AD-A040 105 HONEYWELL INC MINNEAPOLIS MINN SYSTEMS AND RESEARCH --ETC F/G 15/3
PULSED-MODE ENCLOSED-WIRE TRANSDUCER ANALYSIS.(U)
APR 77 L E KOEHLER, T RAHMAN, C TETTEMER F30602-76-C-0378
UNCLASSIFIED RADC-TR-77-129 NL

1 OF 2
ADA040105

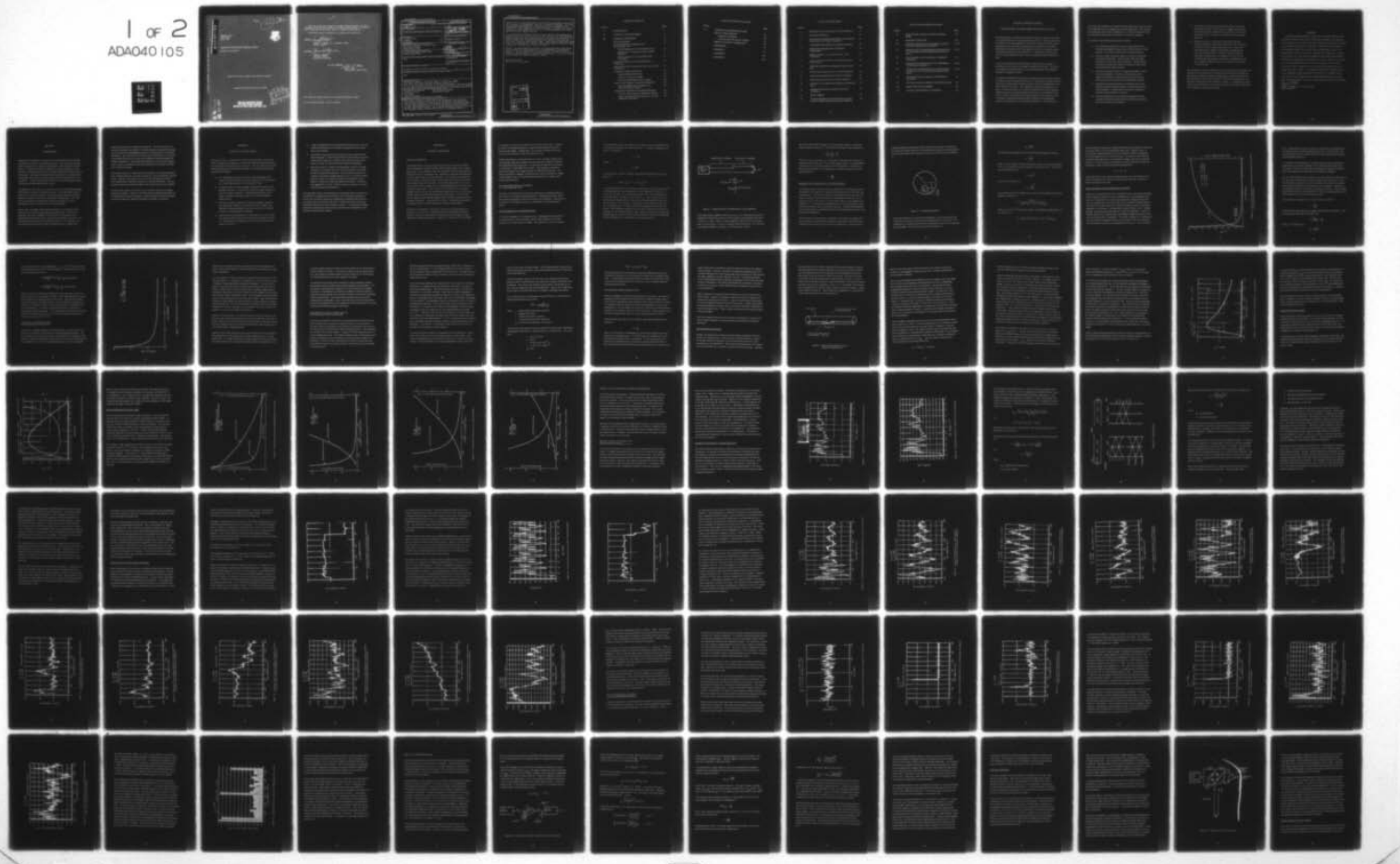

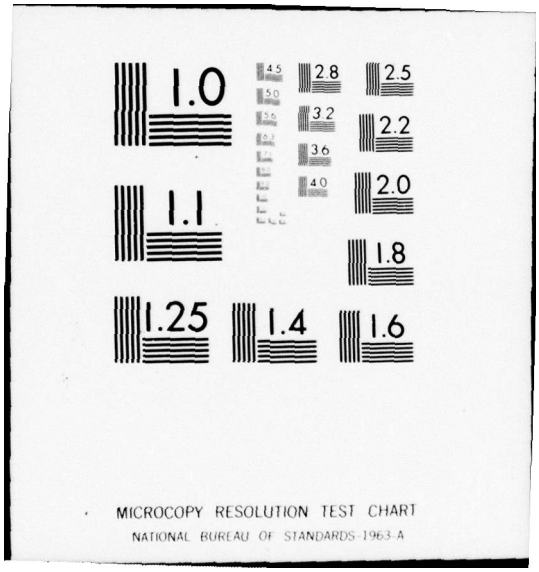
1.0
1.1
1.25
1.4
1.6
1.8
2.0
2.2
2.5
2.8
3.2
3.6
4.0
4.5
5.0
5.6
6.3
MICROCOPY RESOLUTION TEST CHART
NATIONAL BUREAU OF STANDARDS-1963-A

AD A040105

RADC-TR-77-129
Phase Report
April 1977

PULSED-MODE ENCLOSED-WIRE TRANSDUCER ANALYSIS

Honeywell Incorporated

Approved for public release; distribution unlimited.

Laboratory Directors' Fund No. 01707604

DDC
RECEIVED
JUN 2 1977
A

ROME AIR DEVELOPMENT CENTER
AIR FORCE SYSTEMS COMMAND
GRIFFISS AIR FORCE BASE, NEW YORK 13441

AD No.
DDC FILE COPY

PULSED-MODE ENCLOSED-WIRE TRANSDUCER ANALYSIS

This report has been reviewed by the RADC Information Office (OI) and is releasable to the National Technical Information Service (NTIS). At NTIS it will be available to the general public, including foreign nations.

This report has been reviewed and is approved for publication.

APPROVED: Samuel J. Stecher

SAMUEL J. STECHER, Jr., Lieutenant, USAF
Project Engineer

APPROVED: Joseph L Ryerson

JOSEPH L. RYERSON
Technical Director
Surveillance Division

FOR THE COMMANDER: John P. Huss

JOHN P. HUSS
Acting Chief, Plans Office

This effort was funded totally by the Laboratory Directors' Fund.

Do not return this copy; retain or destroy.

UNCLASSIFIED
SECURITY CLASSIFICATION OF THIS PAGE (When Data Entered)

REPORT DOCUMENTATION PAGE

READ INSTRUCTIONS BEFORE COMPLETING FORM

1. REPORT NUMBER: RADC-TR-77-129	2. GOVT ACCESSION NO.
3. RECIPIENT'S CATALOG NUMBER	
4. TITLE (and Subtitle): PULSED-MODE ENCLOSED-WIRE TRANSDUCER ANALYSIS	5. TYPE OF REPORT & PERIOD COVERED: Final Report, June 1976 - December 1976, Phase I
6. PERFORMING ORG. REPORT NUMBER: N/A	
7. AUTHOR(s): L. E. Koehler, T. Rahman, C. Tettemer	8. CONTRACT OR GRANT NUMBER(s): F30602-76-C-0378
9. PERFORMING ORGANIZATION NAME AND ADDRESS: Honeywell Inc/Systems & Research Center, 2600 Ridgway Parkway, Minneapolis MN 55413	10. PROGRAM ELEMENT, PROJECT, TASK AREA & WORK UNIT NUMBERS: 61101F, 01707604, 76
11. CONTROLLING OFFICE NAME AND ADDRESS: Rome Air Development Center (OCDS), Griffiss AFB NY 13441	12. REPORT DATE: April 1977
	13. NUMBER OF PAGES: 134
14. MONITORING AGENCY NAME & ADDRESS (if different from Controlling Office): Same	15. SECURITY CLASS. (of this report): UNCLASSIFIED
	15a. DECLASSIFICATION DOWNGRADING SCHEDULE: N/A

16. DISTRIBUTION STATEMENT (of this Report)

Approved for public release; distribution unlimited.

402 349

17. DISTRIBUTION STATEMENT (of the abstract entered in Block 20, if different from Report)

Same

18. SUPPLEMENTARY NOTES

RADC Project Engineer: Lieutenant Samuel J. Stecher Jr., (OCDS)
This effort was funded totally by Laboratory Directors' Fund.
This is the final report for Phase I of a two-phased effort. The data contained in this report may not necessarily be included in the final report (see reverse)

19. KEY WORDS (Continue on reverse side if necessary and identify by block number)

Enclosed-Wire Transducer
Transmission Line
Line Sensor
Wire-in-Tube Sensor
Randomly Distributed Characteristic Impedance
Time Domain Reflectometry
Reflectometer Sensor

20. ABSTRACT (Continue on reverse side if necessary and identify by block number)

This report contains an analysis and design optimization for pulsed-mode, enclosed-wire transducer. Operating in the pulsed mode, time gating can be used to separate the signals from different portions of a wire-in-tube sensor. A single long transducer and one set of processing electronics can provide multiple range-channel outputs. This study was intended to provide a basis for the subsequent design and feasibility testing of a breadboard sensor.

DD FORM 1 JAN 73 1473 EDITION OF 1 NOV 65 IS OBSOLETE

UNCLASSIFIED
SECURITY CLASSIFICATION OF THIS PAGE (When Data Entered)

Equations for a uniform transmission line with frequency-dependent losses were used to predict the performance limits for an optimized transducer. To account for transducer non-uniformities, we modeled the line as a number of short segments with equal lengths but different impedances. We analyzed the loosely-laid wire-in-tube configuration as well as an optimized geometry with random variations in the conductor spacing.

It is theoretically possible to achieve a range resolution of 30 meters and a signal-to-noise ratio of 25 dB with a 1/2 inch diameter, 2 km long transducer. Range resolution, as well as signal amplitude, are limited by attenuation and multiple reflections. Multiple reflections also produce clutter and cross talk, which limits the sensor dynamic range. These problems become quite significant if the variations in conductor spacing exceed about one millimeter peak-to-peak over a spatial scale of one or two meters.

Because of multiple-reflection problems, the loosely-laid wire-in-tube transducer is limited to usable lengths of a few hundred meters in pulsed-mode operation. We have identified a transducer geometry in which the inner conductor is supported within an eccentric hollow dielectric. This type of sensor should alleviate the multiple reflection effects.

Block 18 continued:
for Phase II of this effort.

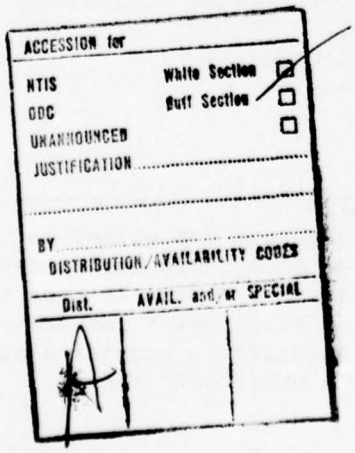

TABLE OF CONTENTS

Section		Page
I	INTRODUCTION	1
II	SUMMARY AND CONCLUSIONS	3
III	TECHNICAL DISCUSSION	5
	Sensor Description	5
	The Enclosed-Wire Transducer as a Transmission Line	6
	Wave Propagation on a Transmission Line	6
	Impedance of a Transducer with a Uniform Dielectric	9
	Signal Attenuation in the Enclosed-Wire Transducer	12
	Mechanical Response of the Enclosed-Wire Transducer	15
	Experimental Characterization of the Wire-In-Tube Transducer	18
	Transducer Design Optimization	21
	Predicted Signal Waveforms	22
	Optimum Transducer Design	28
	Predicted Performance versus Length	30
	Effect of Non-Uniform Transducer Dimensions	35
	Electrical Model of the Loosely-Laid Wire-In-Tube Transducer	35
	Computation Technique for Multiple Reflections	36
	Wire-In-Tube Transducer Simulation Results	44
	Effect of Random Gap Variations in a 1/2-Inch Optimized Transducer	63

TABLE OF CONTENTS (concluded)

Section		Page
III	TECHNICAL DISCUSSION (concluded)	
	Signal-to-Noise Estimates	75
	Excitation Waveforms	81
	Alternate Signal-Processor Designs	84
	Suggested Transducer Configurations	85
	REFERENCES	91
	APPENDIX A	93
	APPENDIX B	103
	APPENDIX C	109

LIST OF ILLUSTRATIONS

Figure		Page
1	Reflection from a Discontinuity in Line Impedance	8
2	Transducer Geometry	10
3	Characteristic Impedance and Reflection Coefficient versus Gap in a 1/2-Inch Transducer	13
4	Attenuation versus Gap for a 1/2-Inch Transducer	16
5	Double-Step Approximation to Conductor Displacement	23
6	Signal Waveform; 0.19-Inch Diameter, 1 km Transducer	27
7	V_{MAX} and τ for 0.5-Inch, 2 km Transducer with 0.05 mm Gap	29
8	Reflection Coefficient and Range Resolution versus Gap	31
9	Performance Estimates for 0.19-Inch Transducer	32
10	Performance Estimates for 0.5-Inch Transducer	33
11	Performance Estimates for 1-Inch Transducer	34
12	Computer Fit to Experimental Reflection-Coefficient Data	37
13	Impedance Variations of Loosely-Laid Wire Transducer	38
14	Bewley Diagram	40
15	Simulated Response Using 200-Element Approximation to Experimentally Determined Impedance	46

LIST OF ILLUSTRATIONS (concluded)

Figure		Page
16	Final 10-meter Loosely-Laid Wire Transducer Model	48
17	Response of Final Model	49
18	Simulated TDR Picture for 1600-Segment Loosely-Laid Wire Transducer (In six parts)	51-56
19	Simulated Time-Varying Response of Loosely-Laid Wire Transducer with Multiple Reflections (In six parts)	57-62
20	Gap Variations in the 1600-Element "Optimized" Transducer	65
21	Partial Time-Amplitude History for 1600-Element Transducer (In two parts)	66-67
22	Partial Time-Amplitude History for 3200-Element Transducer with 1.5 mm Gap Variations (In three parts)	69-71
23	Simulated Processor Outputs for 3200-Element Transducer	73
24	Processor Assumed in Signal-to-Noise Calculations	76
25	Square-Wave Drive Technique	83
26	Eccentric Hollow Dielectric Transducer	89

TECHNICAL REPORT SUMMARY

PULSED-MODE, ENCLOSED-WIRE TRANSDUCER ANALYSIS

The pulsed-mode, enclosed-wire transducer offers the potential for significant improvement over existing buried-line sensors. Other sensors must be deployed in multiple segments to reduce the cumulative effects of background noise and to provide information on the location of an intrusion. Operating in the pulsed mode, time gating can be used to separate signals from different portions of the transducer. A single long transducer and one set of processing electronics can provide multiple range-channel outputs.

Analysis and optimization of this sensor concept involves a number of parameters, and can best be handled by computer simulation. This study was intended to provide a basis for the subsequent design and feasibility testing of a breadboard sensor.

We applied transmission line theory to the pulsed-mode transducer analysis. Although the work was primarily analytical, we performed limited measurements on an experimental transducer section to help in establishing a realistic computer simulation. The transducer analysis was handled in two parts. We used equations for a uniform transmission line with frequency-dependent losses to predict the performance limits of an optimized transducer. For the case where the conductor spacing is not uniform, we had to develop a computation technique which minimizes the bookkeeping involved in calculating all of the multiple reflections. The technique we

used treats the transducer as a lossless transmission line made up of many short segments with equal lengths but different impedances. We analyzed the loosely-laid wire-in-tube configuration as well as an optimized transducer geometry with random variations in the conductor spacing.

Our results can be briefly summarized as follows:

- It is theoretically possible to achieve range resolutions of 30 meters and signal-to-noise ratios of 25 dB with a 1/2-inch diameter, 2 km long transducer and a simple processor.
- Maximum usable transducer length is limited by attenuation and multiple reflections. These factors affect the range resolution as well as the signal amplitude. Multiple reflections due to variations in conductor spacing can also cause crosstalk between range channels.
- The outer conductor should be as large as possible to minimize line attenuation. However, such factors as cost, weight and difficulty of deployment place a practical size limit on the order of one inch on the transducer diameter.
- Optimum electrical performance is obtained with an inner conductor diameter which is about 0.3 times the outer conductor diameter. Performance is relatively constant for diameter ratios between 0.15 and 0.6.
- A gap of approximately one millimeter between the inner and outer conductors represents an acceptable compromise between sensitivity and resolution.

- Variations in the gap must be minimized, both in magnitude and spatial frequency. When the gap variations exceed about one millimeter peak-to-peak over a spatial scale of less than one or two meters, clutter and crosstalk become significant problems.

- Because of clutter, crosstalk and attenuation caused by multiple reflections, the loosely-laid wire-in-tube transducer is not well suited for pulsed-mode operation. This transducer geometry is unlikely to be usable in lengths greater than a few hundred meters. However there are alternate transducer configurations which appear to satisfy the conflicting design requirements--simplicity and ruggedness, low cost, uniform conductor spacing, and sensitivity to mechanical disturbances.

The next logical step in the development of the pulsed-mode, enclosed-wire transducer is an experimental confirmation of the analytical predictions. One or more candidate transducer configurations should be fabricated and then tested under actual field conditions. These tests should confirm the feasibility of the pulsed-mode transducer concept. A combination of experimental and analytical data will provide a firm basis for further refinements in the transducer and processor design.

EVALUATION

This report provides valuable insight into the maximum feasible length transducer to which the pulsed mode concept may be applied. The contractor identified early in the study the inherent limitations associated with pulsing a wire loosely-laid inside of a copper tube. Severe cross talk dispersion and attenuation plagued this concept, and a minimum length of only a few hundred meters could be anticipated. Honeywell then showed how to optimize the geometry of the enclosed wire transducer and calculated the performance limitation for transducers with diameters of one inch. Results of the study of an offset derandomized version of the line indicate that a 100 meter penetration location capability can be achieved from transducer which can extend some 3 km in length. The information provided by the report will be used in subsequent design and feasibility testing of a breadboard sensor. This effort has been funded entirely through Laboratory Directors' Funds under TPO-R6A in support of the Base and Installation Security System Program.

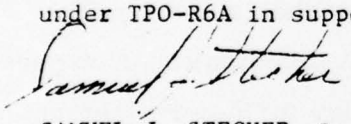

SAMUEL J. STECHER, Jr. Lieutenant, USAF
Project Engineer

SECTION I

INTRODUCTION

Honeywell has completed an analysis of the Pulsed-Mode, Enclosed-Wire Transducer for Rome Air Development Center. This transducer concept offers the potential for significant improvement over existing buried-line sensors. Other sensors must be deployed in multiple segments to limit the effects of background noise and to provide information on the location of an intrusion. Operating the enclosed-wire transducer in the pulsed mode, time gating can be used to separate signals from different portions of the transducer. A single long transducer and one set of processing electronics can provide multiple range-channel outputs.

The objective of our study was to provide a basis for the subsequent design and feasibility testing of a breadboard sensor. This report shows how to optimize the transducer design for pulsed operation and predicts the performance attainable with practical transducer configurations. All of the work was performed at Honeywell's Systems and Research Center, Minneapolis, under the direction of Dr. George Webber.

In our study, we applied transmission-line theory to the analysis of the enclosed-wire transducer operating in the pulsed mode. The work was primarily analytical, although we measured the characteristics of an experimental transducer to form a basis for the computer simulation. The transmission-line analysis was handled in two parts. We analyzed a uniform transmission line with frequency-dependent losses to predict the

performance limits of an optimized transducer. For the case where the conductor spacing is not uniform, we had to develop a computation technique which minimizes the bookkeeping involved in calculating all of the multiple reflections. The technique that we used treats the transducer as a lossless transmission line made up of many short segments with equal lengths but different impedances. We analyzed the loosely-laid wire-in-tube configuration as well as an optimized transducer geometry with random variations in the conductor spacing.

Our results show that an optimized $\frac{1}{2}$-inch diameter, 2-km long transducer with a simple processor can meet or exceed Air Force performance requirements. However, the loosely-laid wire-in-tube configuration suffers a severe performance degradation because of multiple reflections. We have identified alternate transducer designs which should alleviate this problem.

Included in this report are results of our transducer analysis and design optimization studies. There is a brief discussion of signal processing with a sample signal-to-noise calculation. Several alternate transducer designs are recommended for a possible breadboard feasibility verification.

SECTION II

SUMMARY AND CONCLUSIONS

During this study, we showed how to optimize the geometry of the pulsed-mode, enclosed-wire transducer, and we calculated the performance limits for transducers with diameters up to one inch. We also analyzed the effects of non-uniformities in the conductor spacing. Our results can be briefly summarized as follows:

- It is theoretically possible to achieve range resolutions of 30 meters and signal-to-noise ratios of 25 dB with a 1/2 inch diameter, 2 km long transducer and a simple processor.
- Maximum usable transducer length is limited by attenuation and multiple reflections. These factors affect the range resolution as well as the signal amplitude. Multiple reflections due to variations in conductor spacing can also cause crosstalk between range channels.
- The outer conductor should be as large as possible to minimize line attenuation. However, such factors as cost, weight, and difficulty of deployment place a practical size limit on the order of one inch on the transducer diameter.
- Optimum electrical performance is obtained with an inner conductor diameter which is about 0.3 times the outer conductor diameter. Performance is relatively constant for diameter ratios between 0.15 and 0.6.

- A gap of approximately one millimeter between the inner and outer conductors represents an acceptable compromise between sensitivity and resolution.
- Variations in the gap must be minimized, both in magnitude and spatial frequency. When the gap variations exceed about one millimeter peak-to-peak over a spatial scale of less than one or two meters, clutter and crosstalk become significant problems.
- Because of clutter, crosstalk and attenuation caused by multiple reflections, the loosely-laid wire-in-tube transducer is not well suited for pulsed-mode operation. This transducer geometry is unlikely to be usable in lengths greater than a few hundred meters. However, there are alternate transducer configurations which appear to satisfy the conflicting design requirements: simplicity and ruggedness, low cost, uniform conductor spacing, and sensitivity to mechanical disturbances.

The next logical step in the development of the pulsed-mode, enclosed-wire transducer is an experimental confirmation of the analytical predictions. One or more candidate transducer configurations should be fabricated and then tested under actual field conditions. These tests should confirm the feasibility of the pulsed-mode transducer concept. A combination of experimental and analytical data will provide a firm basis for refinements in the transducer and processor design.

SECTION III

TECHNICAL DISCUSSION

SENSOR DESCRIPTION

The pulsed-mode, enclosed-wire transducer uses time-domain reflectometer techniques to provide multiple range channel outputs from a single long sensor. In its simplest form, the transducer can be an insulated wire loosely laid within a conducting tube. Reference 1 describes the operation of such a sensor under d-c bias conditions. The capacitance between the wire and tube is a function of their relative positions. Because the wire is free to move within the outer tube, a mechanical disturbance can cause a relative motion of the conductors and a corresponding time variation in the transducer capacitance. If the transducer is biased with a d-c voltage through a large resistor, the capacitance change results in a time-varying voltage which can be detected with sensitive electronics. In fact, there may be enough electret charge trapped in the insulation so that no external biasing is necessary. The sensor is, in effect, a distributed capacitance microphone which can sense disturbances along its entire length.

Because of its simplicity, sensitivity, and low cost, the enclosed-wire transducer is attractive as a buried-line sensor for perimeter defense. However, several factors limit the maximum transducer length to something on the order of 100 meters. Sensitivity is reduced as the line length

is increased, because of the increase in total shunt capacitance. Cumulative effects of background noise in a long distributed sensor eventually swamp out the signal. Furthermore, it is usually desirable to know the location of an intrusion to within 100 meters or less.

If pulsed excitation is used rather than a d-c bias, intrusion signals from various points along the transducer will be delayed by different amounts of time following the excitation pulse. In this mode of operation, the sensor is essentially a closed-loop radar system. Time gating can be used to separate the signals into range channels for additional processing. This makes it possible to suppress background noise and to provide many range-channel outputs from one continuous long transducer and a single set of processing electronics.

THE ENCLOSED-WIRE TRANSDUCER AS A TRANSMISSION LINE

Basically, the enclosed-wire transducer operating in the pulsed mode can be treated as a non-ideal transmission line. Using equations which relate the transducer geometry to the characteristic line impedance, transmission-line theory can be applied directly to a prediction of transducer performance.

Wave Propagation on a Transmission Line

If a signal is applied to a transmission line, it propagates down the line at a finite velocity so that the voltage at point x lags the phase of the input voltage by an amount β per unit length. The amplitude of the wave at point

x in a non-ideal line is also reduced by an amount α per unit length because of conductor resistance and dielectric losses. A complex propagation constant γ is defined as:

$$\gamma = \alpha + j\beta$$

where:

$$j = \sqrt{-1}$$

At any point on a uniform, infinitely long line the voltage and current are given by:

$$E(x) = E_{in}e^{-\gamma x} \qquad I(x) = I_{in}e^{-\gamma x}$$

A transmission line has a characteristic impedance Z_o which is determined by the line geometry and the properties of the conductors and dielectric material in the line. On an infinitely long line, the ratio of voltage to current is the same at all points and is equal to Z_o. This is also true if the line is finite in length and is terminated in a lumped impedance equal to Z_o. But if the line is not "matched", some energy is not delivered to the load and is accounted for by a reflected wave that propagates back toward the source. This reflection condition will also exist if the line's characteristic impedance is not constant along its path. Figure 1 illustrates a voltage step propagating from a source down a transmission line, and the corresponding reflected voltage from a discontinuity in the line impedance.

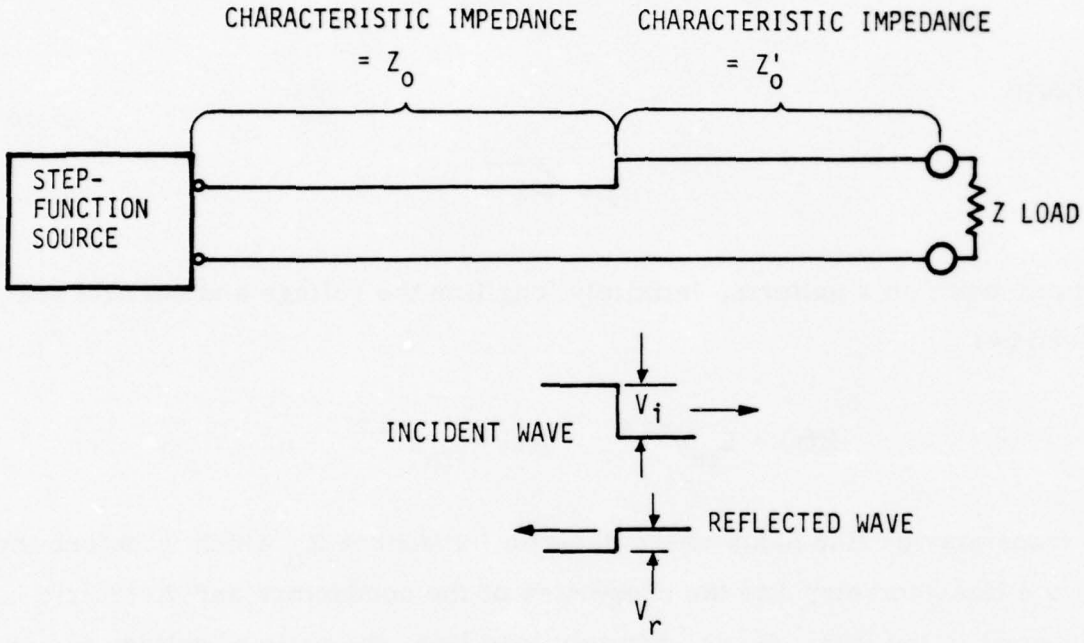

Figure 1. Reflection from a Discontinuity in Line Impedance

If the input pulse is applied to the line at time t_o, the reflected wave from an impedance discontinuity at point x arrives back at the beginning of the line at a time $t = t_o + 2x/c$: where c is the propagation velocity of an electromagnetic wave on the line. In an air-insulated transmission line, c is very close to the speed of light in a vacuum, 3×10^8 meters per second.

The ratio of the reflected voltage V_r to the incident voltage V_i, called the voltage reflection coefficient ρ, is related to the change in line impedance by

$$\rho = \frac{Z_o' - Z_o}{Z_o' + Z_o} = \frac{V_r}{V_i}$$

Note that if Z_o' is less than Z_o, ρ is negative, indicating that the wave reverses sign upon reflection. This will be important later in considering the reflection from a small disturbance in the line impedance. We also note that for small changes in line impedance, the reflection coefficient can be approximated by

$$\rho \simeq \frac{\Delta Z}{2Z_o}$$

Impedance of a Transducer with a Uniform Dielectric

As mentioned above, the characteristic impedance of a transmission line is determined by the goemetry of the line and the properties of the conductors and dielectric. Some form of dielectric coating is needed on the inner conductor to prevent a short in the line if a sharp bend is introduced. If the dielectric layer is fairly thin, it will have little effect on line impedance or sensitivity. A reasonably good approximation to the line impedance can be made by assuming a uniform dielectric constant. Computation procedures for the impedance of an eccentric line with an inhomogeneous dielectric are discussed in Appendix B.

The resistivity of the conductors is typically low enough to be neglected in the calculation of characteristic impedance, even though it gives rise to an attenuation factor which can by no means be neglected. For the eccentric

transducer geometry the characteristic impedance is not only a function of the ratio of the outer conductor to inner conductor diameter, but also depends on the distance of the inner conductor from the axis of the outer tube (Figure 2).

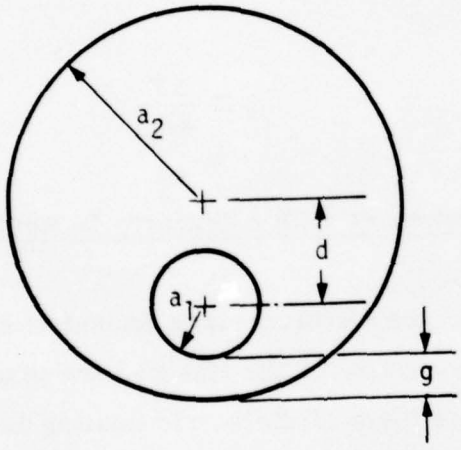

Figure 2. Transducer Geometry

In the determination of characteristic impedance, we will assume that the conductors and dielectric have the same permeability as free space. The impedance of a transmission line can be expressed in terms of its inductance per unit length L and its capacitance per unit length C by

$$Z_o = \left(\frac{L}{C}\right)^{\frac{1}{2}}$$

The velocity of propagation in the transverse electromagnetic mode is

$$V = \frac{c}{(\epsilon_r)^{\frac{1}{2}}}$$

where c is the velocity of light in free space, and ϵ_r is the relative permittivity of the dielectric material filling the transmission line. The velocity can also be expressed as

$$V = (LC)^{-\frac{1}{2}}$$

so that we can define Z_o as

$$Z_o = \frac{(\epsilon_r)^{\frac{1}{2}}}{cC}$$

The capacitance per unit length of an eccentric cable uniformly filled with a dielectric material is

$$C = \frac{2\pi\epsilon_o\epsilon_r}{\cosh^{-1}[(a_1^2 + a_2^2 - d^2)/2a_1a_2)]}$$

where $\epsilon_o = 8.85 \times 10^{-12}$ farads per meter. Combining the expressions, we can write Z_o as

$$Z_o = 60(\epsilon_r)^{-\frac{1}{2}} \cosh^{-1}[(a_1^2 + a_2^2 - d^2)/2a_1a_2]$$

The characteristic impedance is highest when the inner conductor is centered, and lowest when it is nearly touching the outer tube. Figure 3 shows Z_o versus inner-conductor position for an air-dielectric cable consisting of a 0.14-inch diameter wire in a $\frac{1}{2}$-inch ID tube. Also shown is the reflection coefficient resulting from a 0.01 millimeter change in the inner-conductor position. We have expressed the position in terms of the gap g between the conductors, which is related to the other dimensions by

$$d = a_2 - (a_1 + g)$$

The sensitivity to small relative displacements is zero when the inner conductor is centered, and reaches a maximum when the inner conductor is nearly touching the tube wall.

Signal Attenuation in the Enclosed-Wire Transducer

Even in an air-insulated line with no dielectric losses, the finite conductivity of the conductors results in a loss of amplitude as a wave propagates down the line. Furthermore, the losses become greater at higher frequencies. This is due primarily to the "skin effect" which confines the high-frequency currents to the surface region of a conductor and gives rise to a frequency-dependent a-c resistance. Although the exciting waveform is a d-c voltage change, we cannot assume that only d-c losses are important. Actually, a Fourier analysis of an instantaneous step voltage change reveals that it contains an infinite band of frequencies. If the step is applied to a transmission line with frequency-dependent losses, the rise time of the step waveform will continuously increase as it propagates down the line. As we will show

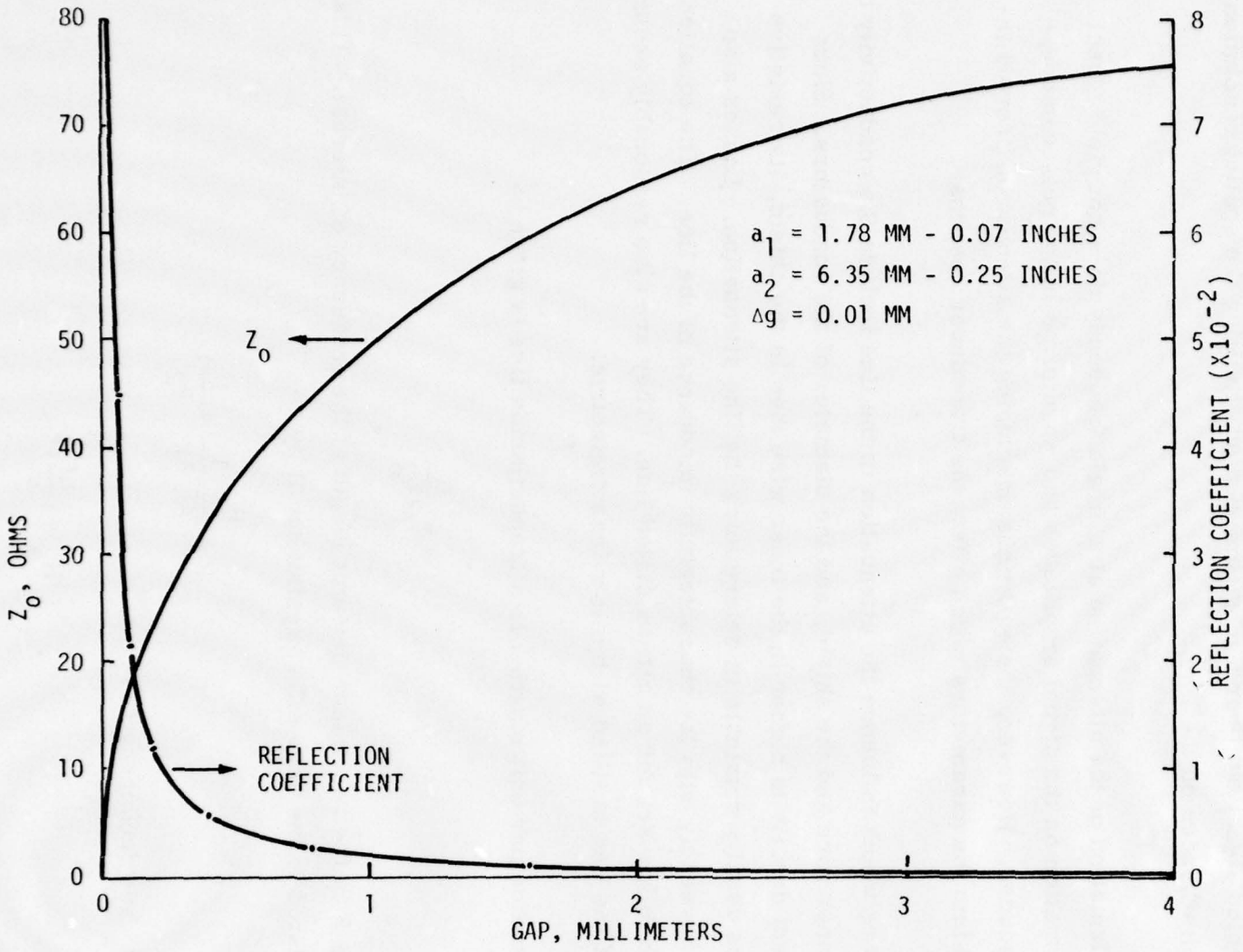

Figure 3. Characteristic Impedance and Reflection Coefficient versus Gap in a 1/2-Inch Transducer

later, a degradation in rise time results in a reduction in the amplitude of the reflection from a small disturbance in the line. It also "smears" the reflected signal out over a long time period, limiting the spatial resolution of disturbances on the line.

A calculation of the attenuation at a single frequency does not yield direct information on the signal amplitudes and waveforms in the pulsed-mode transducer. However, the equations describing the attenuation provide insight into the parameters which affect the transducer response.

Factors which influence the attenuation in the line include the conductivity of the inner wire and the shield, and the diameter of the conductors. Since current density is higher in the inner wire than in the shield, its resistive losses usually dominate in determining the line attenuation. Losses also vary inversely with the characteristic impedance of the line. The equations which follow are for an air-insulated line. They are also reasonably accurate if the line is filled with a low-loss dielectric.

Attenuation per unit length α in a transmission line is given by

$$\alpha = \frac{R}{2Z_o}$$

where R is the resistance per unit length at the frequency of interest. This is related to the skin-effect resistance R by

$$R = \frac{R_s}{2\pi}\left(\frac{1}{a_1} + \frac{1}{a_2}\right)$$

and R_s at a frequency f is

$$R_s = \left(\frac{\pi\mu f}{\sigma}\right)^{\frac{1}{2}}$$

For copper conductors, the permeability $\mu = \mu_o = 4\pi \times 10^{-7}$ henries/meter and the conductivity σ in 5.8×10^{7} mhos/meter. The attenuation for a copper transmission line is then

$$\alpha = \frac{2.08 \times 10^{-8}}{Z_o} (f)^{\frac{1}{2}} \left(\frac{1}{a_1} + \frac{1}{a_2}\right) \text{ nepers/meter}$$

or

$$\alpha = \frac{1.8 \times 10^{-4}}{Z_o} (f)^{\frac{1}{2}} \left(\frac{1}{a_1} + \frac{1}{a_2}\right) \text{ dB/kilometer}$$

Figure 4 shows the attenuation in dB per km versus gap for a $\frac{1}{2}$-inch diameter transducer at a frequency of 5 MHz. This is approximately the bandwidth needed for a range resolution of 30 meters. Since the drive signal and reflected signal are both attenuated, the total effective attenuation per kilometer of transducer length is twice the value shown. Comparing this curve with Figure 3, we note that the high sensitivity at small gaps is accompanied by high attenuation. For a resolution of 100 meters, the bandwidth can be reduced by a factor of 3.33 and the attenuation would be reduced by the factor $(3.33)^{\frac{1}{2}} = 1.82$.

MECHANICAL RESPONSE OF THE ENCLOSED-WIRE TRANSDUCER

To perform a complete analysis of the pulsed-mode, enclosed-wire transducer, it is necessary to know the exact transmission-line geometry. We are interested in the static variations in the dimensions of a deployed transducer, as well as the conductor motion caused by a time-varying disturbance. In subsequent discussions, we use experimental data as well as computer

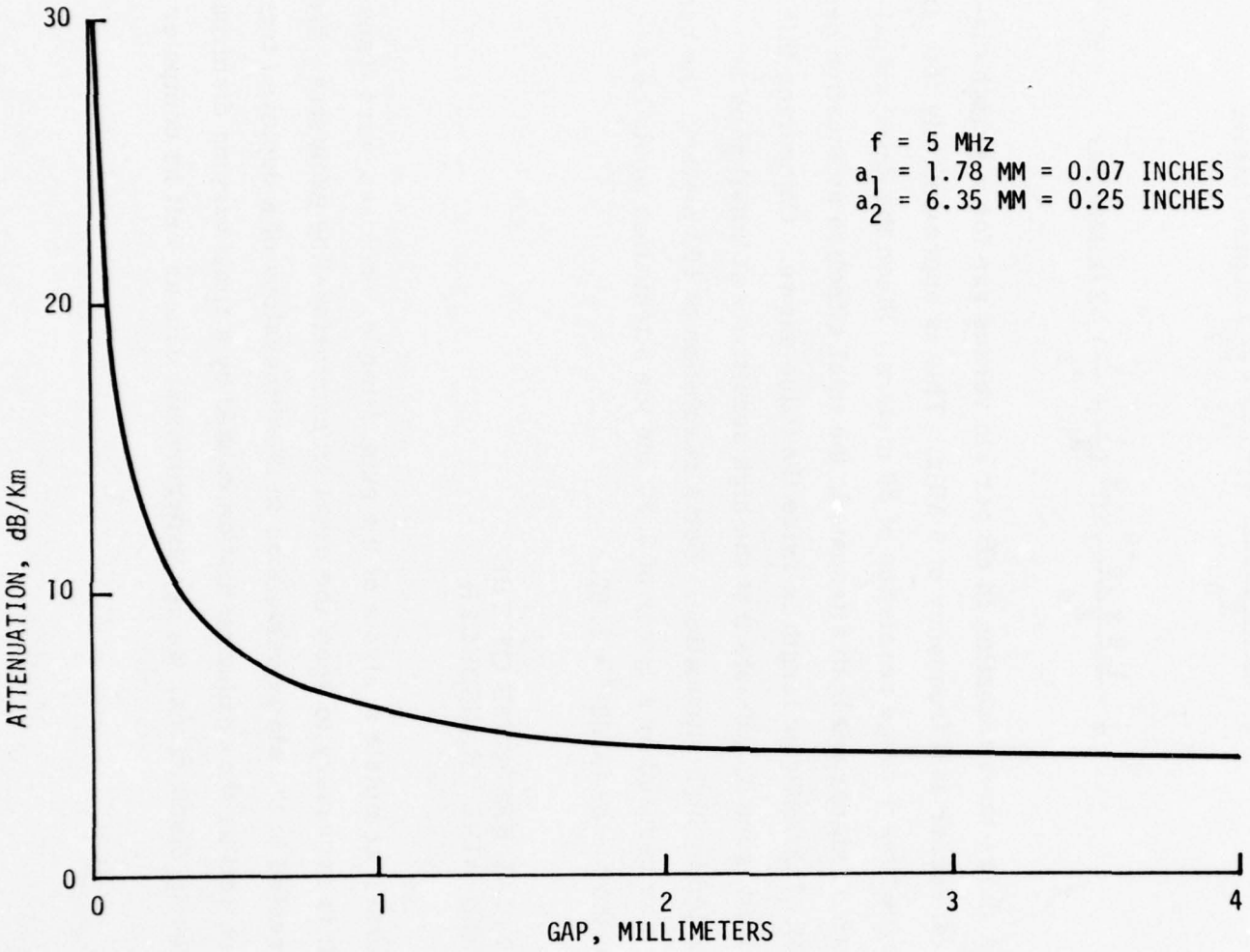

Figure 4. Attenuation versus Gap for a 1/2-Inch Transducer

simulations to establish mechanical models for the static dimension variations. We use these models to show the effects of non-uniformity on transducer performance.

It is very difficult to make a quantitative estimate of the transducer's time-varying response. As pointed out in Reference 1, there are several modes of response, depending upon the disturbance frequency. At very low frequencies, the dominant cause of relative motion between the wire and the tube is a deformation of the tube between inner-conductor support points. Mechanical resonances in the inner conductor and its support structure give rise to the so-called "strumming" mode. For the loosely-laid wire-in-tube sensor, these resonances lie in the 20 to 40 Hz range. When the excitation frequency is high enough, the inner conductor remains relatively stationary as the tube vibrates. In all of these modes, the relative motion is strongly influenced by the inner conductor size and stiffness, the way in which it is supported, and the surrounding soil conditions.

Except for resonant effects, the relative motion of the inner and outer conductors cannot exceed the deformation of the soil in which the transducer is buried. Thus, we can estimate the maximum amplitude of the time-varying conductor displacement by calculating the soil motion under loading conditions representing a walking intruder.

Appendix A gives the results of a quasi-static solution for the soil displacement produced by a 200-pound load distributed uniformly over an 8-inch radius disk. At a depth of eight inches directly below the load, the vertical soil displacement is 722 microinches (approximately 0.02 millimeter); the

maximum displacement decreases to 451 microinches (0.011 millimeter) at a burial depth of 16 inches. At 40 inches (1 meter) from the center of the load, the vertical soil displacement is nearly constant at 110 microinches (0.0028 millimeter) down to burial depths of 24 inches.

We will show later that the static variations in inner-conductor relative displacement must be minimized to reduce attenuation and crosstalk. It is impractical to keep the outer conductor of a buried transducer straight. Therefore it will probably be necessary to support the inner conductor at intervals not much greater than one meter in order to restrict its maximum relative displacement. Based upon these considerations and the soil-displacement computations, we have assumed that the time-varying inner-conductor displacement has a peak amplitude of 400 microinches (0.01 millimeters) and an effective length of one meter.

EXPERIMENTAL CHARACTERIZATION OF THE ENCLOSED-WIRE TRANSDUCER

Our study was primarily analytical, but we performed limited field experiments to help define a simulation analytical model for the transducer. A 10-meter section of transducer was fabricated and installed in the line sensor test facility at the Honeywell Ordnance Proving Ground. The transducer was the basic wire-in-tube sensor, a number 26 Teflon-insulated wire in a $\frac{1}{4}$-inch refrigeration tube. Time-domain reflectometer measurements were made to determine the static impedance variations along the length of the transducer. Results of these measurements and their incorporation into the transducer model are treated in detail in the discussion of non-uniform transducer effects.

We also measured the time-varying reflection coefficients in response to a known soil disturbance. A cyclic signal generator was used to impart a 10-Hz, 100-pound peak-to-peak load to the soil surface. The generator was placed above the midpoint of the transducer, which was buried about eight inches deep in sand.

The time-domain reflectometer controls were set to display the reflection coefficient at a single point on the transducer, selectable by varying the delay-time potentiometer. The vertical deflection output of the TDR was recorded on a strip chart recorder, along with the outputs of geophones adjacent to the transducer and directly beneath the 10-Hz cyclic signal generator. Recordings of the TDR output were made at time-delay increments of 5 nanoseconds, corresponding to position increments of about 0.6 meters along the line transducer. With a peak-to-peak soil displacement of 300 microinches, as indicated by the vertical-axis geophone, the peak-to-peak variation in reflection coefficient near the signal generator was about 8.6×10^{-3}. The noise level with this instrumentation was fairly high, and it was difficult to distinguish the signal from the noise at points more than two meters from the signal generator. In fact, except for one measurement point, the signal appeared to consist mostly of the second harmonic of the excitation. This implies a "strumming" mode excitation of the wire at a harmonic of the mechanical input frequency.

We also measured the velocity of propagation in the transducer by using a short-circuit load at the far end to provide distinct time marker. The round-trip propagation time within the 10-meter test section was 80 nanoseconds. This corresponds to an average propagation velocity of 0.833

times the free-space velocity of light. The average velocity factor is about midway between the free-space value and the velocity factor of a cable with solid Teflon dielectric.

With the transducer shorted, the fall time of the reflected step-function signal provides a measurement of the round-trip waveform distortion in the transducer. The time for the reflected step to decay to 50 percent of its final value was approximately three nanoseconds. This is much longer than the fall time calculated on the basis of frequency-dependent line losses.

For a step excitation, the 50 percent risetime ($T_{50\%}$) of a coaxial line is approximately given by the formula

$$T_{50\%} \approx \frac{\mu \ell^2}{16 \pi^2 r^2 \sigma Z_o^2}$$

where μ = permeability of the inner conductor

ℓ = length of the cable

r = radius of the inner conductor

σ = conductivity of the inner conductor

Z_o = characteristic impedance of the cable

The fall time of the reflected step on a shorted 10-meter line is obtained by computing the rise time of a step excitation on a 20-meter line. For a #26 wire,

$\mu = 4\pi \times 10^{-7}$ H/M

$\ell = 20$ m

$r = 0.009 \times 2.54 \times 10^{-2}$ m

$\sigma = 5.85 \times 10^{7}$ (Ω meter)$^{-1}$

$Z_o = 85\Omega$

$$T_{50\%} = 0.144 \times 10^{-9} \text{ secs}$$

This calculation led us to conclude that the pulse degradation on the test transducer would have to be accounted for by losses due to multiple reflections. A valid numerical solution of the line response must therefore show a fall time for the shorted-line case which is at least in rough agreement with the observed value.

TRANSDUCER DESIGN OPTIMIZATION

From the standpoint of electrical performance of the sensor, the important quantities are the amplitude and time width of the signal resulting from a small relative disturbance of the conductor over a short section of its length. A walking intruder may produce a typical soil displacement of about 0.01 millimeters at a burial depth of 0.25 meters (10 inches), and the disturbance extends over an effective distance of about one meter. These values for the transducer displacement were used in our design optimization studies.

Time duration of the signal can be related to the range resolution of the sensor by

$$\Delta R = \frac{c}{2\tau}$$

where c is the velocity of propagation for an electrical signal in the transducer (for air-insulated line, $c = 3 \times 10^8$ meters per second) and τ is the time width of the signal from a disturbance. We are assuming that two pulses can be resolved if their separation is greater than their width. If the transducer had no losses and had no multiple reflections, the width of a

signal reflected by a disturbance would be determined only by the length of the disturbance. However, the effects of frequency-dependent losses and multiple reflections in a real transmission-line transducer not only decrease the signal amplitude, but also broaden it in time. Transducer geometry factors influencing the signal amplitude and duration are the inner and outer conductor dimensions, the nominal gap between the conductors, the amount of variation in the gap, and the distance from the generator end of the line to the disturbance.

Signal amplitude in the pulsed-mode transducer is directly related to the drive voltage. However, the signal-to-noise ratio cannot be improved indefinitely by raising the drive level. A limit is reached where fluctuations in the drive signal become the dominant noise source. Rather than expressing signal amplitude in absolute units, the effective reflection coefficient is a more meaningful term. This is related to the ratio of the reflected signal to the drive signal.

The drive voltage level used in our computer simulations was chosen such that the signal amplitude is numerically equal to the effective reflection coefficient.

Predicted Signal Waveforms

Earlier, we showed how to derive the characteristic impedance of the enclosed wire transducer as a function of inner conductor position, and how the voltage reflection coefficient can be calculated when there is a step discontinuity in line impedance. Inner-conductor displacement with respect to the outer shield will, of course, be gradual rather than abrupt. However,

the total reflection can still be computed with the same equations simply by representing the inner-conductor position as a series of small discontinuities and superposing all of the reflections (with the appropriate time displacement) to give the resultant reflected waveform. Because of the time "smearing" of the incident pulse due to high-frequency losses in the line, information on the exact shape of a small disturbance in the center-conductor position will be lost on a long line. In fact, it is a reasonably valid assumption to approximate the gradual center-conductor position change by a double step as shown in Figure 5. This reduces the computation to a superposition of the reflections from the two discontinuities.

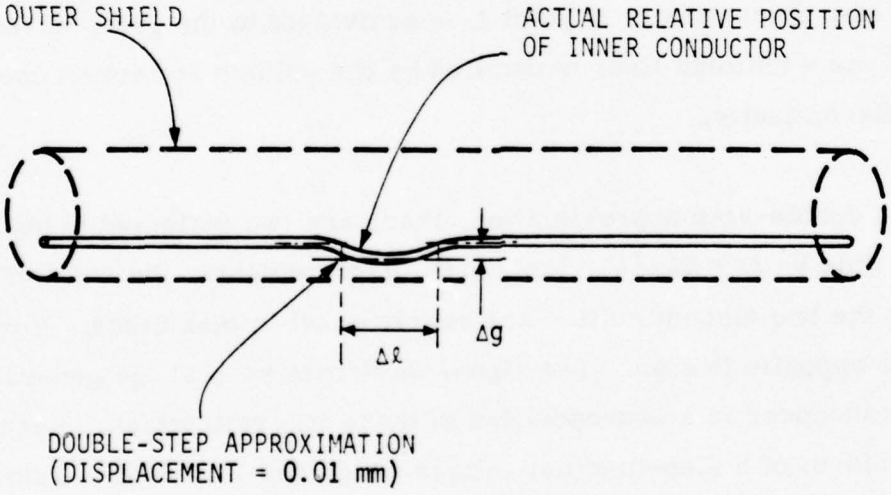

Figure 5. Double-Step Approximation to Conductor Displacement

Figure 5 shows the center conductor distorted with respect to the outer conductor, even though the reverse may be true. Relative displacement is the parameter of interest.

Since we are interested in the reflected wave as it appears back at the input end of the line, the attenuation and distortion of the wave in propagating back through the line must also be considered. The line has the same propagation constants for waves traveling in either direction, so we can treat the reflection from the discontinuity at point L on the line as if the incident wave at the location of the discontinuity is simply scaled down by the linear factor ρ, and then continues along an identical line section of length L. Mathematically, it makes no difference whether we multiply by ρ when the wave gets to position x or wait until it has reached 2L. Thus, the reflected waveform appearing at the driven end of a pulsed line resulting from a step discontinuity at point L is equivalent to the pulse waveform at point 2L on a uniform line, multiplied by the voltage reflection coefficient of the discontinuity.

With the double-step approximation, there are two reflected signals separated in time by $\Delta t = 2\Delta\ell/V$. For small displacements, the reflection coefficients at the two discontinuities are nearly equal in magnitude. However, they are opposite in sign. The signal waveform seen at the generator end of the transducer is a superposition of these two reflections. Let us express the waveform of a step-function voltage which has travelled a distance 2L down a transmission line as $V(t)_{2L}$. Then the signal waveform from a small disturbance can be approximated by

$$V_s = \rho[V(t)_{2L} - V(t-\Delta t)_{2L}]$$

With this expression we can readily calculate the signal waveform if we know the step-function response of the transmission line.

Figure 6 represents the signal which would appear at the input of a transducer consisting of a 2.03×10^{-4} meter radius (No. 26) copper inner conductor in a 2.41×10^{-3} meter radius copper tube ($\frac{1}{4}$ inch refrigeration tubing). There is a uniform 0.5-millimeter gap between the inner conductor and outer conductor, except for a one-meter long disturbed section where the gap is 0.49 millimeters, located 1000 meters from the driven end. The excitation signal is a two-volt step function, and the generator impedance is equal to the nominal cable impedance. Under these conditions, the "TDR picture" would be a constant 1-volt level from t = 0 until t_1, the instant where the first reflection from the disturbance arrives back at the generator end. For an air-insulated line, t_1 would be 6.67 microseconds. Starting at t_1, the waveform of Figure 6 would be added to the constant 1-volt level. (Note that the polarity of this superimposed wave is negative because the disturbed section of transducer has a lower impedance than the rest of the transmission line.) This waveform corresponds to the difference signal which appears when a disturbance produces a one-meter long, 0.01-millimeter displacement in the position of the inner conductor.

The maximum amplitude of the signal and its time duration are shown in Figure 6 as V_{MAX} and τ. Actually, the total time duration is extremely long, but most of the energy is contained between the half-voltage points. Therefore, we have used this definition (full width at half maximum) for the time duration of the signal. V_{MAX} represents the effective reflection coefficient; τ determines the time resolution and thus the spatial resolution

of the transducer. For this example, V_{MAX} is about 15.6 microvolts (effective reflection coefficient = 1.56×10^{-5}) and τ is 6.2×10^{-7} seconds. The corresponding range resolution is about 93 meters.

To calculate the waveform of a step-function signal which has propagated down a long transmission line, we used equations developed by Wigington and Nahman (Reference 2). These equations and the computation procedures used are described in Appendix C. We also computed signal waveshapes for a case in which the line impedance variation is expressed as a continuous analytical function. An inverse Fourier transform was used to derive the time response from the analytical expressions for line impedance and the transfer function of a lossy transmission line. Results of these independent computations are included in Appendix C. They show that the step approximation for the conductor displacement is indeed valid for long transducers, where the signal waveform is determined almost entirely by the transfer function of the transmission line. On a long transducer, the amplitude of the reflected signal is proportional to the integral of the displacement function along the length of the disturbance. A 0.01 millimeter displacement over a 1-meter length will therefore produce almost the same signal amplitude and duration as a 0.001-millimeter displacement over a 10-meter length.

Using a double-step approximation for the inner conductor displacement, we have calculated the amplitude and time widths of reflected signals in uniform transducers with outer conductor ID's of 0.19, 0.5 and 1 inch.

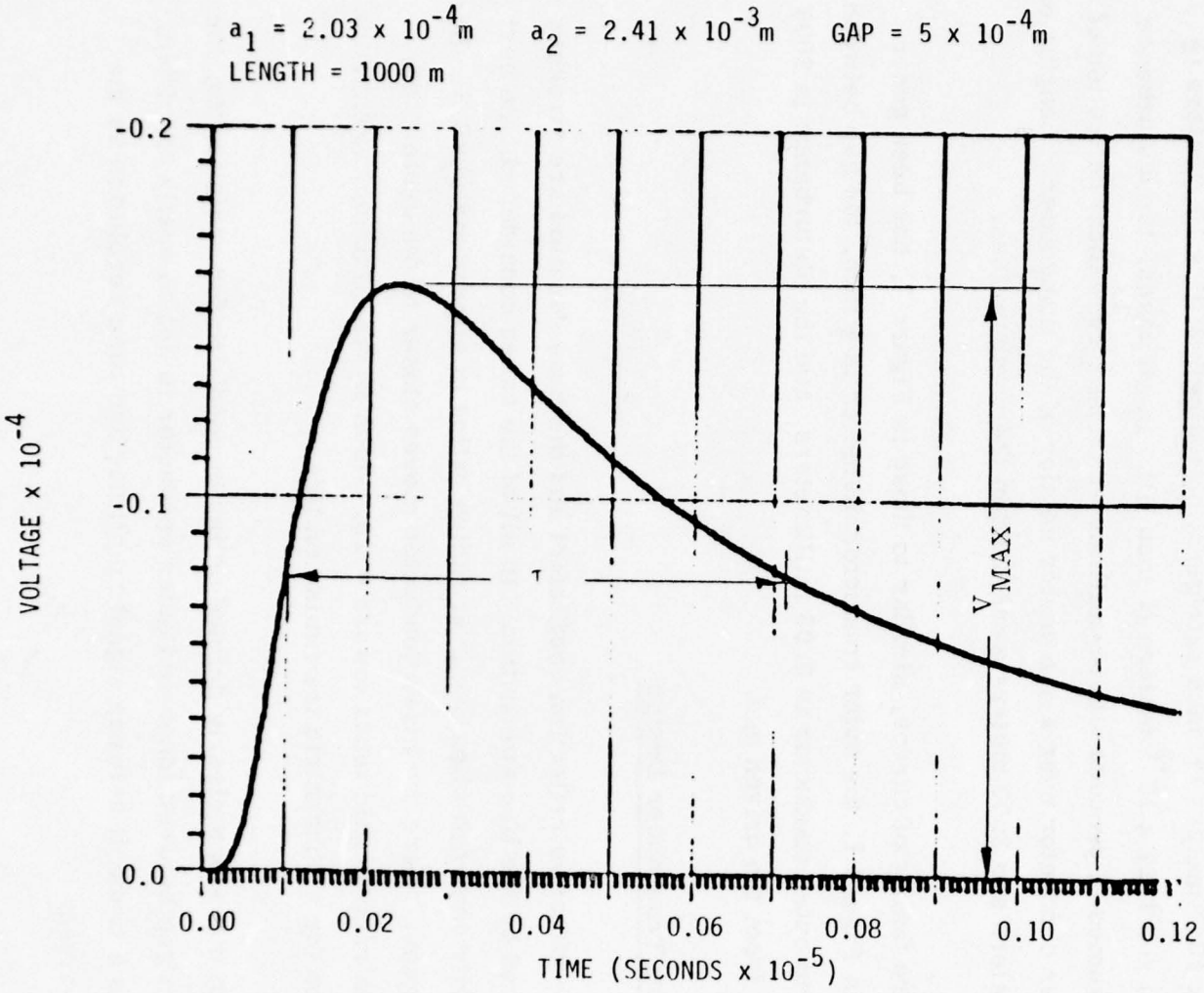

Figure 6. Signal Waveform; 0.19-Inch Diameter, 1 km Transducer

To show the effects of conductor geometry on sensitivity and resolution, we computed and plotted V_{MAX} and τ versus the radius ratio (inner conductor/outer conductor) for various conductor gaps and for outer conductor radii of 2.4×10^{-3} meters ($\frac{1}{4}$ inch refrigeration tubing), 6.35×10^{3} meters ($\frac{1}{2}$ inch ID) and 1.27×10^{-2} meters (1 inch ID). In all cases, the disturbance was assumed to produce a 0.01-millimeter (3.94×10^{-4} inch) deflection of the inner conductor over a one-meter section of the transducer. Lengths of 1000 meters and 2000 meters were used in the computations.

An entire family of curves, similar to those in Figure 7, has been generated. In Figure 7, the outer conductor diameter is $\frac{1}{2}$ inch, the gap between inner and outer conductor is 0.05 millimeters, and the disturbance is 2000 meters from the driven end.

Optimum Transducer Design

Both the effective reflection coefficient and the time duration are strongly influenced by the line attenuation. In all of the cases considered, the best sensitivity and resolution occur at radius ratios of approximately 0.3. For larger gaps, where the inner conductor moves closer to the center, the optimum radius ratio tends toward 0.28, which is the minimum attenuation condition for a concentric transmission line.

Although there is a clearly defined optimum condition for radius ratio, the optimum gap between inner and outer conductor is not so easily specified. There is a tradeoff between signal amplitude and time resolution as the gap is varied.

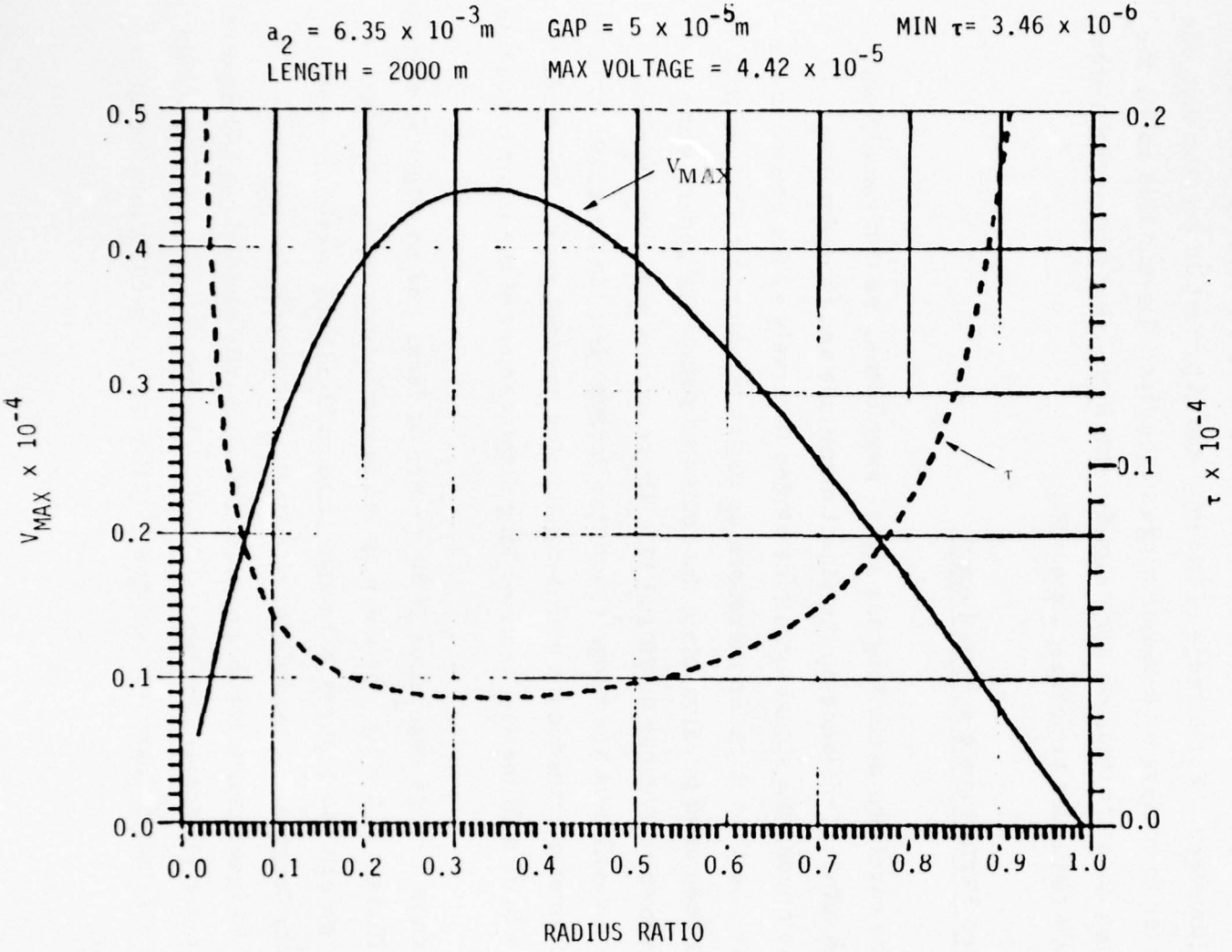

Figure 7. V_{MAX} and τ for 0.5-Inch, 2 km Transducer with 0.05 mm Gap

Figure 8 shows the effective reflection coefficient and range resolution of an "optimum" $\frac{1}{2}$-inch diameter transducer as the gap is varied from 0.05 to 5 millimeters. For a range of two km, the gap must be greater than one millimeter to achieve a 30-meter range resolution. Beyond this point, the resolution does not improve very rapidly with increasing gap, and the signal amplitude continues to decrease steadily.

Predicted Performance versus Length

From the equations describing the signal waveforms, we can readily estimate the effect of distance on the signal amplitude and time duration. At large distances, the signal amplitude varies inversely as the square of the distance; the time duration increases as distance squared. This relationship has been used to extrapolate the computed points and generate the curves shown in Figures 9, 10 and 11. These curves give the effective reflection coefficient and range resolution versus distance for 0.19, 0.5 and 1-inch diameter transducers with 1-millimeter nominal gaps. The disturbance is a 0.01 millimeter, 1-meter long displacement of the inner conductor.

If we choose a range resolution of 30 meters or less, and an effective reflection coefficient of 3×10^{-5} or more as the acceptance criteria for transducers, we can use Figures 9 through 11 to establish the maximum usable transducer lengths. A transducer of $\frac{1}{4}$-inch refrigeration tubing with a Number 16 inner conductor can operate satisfactorily up to about 850 meters. With an outer conductor diameter of $\frac{1}{2}$ inch, lengths up to two km are possible, and a 1-inch transducer can theoretically be deployed in lengths up to three km.

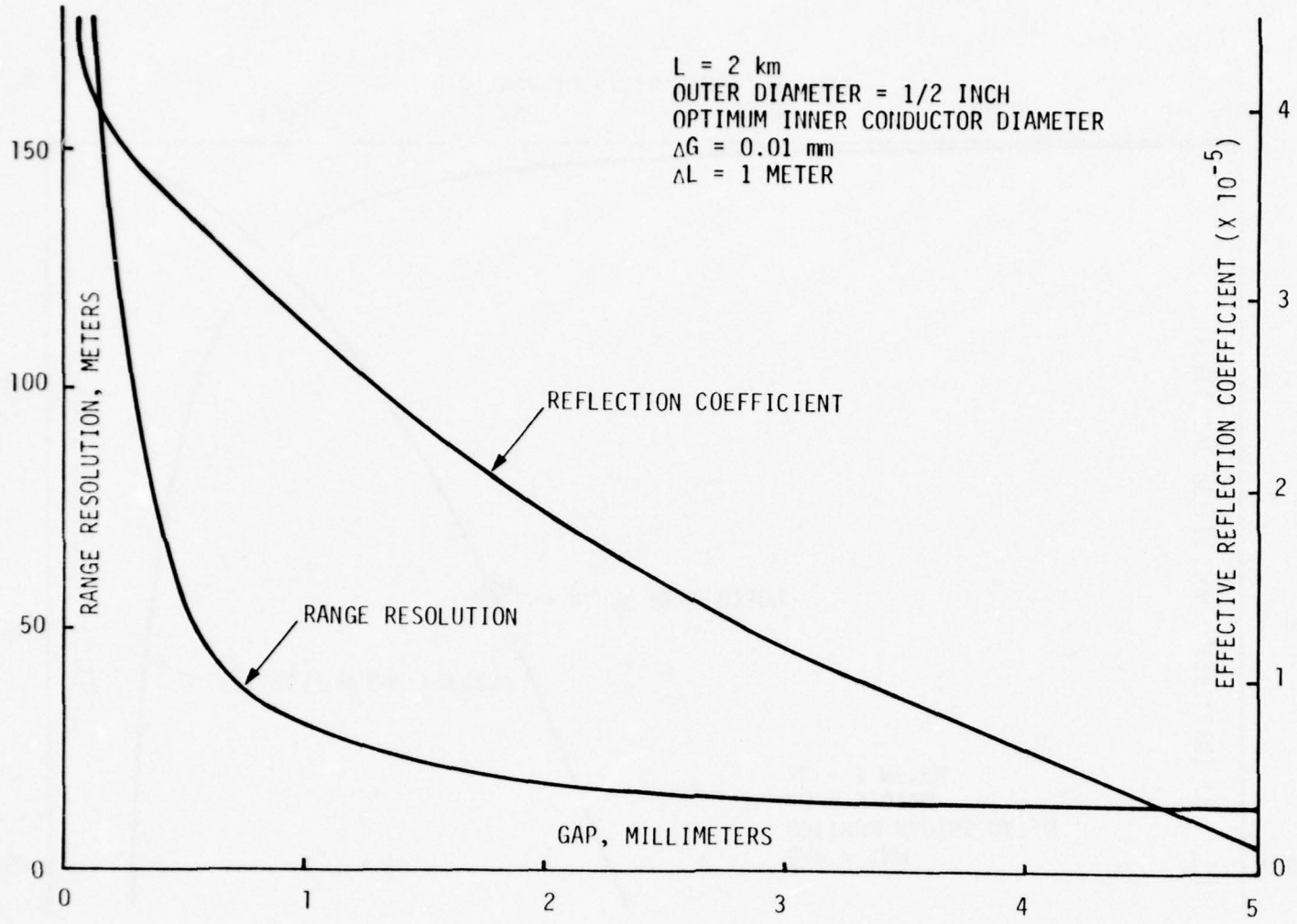

Figure 8. Reflection Coefficient and Range Resolution versus Gap

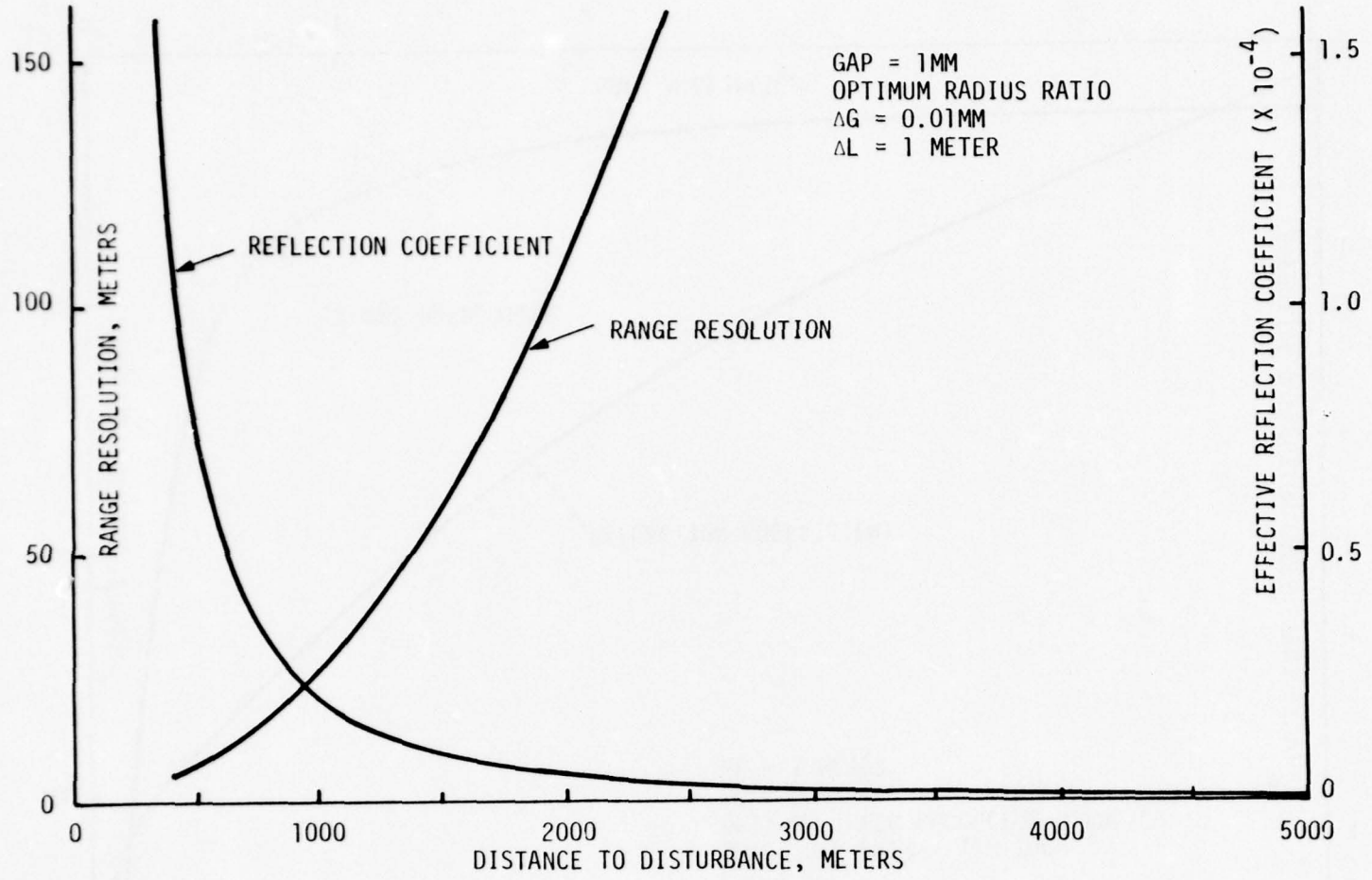

Figure 9. Performance Estimates for 0.19-Inch Transducer

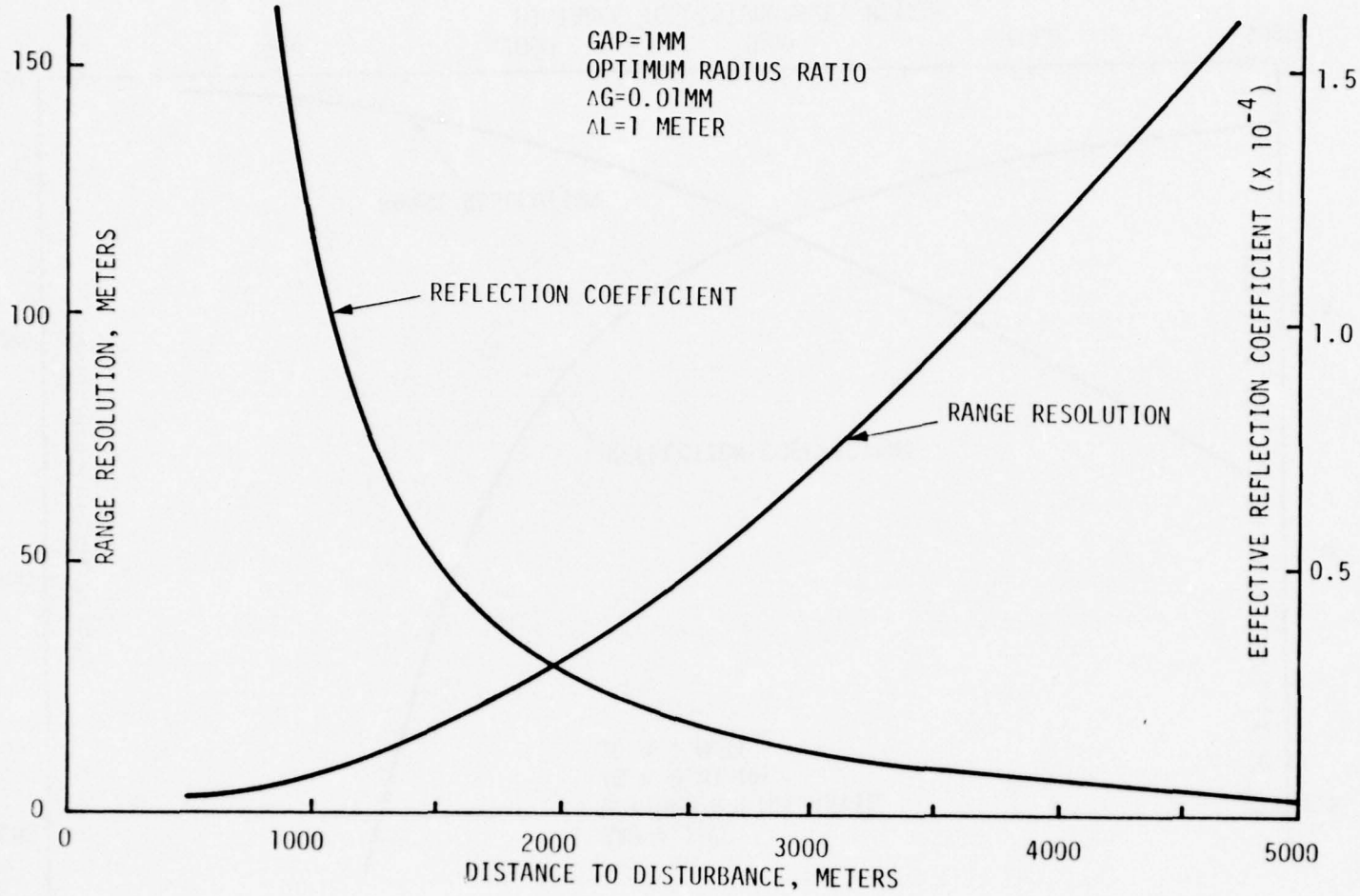

Figure 10. Performance Estimates for 0.5-Inch Transducer

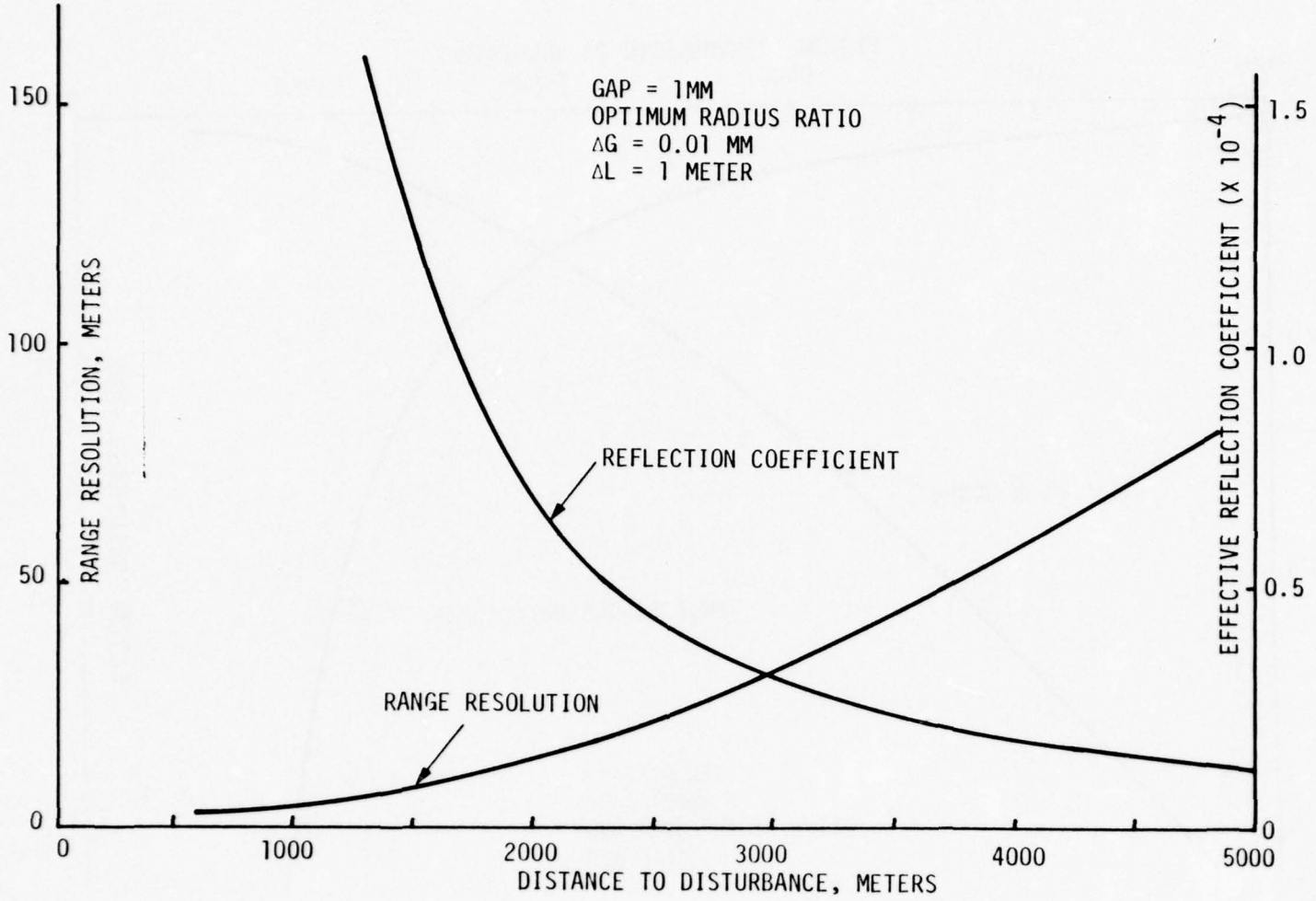

Figure 11. Performance Estimates for 1-Inch Transducer

EFFECT OF NON-UNIFORM TRANSDUCER DIMENSIONS

In all of the above calculations, a uniform conductor spacing was assumed. If the transducer consists of a loosely laid wire in a tube, the spacing will be far from uniform. This will increase the average attenuation and will result in regions of low sensitivity. Furthermore, multiple reflections of the incident step waveform and the return signal from a disturbance will result from the impedance variations along the line length. This causes additional time smearing and reduction in signal amplitude. It also results in a form of crosstalk, because echoes from a disturbance signal will appear in all subsequent range channels.

Because of the complexity of the computations involved, it was not practical to consider the effects of multiple reflections and frequency-dependent losses at the same time. However, we did perform separate computations of multiple reflections on a "lossless" transmission line to show the effect of dimensional variations in the transducer.

Electrical Model of the Loosely-Laid Wire-in-Tube Transducer

To simulate the electrical characteristics of the loosely-laid wire-in-tube sensor, a computer-generated curve was fitted to the time-domain reflectometer measurements on the 10-meter test section of line. We considered deriving a polynomial expression which would pass through selected experimental data points. However, this degree of sophistication was not necessary for the way in which the model was actually used. An adequate model was produced by a linear interpolation method in which the data points

entered were selected to provide a reasonable straight-line fit to the experimental curve. Figure 12 is a computer-generated plot of the reflection-coefficient data. The inset is an oscilloscope camera photograph of the TDR display (with the time axis reversed). Figure 13 is the computed impedance of the line, based upon the reflection-coefficient data. In these figures, the horizontal axis is shown as a time scale. A subsequent measurement was made with the end of the line shorted to provide a definite marker (multiple reflections in the line make it difficult to determine the exact point in Figures 12 and 13 where the 10-meter transducer was terminated in a 75-ohm resistor). It was found that the round-trip propagation time within the 10-meter test section was 80 nanoseconds, corresponding to a velocity factor of 0.833 with respect to free-space propagation. To relate the time scales of Figures 12 and 13 to a physical distance along the transducer, note that zero distance on the transducer corresponds to t = 5 nanoseconds, and the end of the line corresponds to t = 85 nanoseconds. The initial 5-nanosecond delay represents a short section of flexible 50-ohm line between the TDR and transducer.

Computation Technique for Multiple Reflections

The major problem of generating a model for the lossless non-uniform wire transducer is to develop a mathematical technique for incorporating multiple impedance variations while reducing the associated bookkeeping tasks. From the experimental data on the test section of transducer it is seen that impedance variations occur on a spatial scale of less than one meter. Analysis of a line hundreds of meters long involves hundreds or thousands of discontinuities. This can be a staggering bookkeeping problem if the mathematical method is poorly chosen. Memory limitations of the computer further compound the problem.

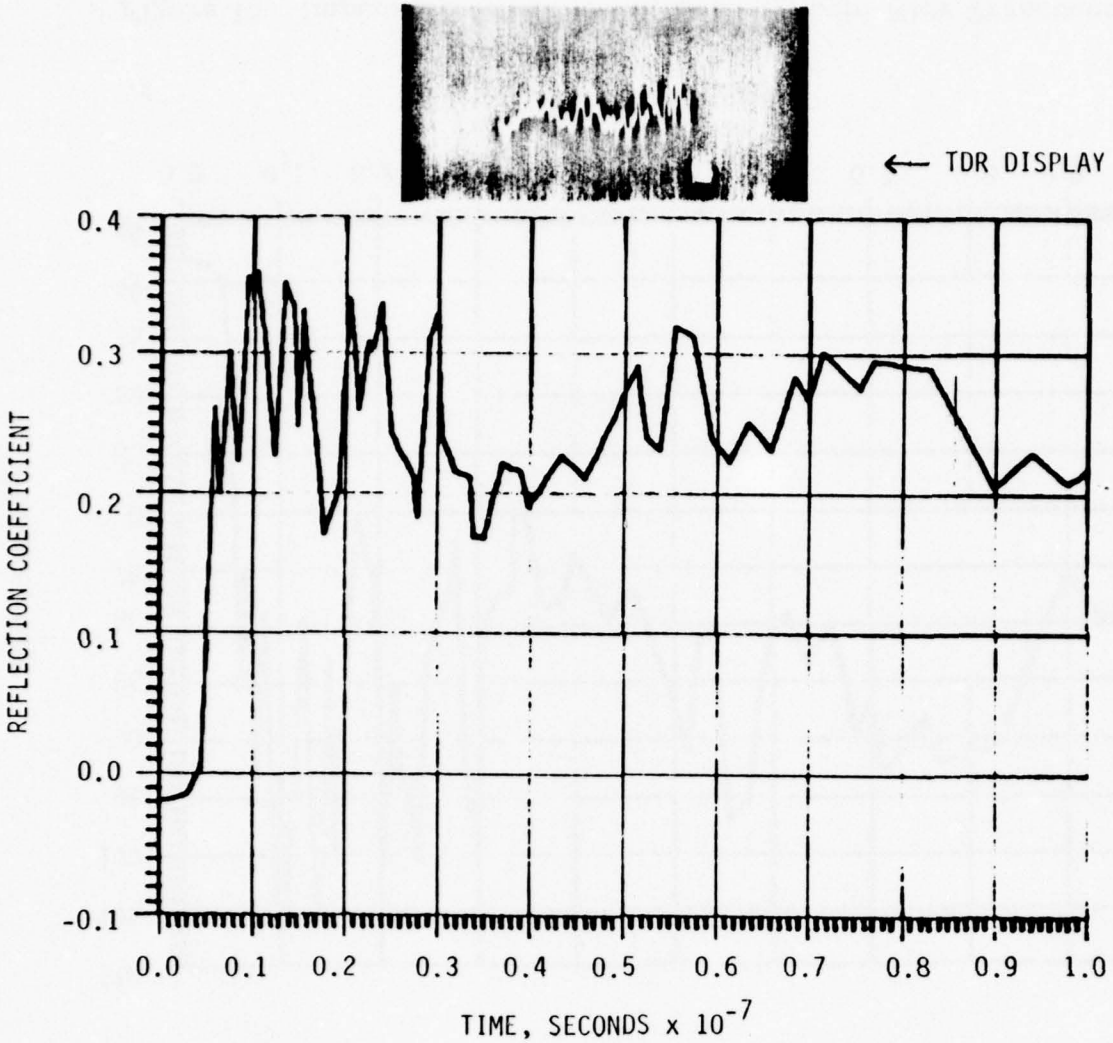

Figure 12. Computer Fit to Experimental Reflection-Coefficient Data

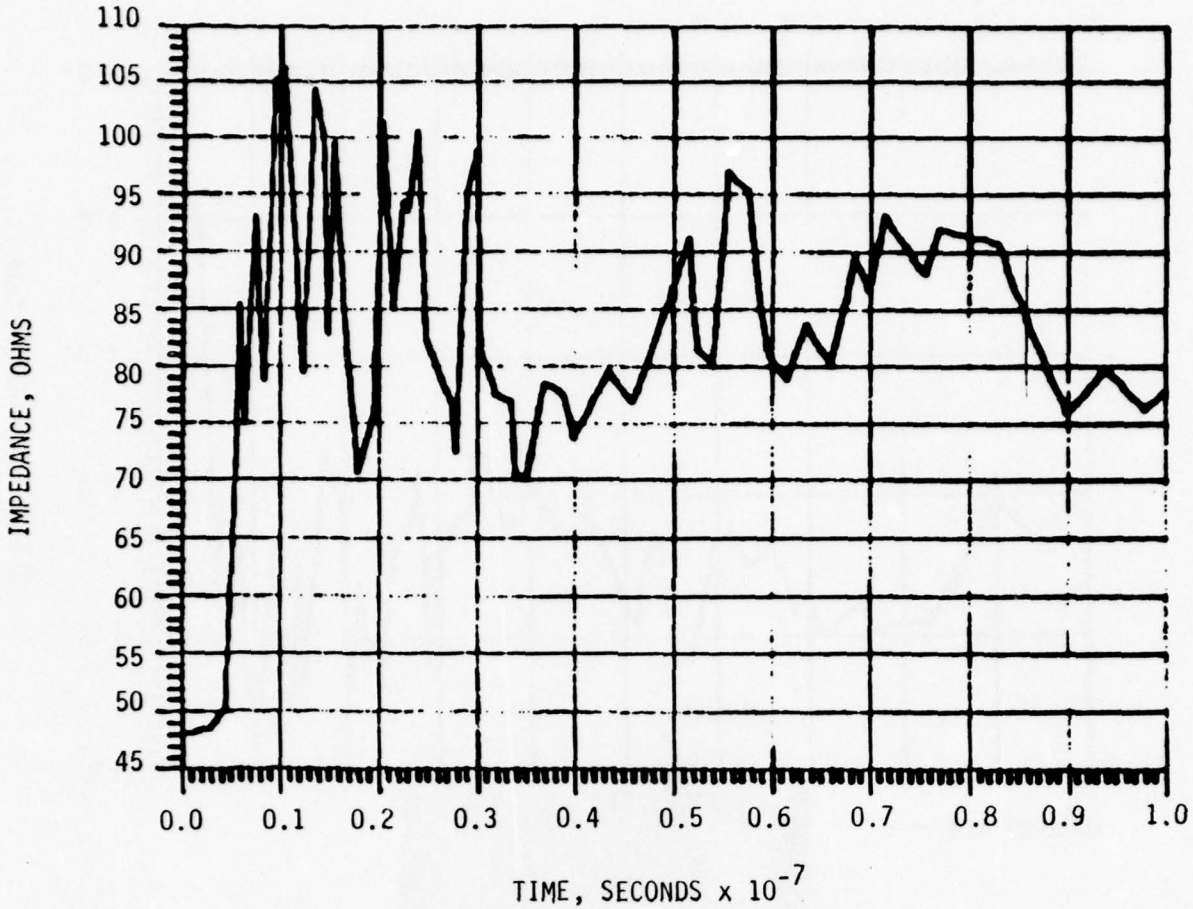

Figure 13. Impedance Variations of Loosely-Laid Wire Transducer

By treating the non-uniform line as a series of short line segments with equal lengths, the time history of the propagated and reflected wave can be kept track of by using a method proposed by Bewley (Reference 3). His method is graphically represented in Figure 14. Each transmission line junction or impedance mismatch can be expressed as a voltage and current level at that junction. The equations for the voltage and current levels for a given junction K are

$$I_K = \frac{V_{k-1} - V_{k+1} - Z_{k-1} I_{k-1} + Z_k I_{k+1}}{Z_k + Z_{k-1}}$$

and

$$V_k = V_{k-1} + Z_{k-1} I_{k-1} - Z_{k-1} I_k$$

The above equations hold for all junctions other than the special cases at the generator and load ends.

The equations for the junction between the generator and first line element are

$$V_1 = \frac{R_g}{R_g + Z_1} [V_{k+1} - Z_1 I_2] + \frac{V_s Z_1}{R_g + Z_1}$$

and

$$I_1 = \frac{V_s - V_1}{R_g}$$

where

R_g = impedance of the generator

V_s = source voltage

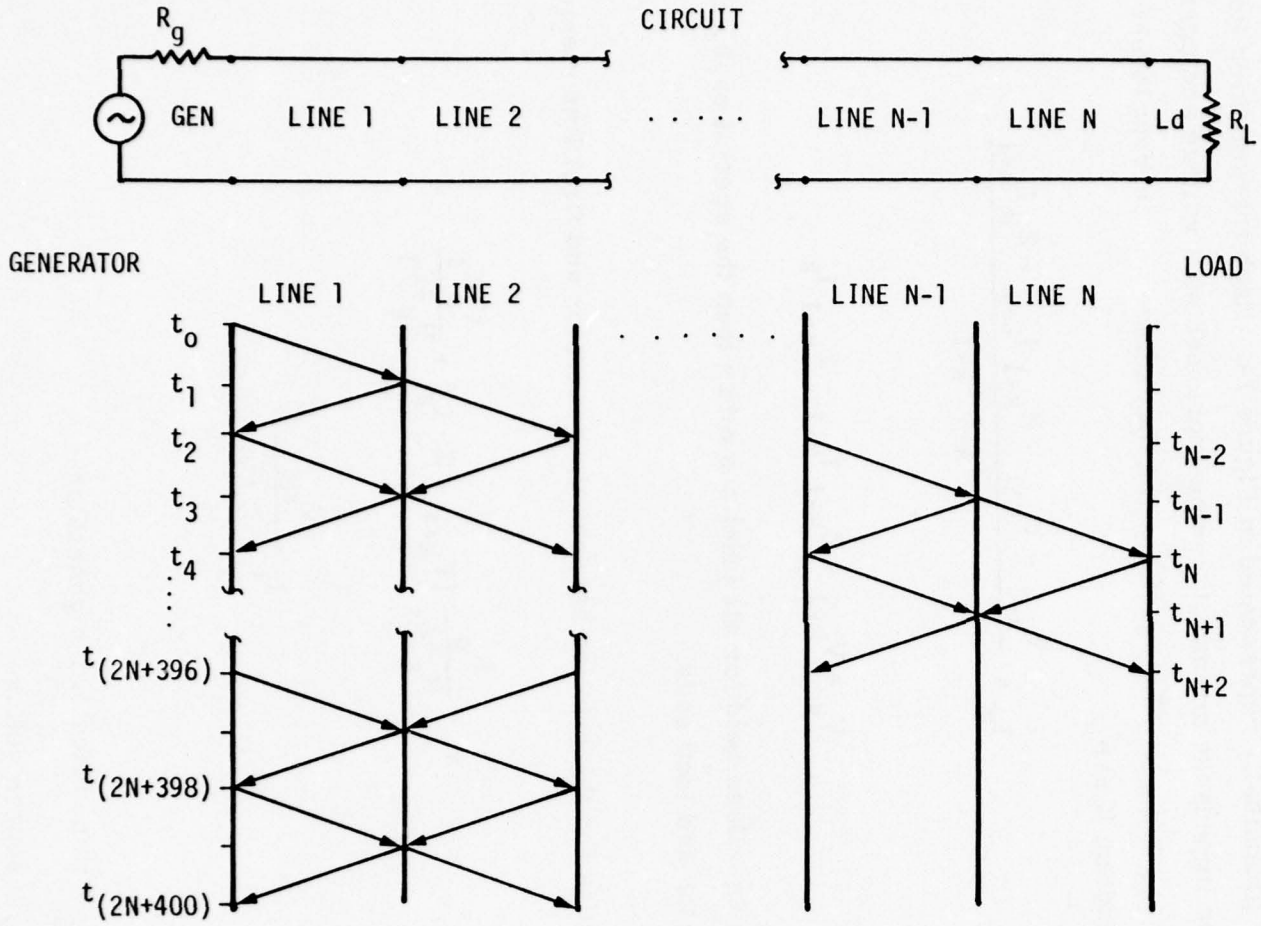

Figure 14. Bewley Diagram

The junction between the last line element and the load is characterized as

$$V_L = \frac{R_1(V_N + Z_N I_N)}{R_L + Z_N}$$

and

$$I_L = \frac{V_L}{R_L}$$

where

R_L = load impedance

N = the last line element

Examination of the previously mentioned equations shows the dependence of a given junction K on its left and right junctions, K-1 and K+1 respectively. With this model, keeping a time history of the voltages at any given line junction is possible, although we are only concerned with the history at the generator end.

Two more observations can be made from the Bewley diagram. We assume that the line segments are of equal length, and that the velocity of propagation of the traveling wave in each line section is constant. All reflections occur at multiples of the time it takes to traverse one line segment. We therefore need to compute reflections only at these discrete intervals. The second observation is that a traveling wave does not reach junction K until time k. Hence, no information from that junction is received at the generator until time 2k.

Due to our computer limitations, incorporation of the math model into a computer package was a four step process. The four steps were:

1) Generate the line impedances

2) Plot the line impedances versus line element

3) Calculate the history at the generator end

4) Plot the history versus time

Originally, the line impedances were taken from the experimental time-domain reflectometer data on a 10-meter transducer section. The 10-meter impedance data was repeated as often as necessary to represent the length of line that was being simulated. This scheme turned out to give anomalous reflections due to the false periodicity induced by using the 10-meter TDR data. In actuality, the center conductor of the sensor would be randomly lying within the outer conductor. Therefore, the line impedances should be generated in a random manner to avoid introducing any false periodicity. To avoid generating a line that would have large changes in impedances from one segment to the next, a filter was devised. This filter consisted of averaging four consecutive random numbers. This eliminates large fluctuations in impedance values between adjacent line elements.

Generation of the N random line impedances was accomplished in the following manner. The parameters of the transducer, outer conductor radius, inner conductor radius, and inner conductor placement with respect to outer conductor were entered. Filtered random numbers were drawn to determine the plus and minus offset of the inner conductor with respect to its nominal placement within the outer conductor. The impedance of each line segment was then calculated from the equation for an eccentric coaxial transmission line. Once the N line impedances were generated, they were written onto magnetic tape for later use.

The previously described algorithm for finding the time history at the generator end was implemented in the following manner. The source voltage, generator impedance, load impedance, and line impedances which were previously calculated and stored on magnetic tape were entered into the simulation program. It should be noted from the Bewley diagram, Figure 14, that for each time interval it is necessary to calculate only voltages and currents at every other line junction. Hence, at t_o the initial voltage wave is calculated. At odd numbered times, the junctions between Elements 1 and 2, 3 and 4, etc. are updated, and at even times the junctions between Elements 2 and 3, 4 and 5, etc., are updated. The junctions at the generator and load ends are updated during even time intervals.

For every time interval, the voltage level at the generator and the corresponding time interval are stored in a buffer. After 200 time intervals have been calculated, the buffer is then written on tape. The process is then repeated for the next 200 time intervals until the maximum time limit is reached. The present time stop is set to $2N + 400$ time intervals. This allows the wave sufficient time to travel the length of line and back to the generator.

Since the algorithm structure requires N line impedances, voltages and currents to be retained in memory, there must be some upper limit for the value of N. This limit will vary from machine to machine, so in our case, using a SDS 9300 computer, the value for N is 3200. Without restructuring the model or using peripheral devices, such as tape drives which slow down the execution of the program, the maximum number of line elements that can be handled is 3200.

In addition to the two programs that were just described, the line generator and the line simulator, there are two more programs which generate a plot of the previously calculated data.

The first routine displays the generated line impedances, stored on tape, versus the corresponding line element. The second program is slightly more complicated. This routine has two options available to the user. The first option is to read a tape containing the generator history information and the corresponding time interval, then graphically display that information in the form of generator history versus time. The second option involves reading two tapes containing two different sets of data, comparing the sets, and then displaying them as generator history versus time. The two sets of data are the results of two line simulation runs for the same length transducer where one run has one or more perturbations introduced to the line for simulation of intruders. The results of one run are subtracted from the other, thus allowing us to observe the time-varying signals from simulated intrusions.

Wire-in-Tube Transducer Simulation Results

Initial computations were made on a simplified model of the transmission line in which the 10-meter section was broken into 20 segments. The impedance of each segment was taken as the average value from the experimental data over the corresponding interval. A short-circuit termination was simulated to provide information on the fall time. It was hoped that this model would be adequate, because the solution of a 1-kilometer line could then be accomplished with a 2000 element calculation which is easily

within the capabilities of our computing facility. However, the numerical computation of the reflected voltage for this model showed a fall time of zero for the reflection from the short-circuit termination.

Subsequent computations were based upon a 200-element approximation to the experimentally-determined transducer impedance. The computed response shown in Figure 15 is plotted on a normalized time scale, where each time unit represents the time required for the incident wave to traverse one line segment. Thus it takes 400 time units for the step-function voltage to travel down the line to the shorted end and for the reflections to return to the input end of the 200-segment line.

To relate this to the TDR data shown in Figure 12, each time unit here corresponds to 0.25 nanoseconds.

The computed response for this model shows that the fall time at t = 400 is still virtually instantaneous. In other respects, the response appears to be correct for the impedance model used.

Neither the resistance losses nor multiple reflections, as computed by our numerical technique, could explain the observed fall time. Since the computation technique appeared to be valid in other respects, and the 200 element approximation was very close to the measured line-impedance variations in the test transducer, we suspected that the actual measured impedances were incorrect. We know that the inner conductor insulation must at some points be touching the outer tube, and at other points the inner conductor may lie nearly along the axis of the outer cylinder. If the TDR had infinite resolution we would expect the impedance to go from a maximum of about 140 ohms

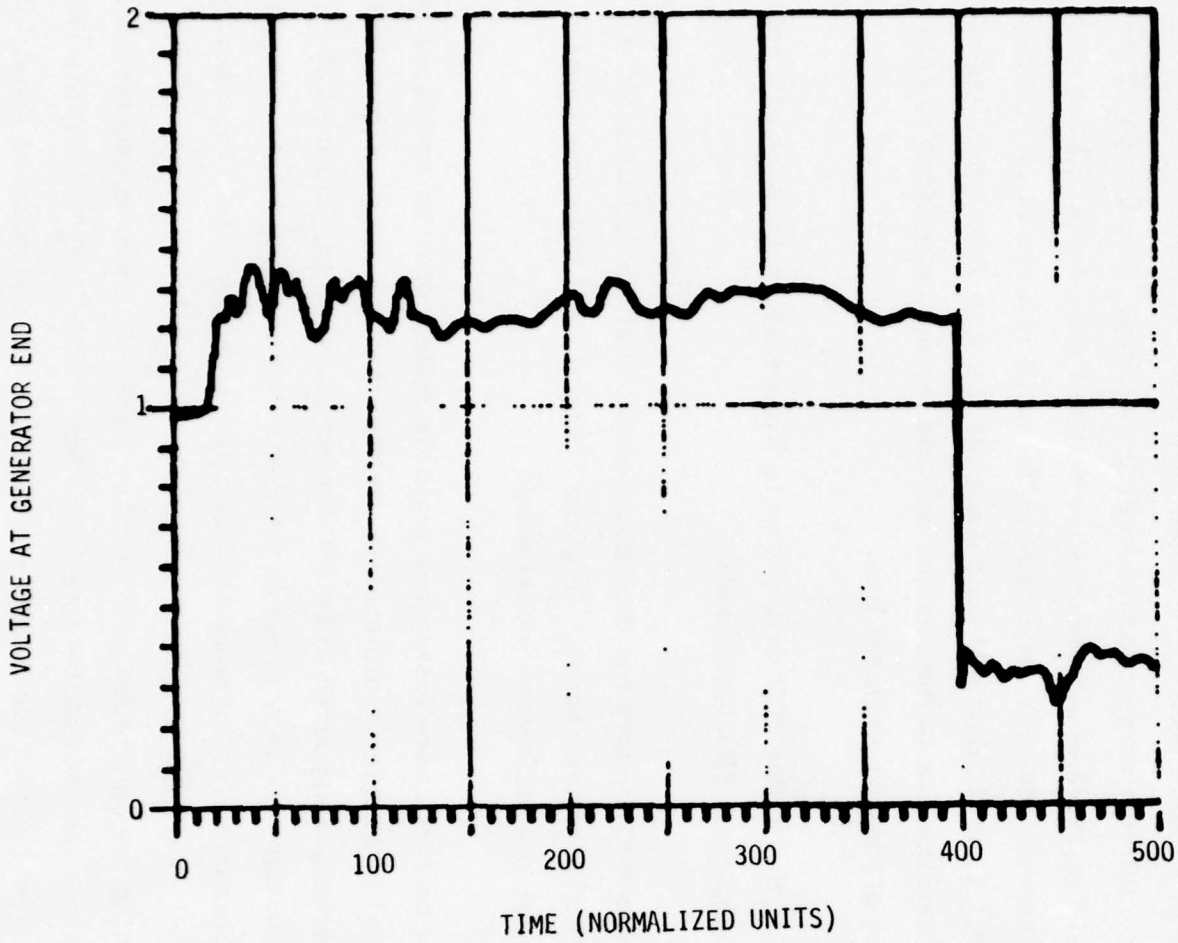

Figure 15. Simulated Response Using 200-Element Approximation to Experimentally Determined Impedance

to a minimum of 50 or 60 ohms. Since the impedances derived from the TDR measurements only ranged from about 70 to 105 ohms, there is indeed a strong reason to suspect that TDR resolution caused some "smoothing" of the measured line characteristics. We therefore changed the model by doubling the peak-to-peak variations about the 85-ohm nominal impedance value. The computed response of this line exhibited a finite fall time, but it still took much less than three nanoseconds to reach 50 percent of the final value.

Taking a further critical look at the measured impedance data, we noted that the far end of the transducer seemed to have fewer and less extreme impedance variations than the first few meters of line. There is no reason why this should be true; in fact the inner conductor must touch the wall at least every meter or so along the entire line because it was not under tension. Evidently the waveform degradation of the line itself was introducing additional smoothing after the first few meters of line.

To correct for this effect, we simply took the impedance data from the first few meters of transducer and repeated it periodically until we had "extended" this new model to 200 segments. Finally, we doubled the impedance variations to produce the model shown in Figure 16; the computed response of this line is given in Figure 17. Now the 50 percent fall time lies between 10 and 20 units (2.5 to 5 nanoseconds) and the reflected waveform shows the same smoothing effect on the last half of the line as we see in the TDR data. This final model is probably a fairly accurate simulation of the real impedance variations in a loosely-laid wire transducer, and the waveform degradation in such a transducer is predicted by the numerical computation.

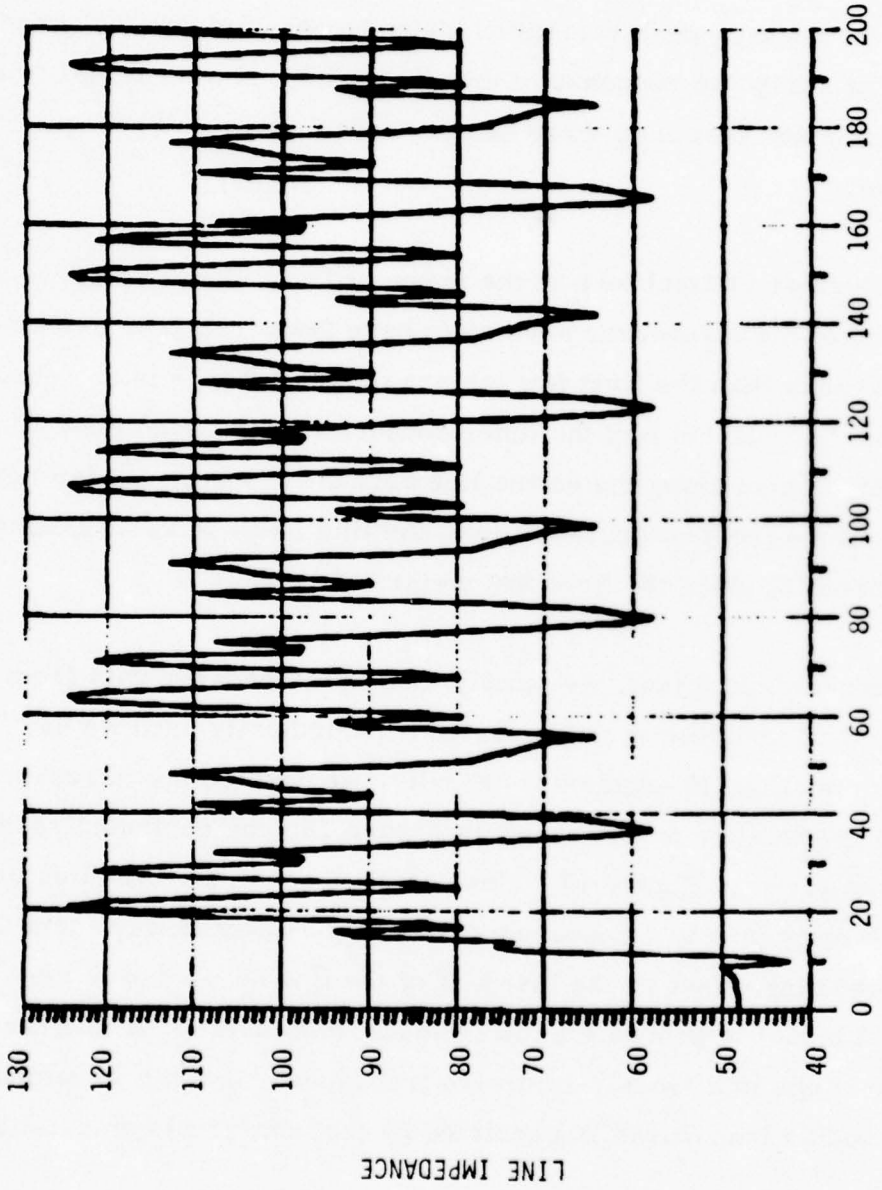

Figure 16. Final 10-meter Loosely-Laid Wire Transducer Model

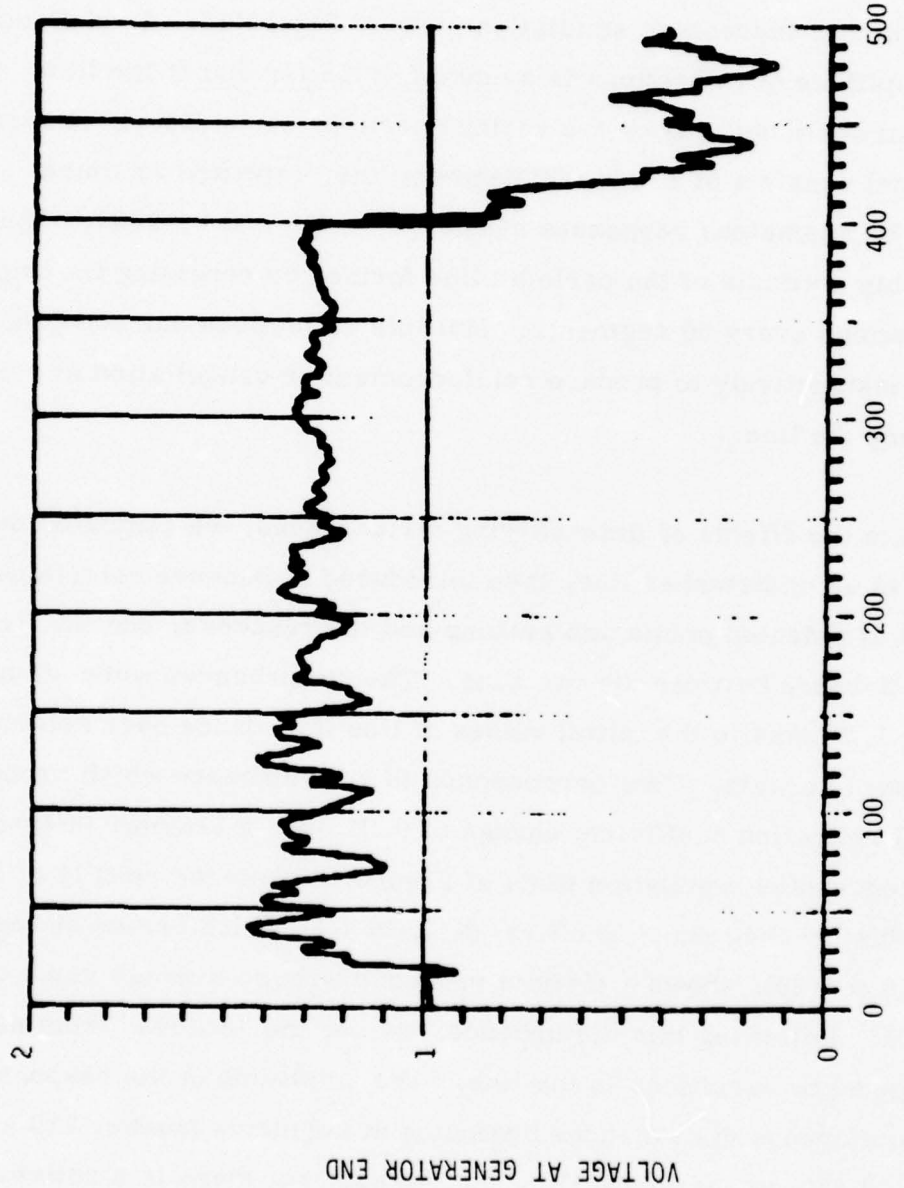

Figure 17. Response of Final Model

We extended the above model to 1600 elements and calculated its step response. When the generator impedance is matched to the average transducer impedance of about 85 ohms, and the transducer is terminated with an 85 ohm resistor, the simulated "TDR picture" of a 1600-element line is shown in the six successive simulation plots of Figure 18. A substantial loss in amplitude of reflections is evident for the far end of the line. (Note the vertical scale changes on the various portions of the line.) The transducer model consists of a basic 50 segment line, repeated 32 times. There appear to be anomalous responses at about t = 1400 and t = 2800. These are probably artifacts of the periodic line formed by repeating the impedance variations every 50 segments. Multiple reflections can add constructively or destructively to produce reinforcement or cancellation at certain points along the line.

To simulate the effects of time-varying disturbances, we computed the response of an undisturbed line, then introduced impedance variations in the model at selected points and recomputed the response, and finally plotted the difference between the two runs. The disturbances were simulated by adding 1.7 ohms to the initial values of line impedance over selected 20-segment intervals. This corresponds to a disturbance which produces a nominal reflection coefficient change of 0.01 over a 1-meter interval. The six successive simulation plots of Figure 19 show the results of a multiple-disturbance run. The first disturbance, which begins at segment number 10 (t = 20), shows a distinct response with an average value of about 0.01. Following this disturbance, we see the "echoes" from subsequent impedance variations in the line. The amplitude of the response from other simultaneous disturbances beginning at segments number 110 and 310 (t = 220 and 620) is not appreciably diminished, but there is a noticeable broadening of the time response.

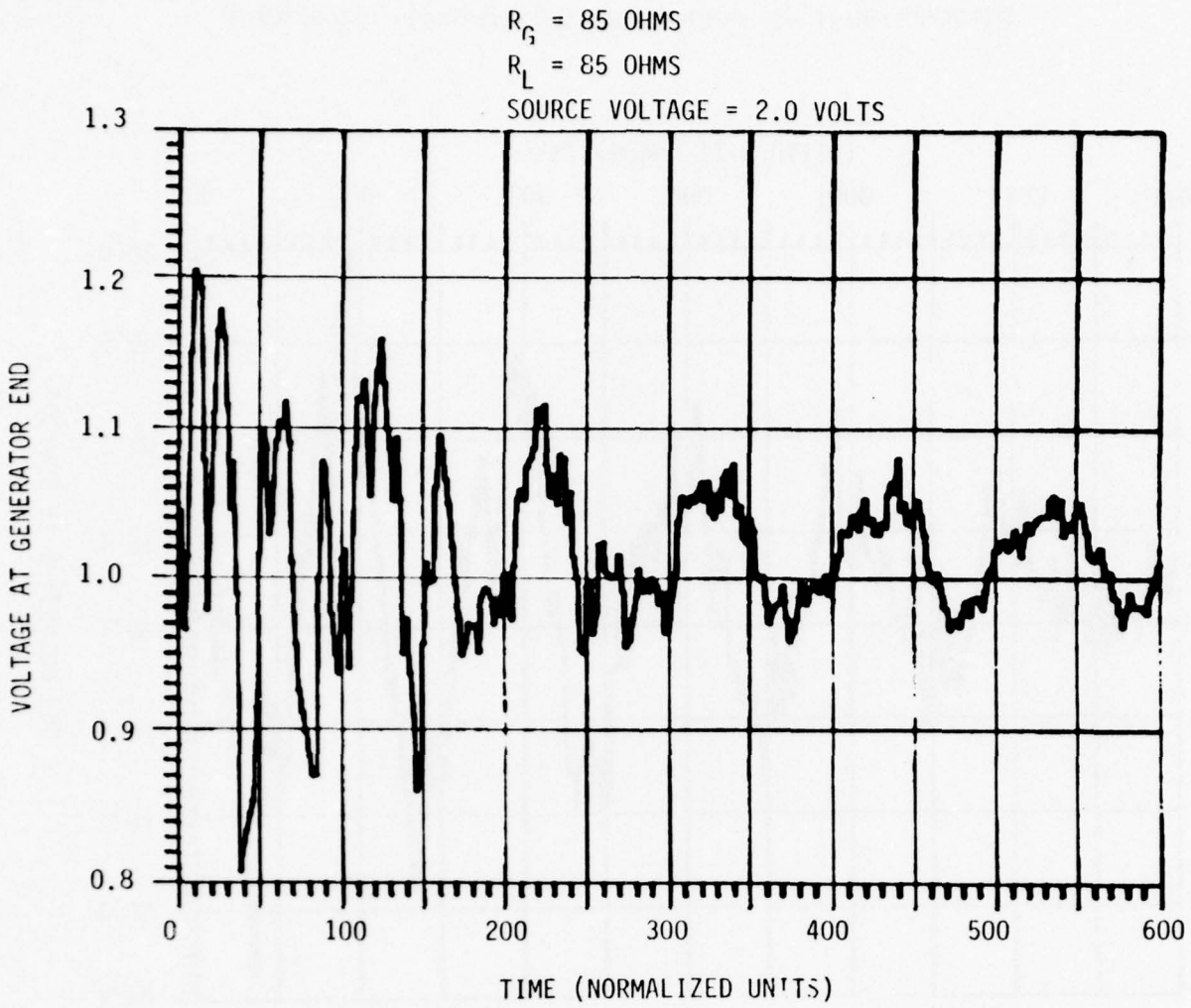

Figure 18. Simulated TDR Picture for 1600-Segment Loosely-Laid Wire Transducer

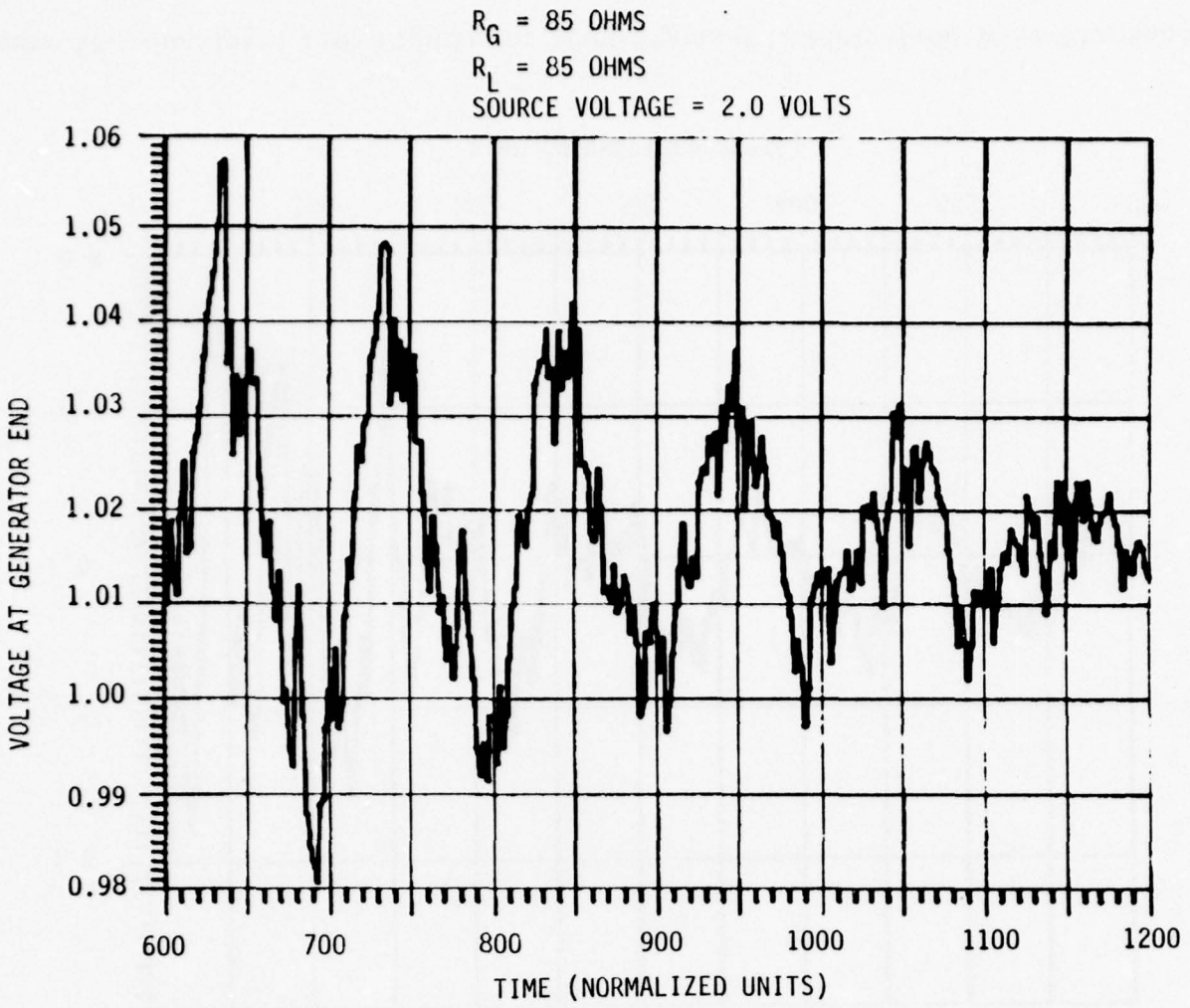

Figure 18. Simulated TDR Picture for 1600-Segment Loosely-Laid Wire Transducer (continued)

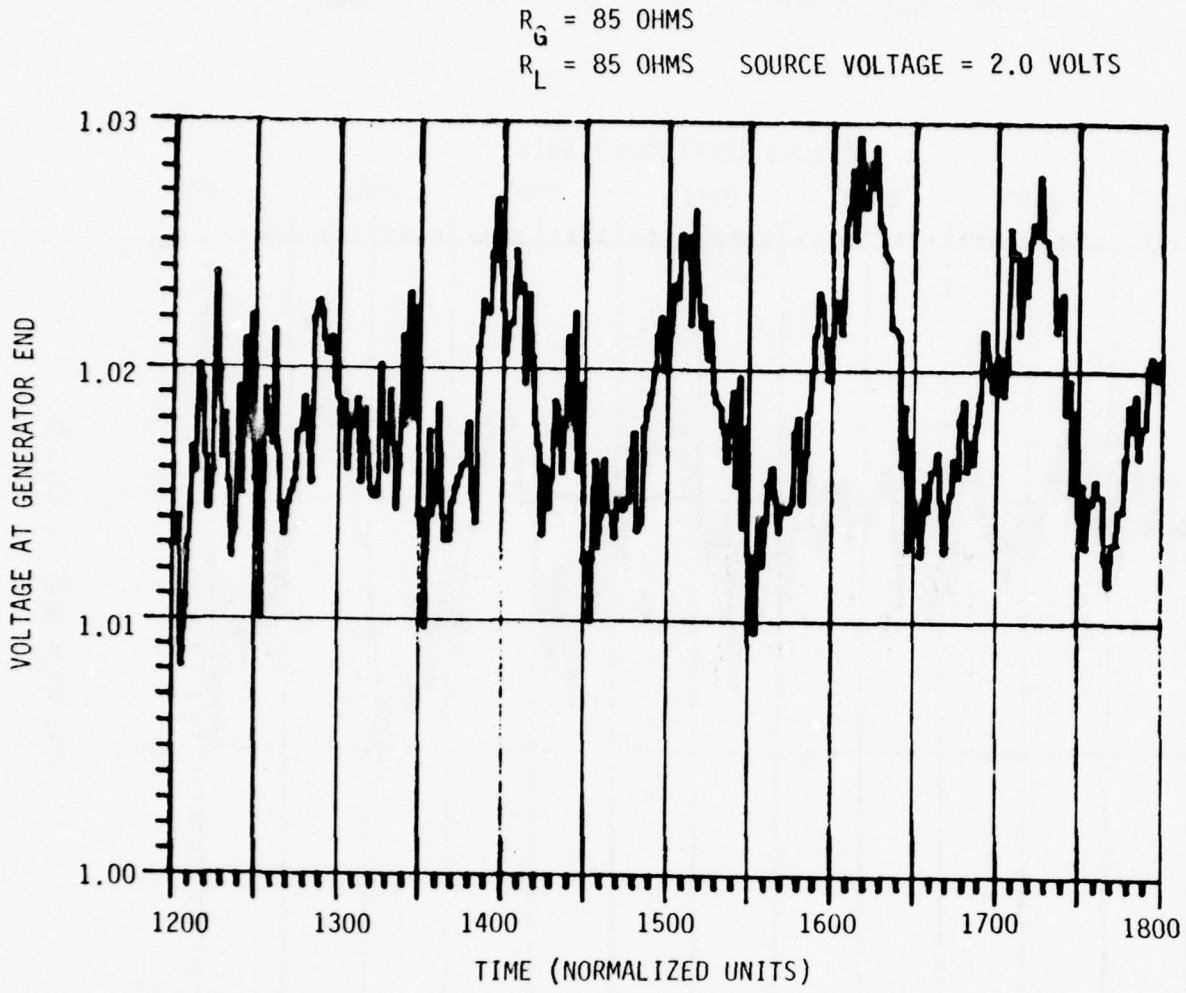

Figure 18. Simulated TDR Picture for 1600-Segment Loosely-Laid Wire Transducer (continued)

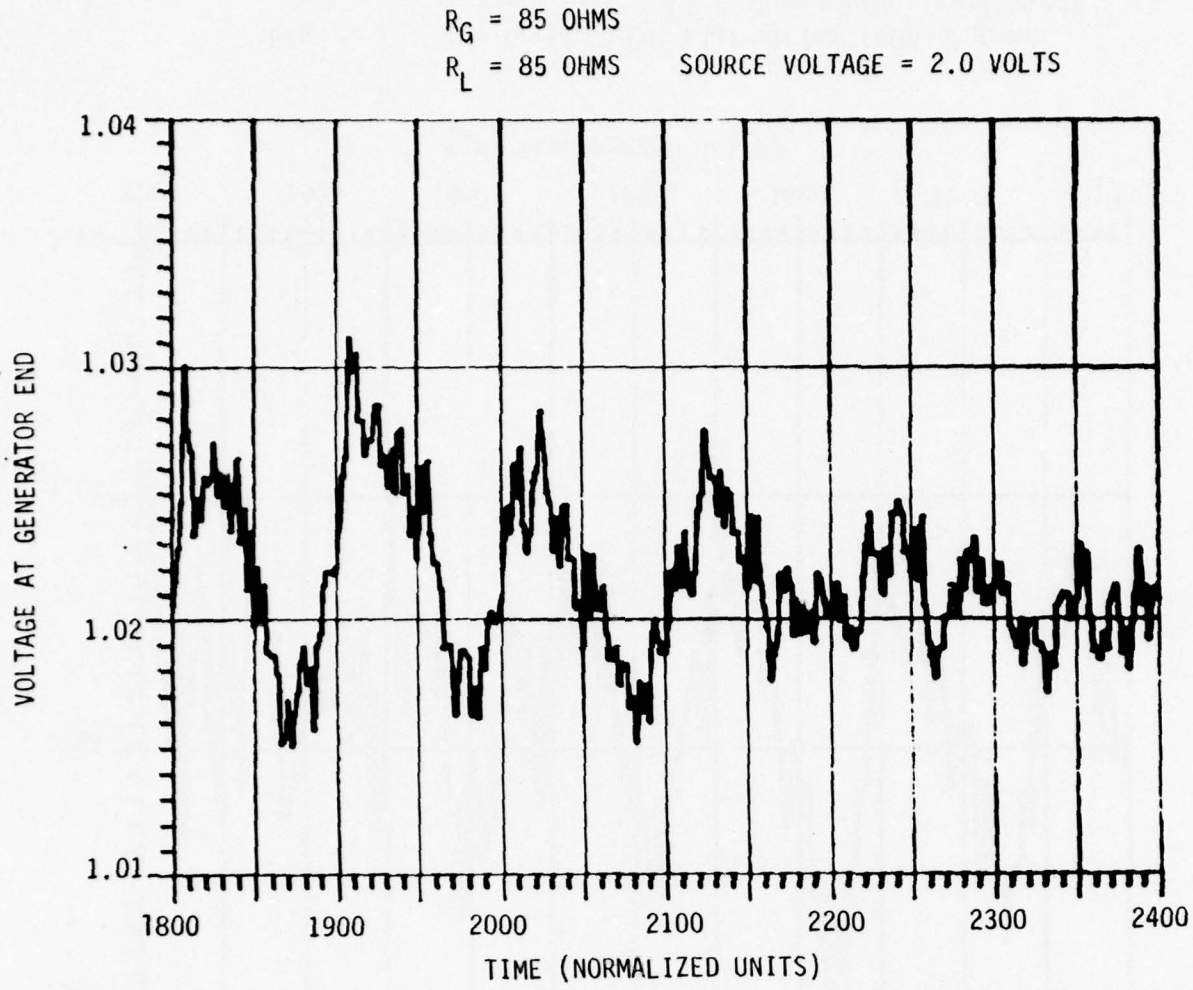

Figure 18. Simulated TDR Picture for 1600-Segment Loosely-Laid Wire Transducer (continued)

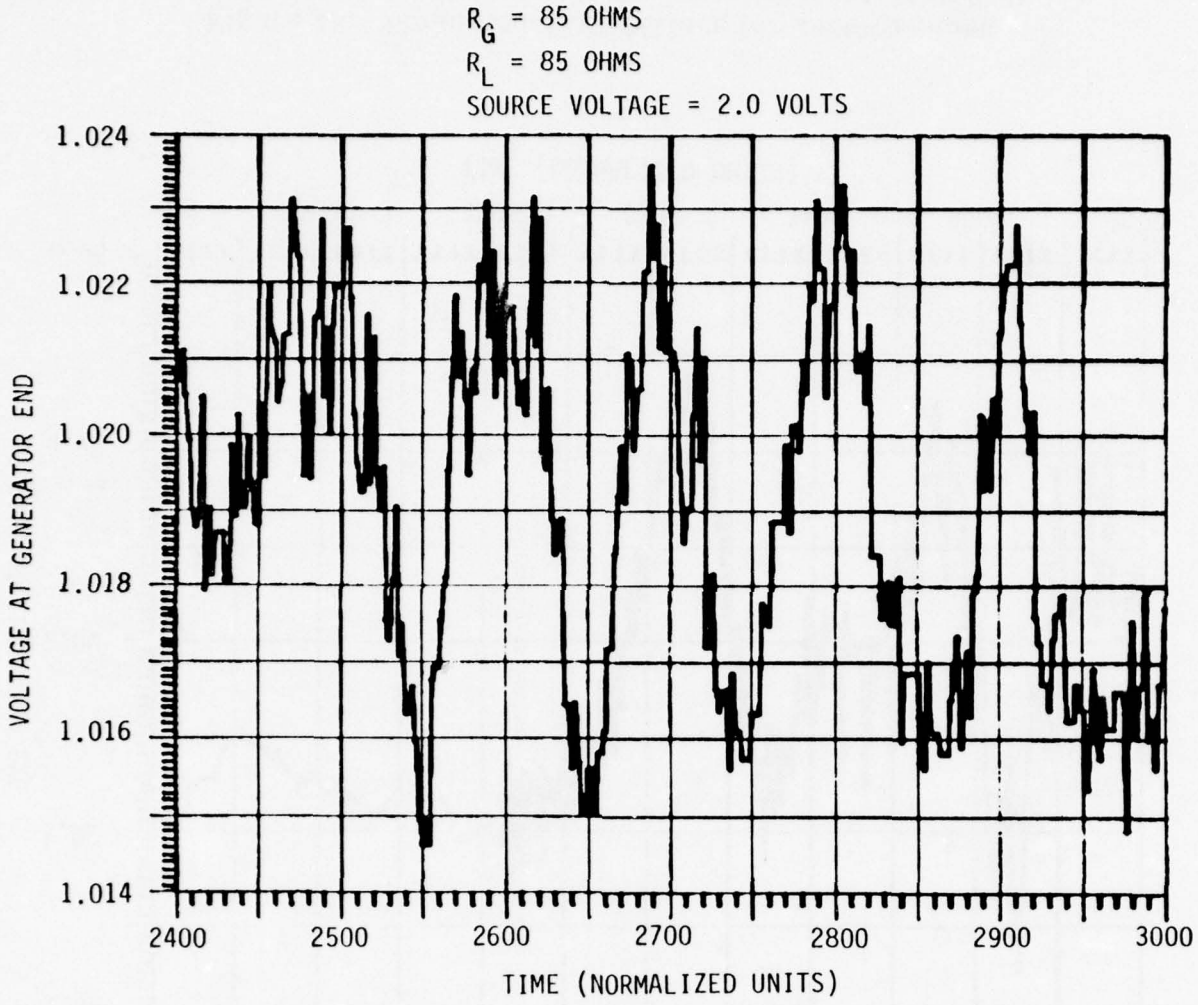

Figure 18. Simulated TDR Picture for 1600-Segment Loosely-Laid Wire Transducer (continued)

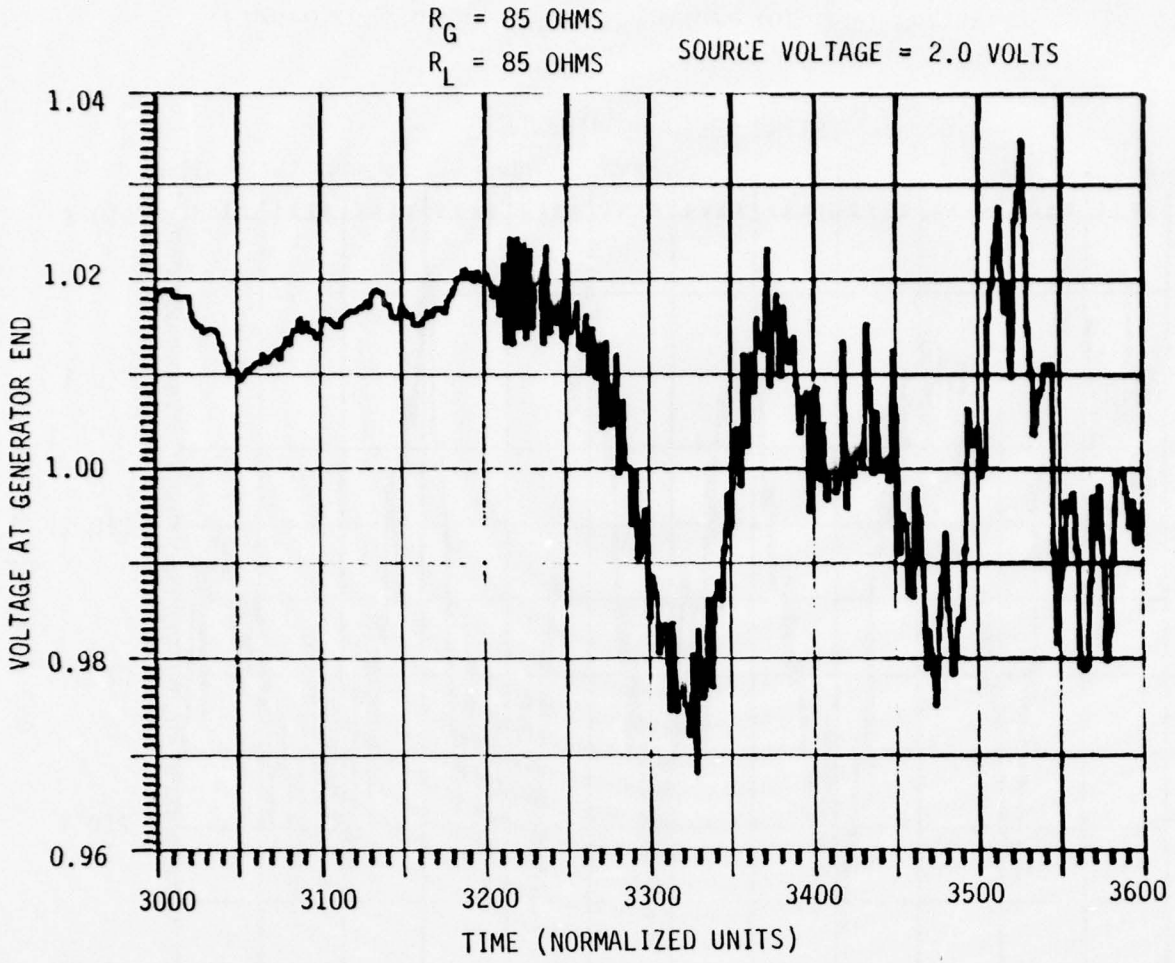

Figure 18. Simulated TDR Picture for 1600-Segment Loosely-Laid Wire Transducer (concluded)

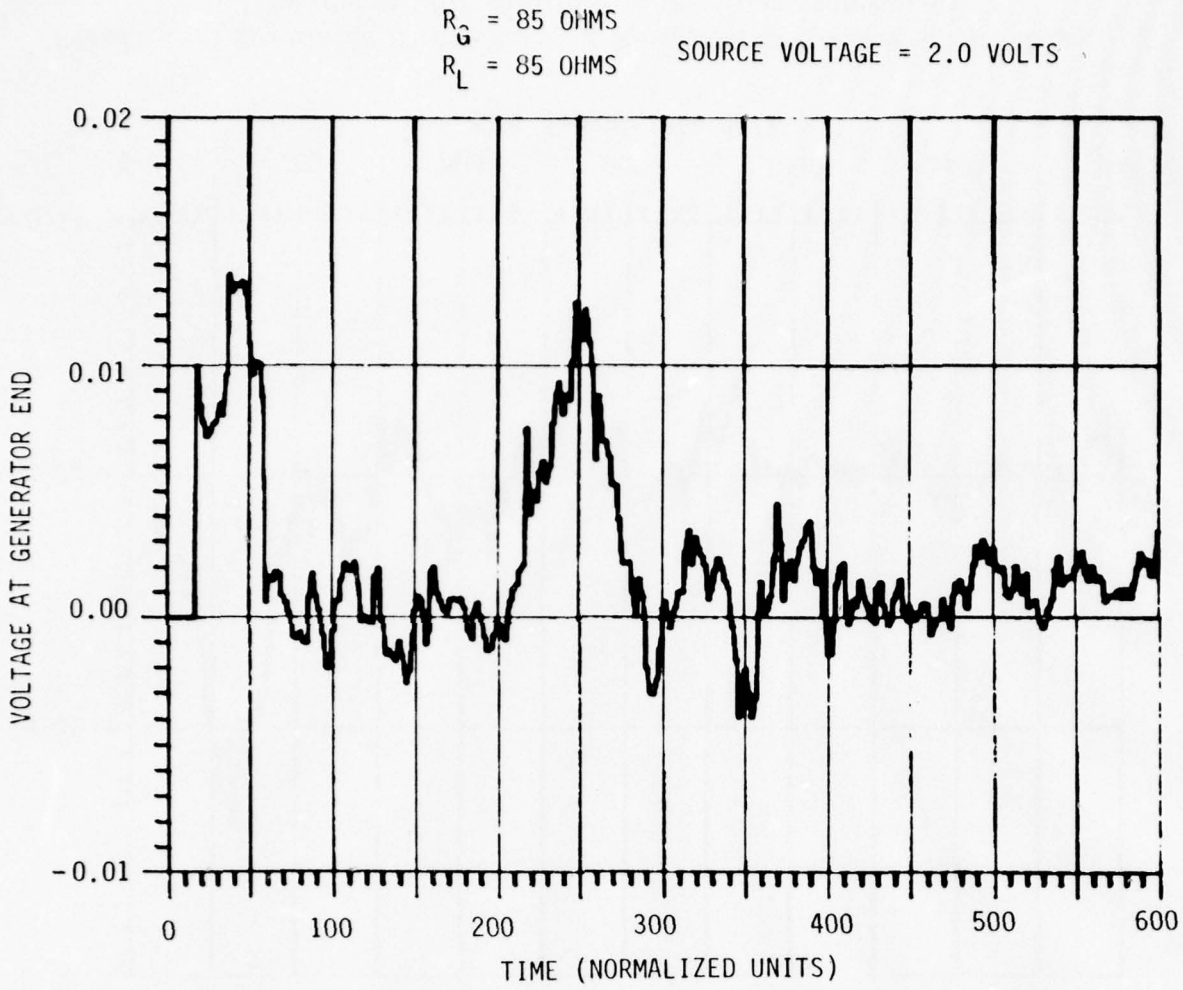

Figure 19. Simulated Time-Varying Response of Loosely-Laid Wire Transducer with Multiple Reflections

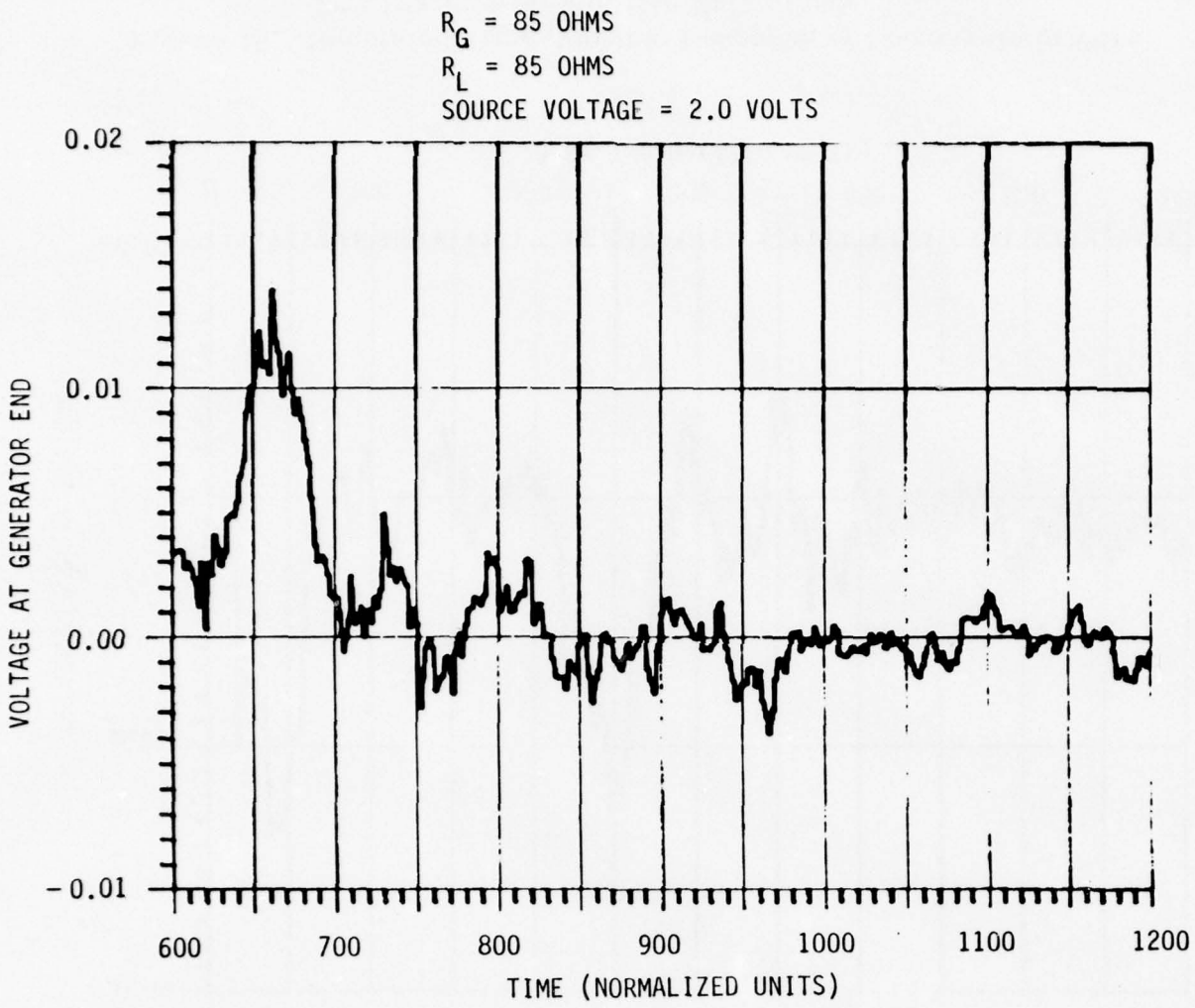

Figure 19. Simulated Time-Varying Response of Loosely-Laid Wire Transducer with Multiple Reflections (continued)

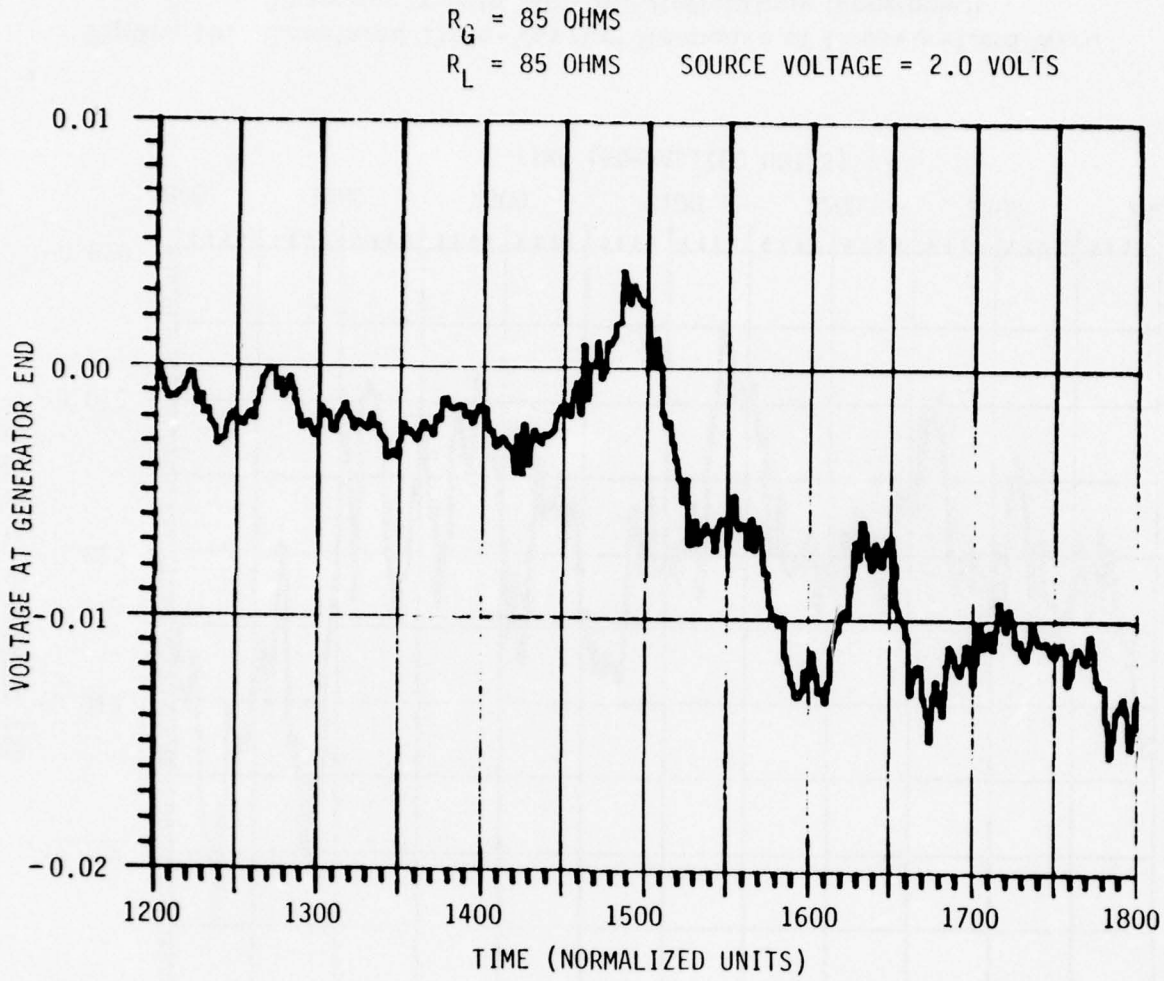

Figure 19. Simulated Time-Varying Response of Loosely-Laid Wire Transducer with Multiple Reflections (continued)

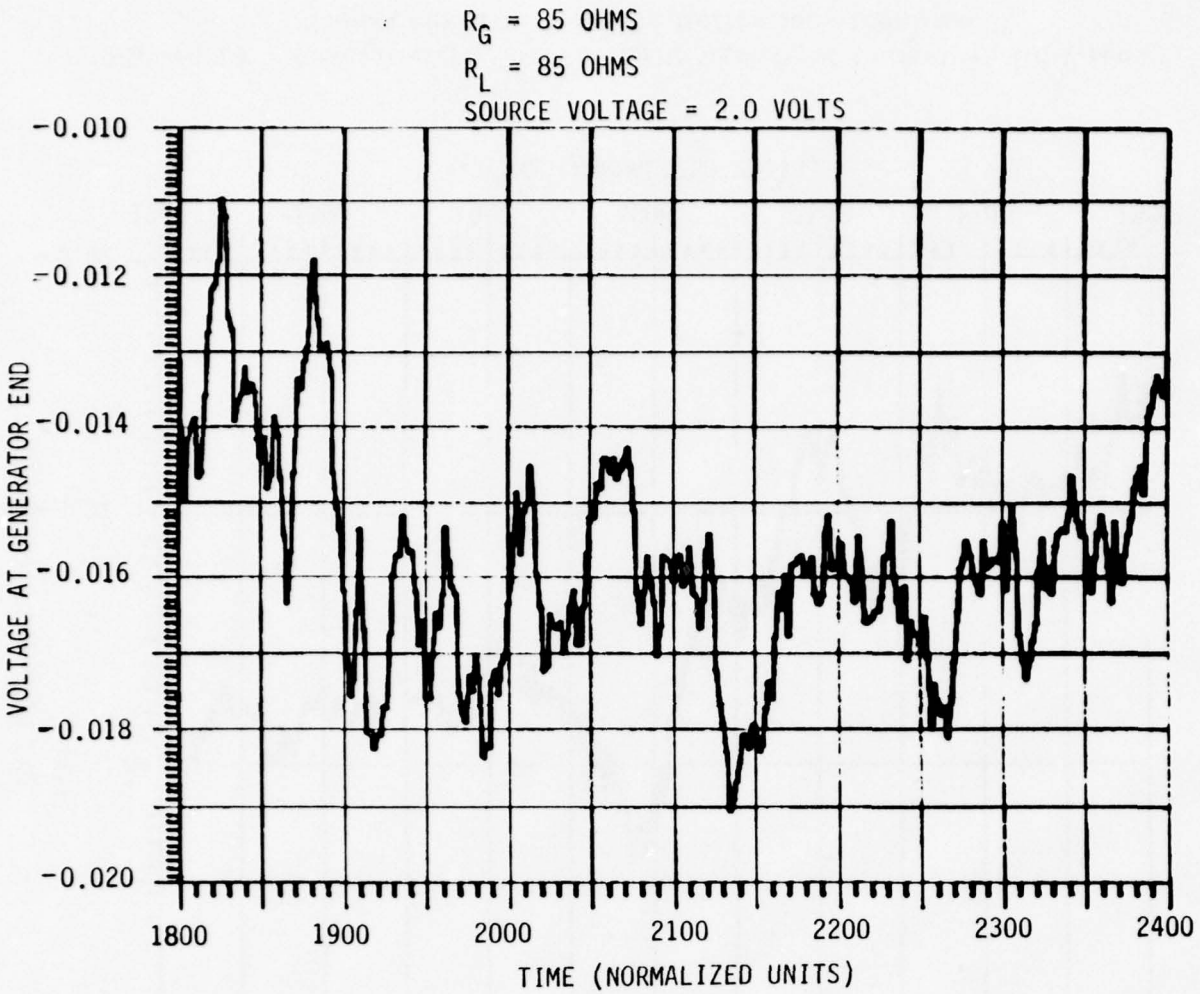

Figure 19. Simulated Time-Varying Response of Loosely-Laid Wire Transducer with Multiple Reflections (continued)

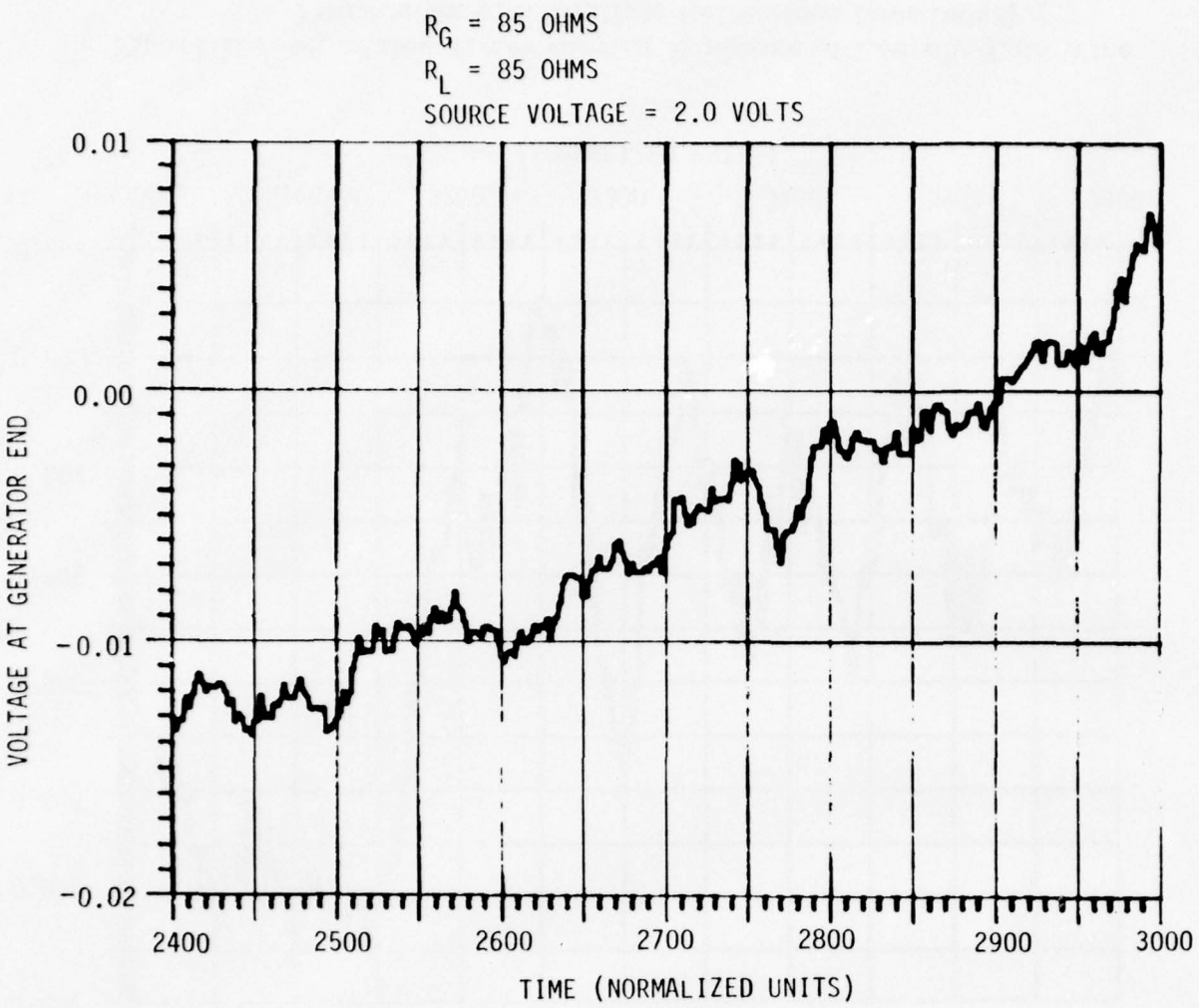

Figure 19. Simulated Time-Varying Response of Loosely-Laid Wire Transducer with Multiple Reflections (continued)

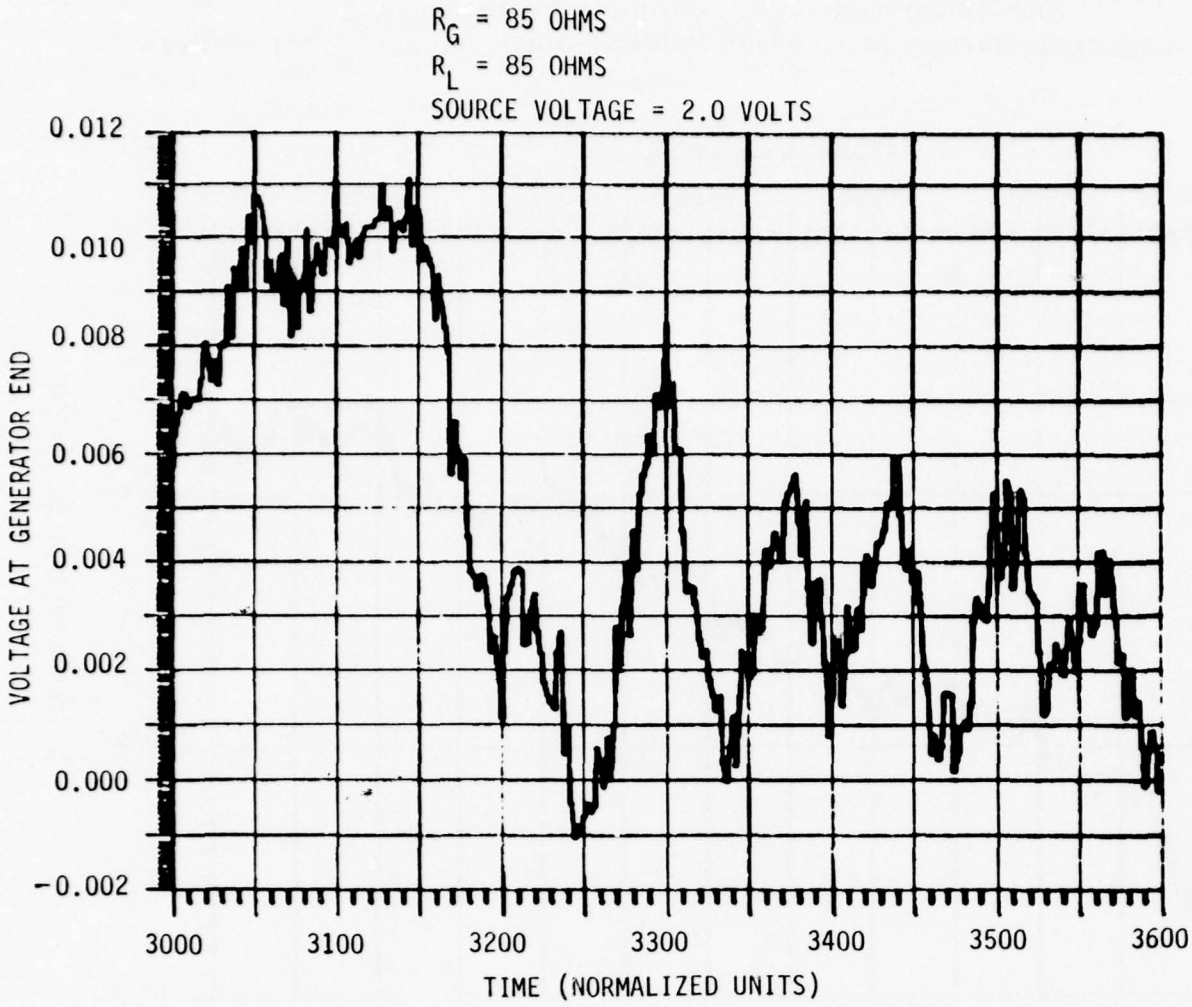

Figure 19. Simulated Time-Varying Response of Loosely-Laid Wire Transducer with Multiple Reflections (concluded)

Again, the line shows anomalous behavior at about t = 1400. The calculated response shows time-varying reflections from undisturbed portions of the line which are comparable in magnitude to the signals from actual disturbances. The last disturbance at segment number 1510 (t = 3020) is difficult to discern among the echoes from the other disturbances.

In an attempt to remove the anomalous behavior at t = 1400 and t = 2800, we tried changing the model to increase the fundamental length from 50 to 200 segments. This was done by using a time inversion of the first 50 segments between 50 and 100, an inversion about the average value of impedance for segments 100 through 150, and another time inversion to generate segments 150-200. Although the resulting response was altered, there were still regions of anomalous reflections.

We did not make further refinements of the loosely-laid, enclosed-wire transducer model because this transducer appears far from optimum for pulsed-mode operation. The simulated 1600-element transducer represents a physical length of 80 meters. Even at this length, attenuation and crosstalk problems are severe. Without a highly sophisticated processor, the maximum usable length of a loosely-laid wire-in-tube transducer will probably be less than a few hundred meters.

Effect of Random Gap Variations in a 0.5-Inch Optimized Transducer

Further computations of multiple-reflection effects were carried out for a 0.5-inch diameter transducer. The inner conductor diameter was chosen as 0.14 inch and the nominal gap was set at one millimeter. These

dimensions were shown earlier to provide nearly optimum electrical characteristics for a uniform transducer. To avoid the anomalous results obtained with periodic impedance variations, we used a transducer model in which the dimensional variations are completely random. This model was created by using a random-number generator routine in the computer to represent the inner conductor displacement. The inner conductor displacement cannot vary abruptly between its extreme positions in a real transducer. We therefore used a "filtering" process consisting simply of a four-number running average to smooth the random-number generator output.

For the first simulation we used a 1600-element transducer with peak-to-peak fluctuations of about 0.7 millimeters about the 1-millimeter nominal gap. Figure 20 is a plot of the first 300 elements in this transducer model showing the variation in gap.

To simulate the effect of a time-varying disturbance, we first calculated the time history of the voltage at the generator end of the transducer. Then the transducer model was altered by adding 0.01 millimeter to the gap for Elements 100 through 103, and Elements 1500 through 1503. The voltage response was computed again, and the "undisturbed" response then subtracted. When plotted, the result is a time-amplitude history showing, in effect, the outputs of a very large number of processed range channels when two similar time-varying disturbances are present simultaneously.

Figure 21 (two parts) shows portions of the time-amplitude plot for the 1600-element transducer. The round-trip time delay for each transducer element is two time units. We can think of each time unit as a separate time-gated range channel, with the corresponding range increment equal

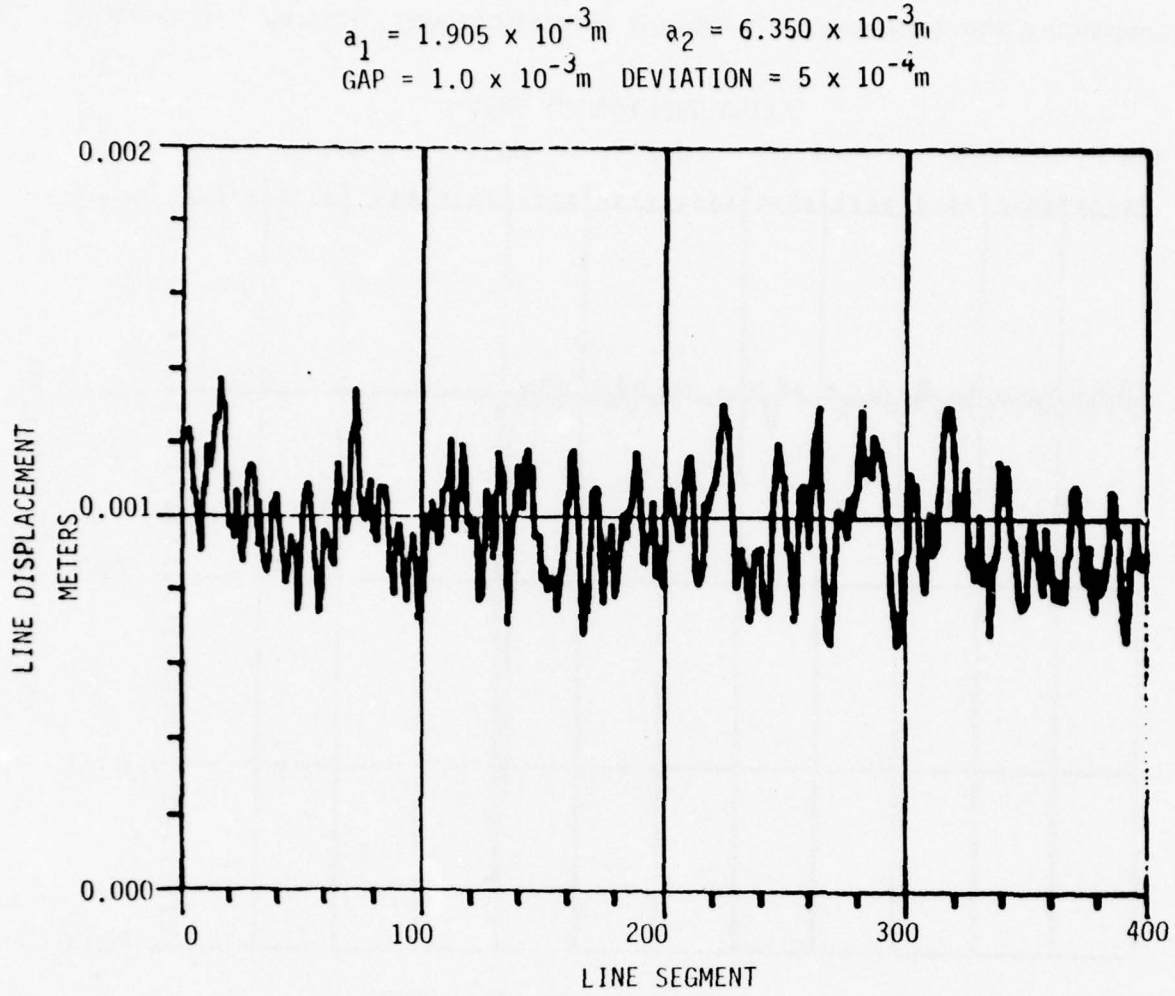

Figure 20. Gap Variations in the 1600-Element "Optimized" Transducer

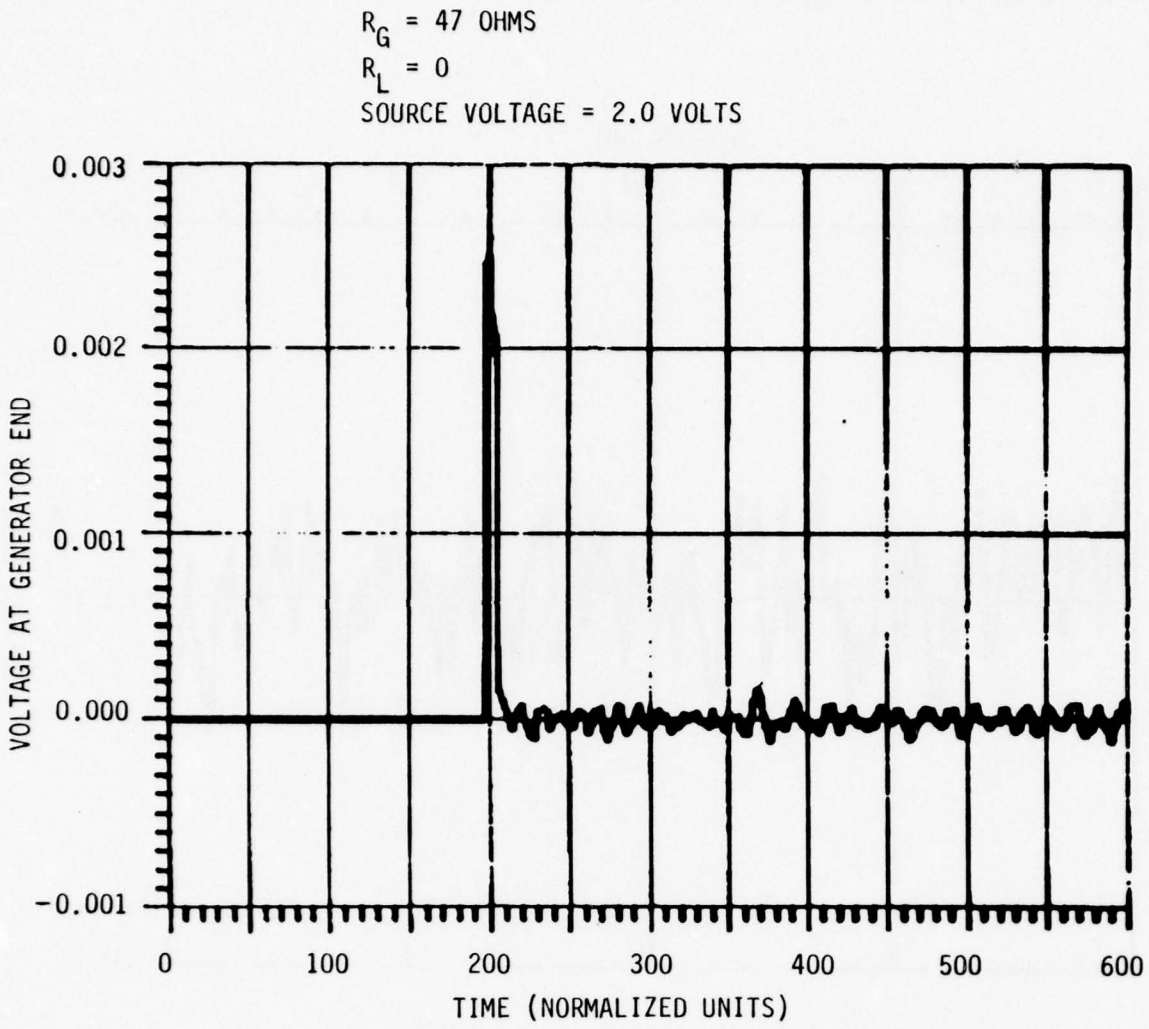

Figure 21. Partial Time-Amplitude History for 1600-Element Transducer

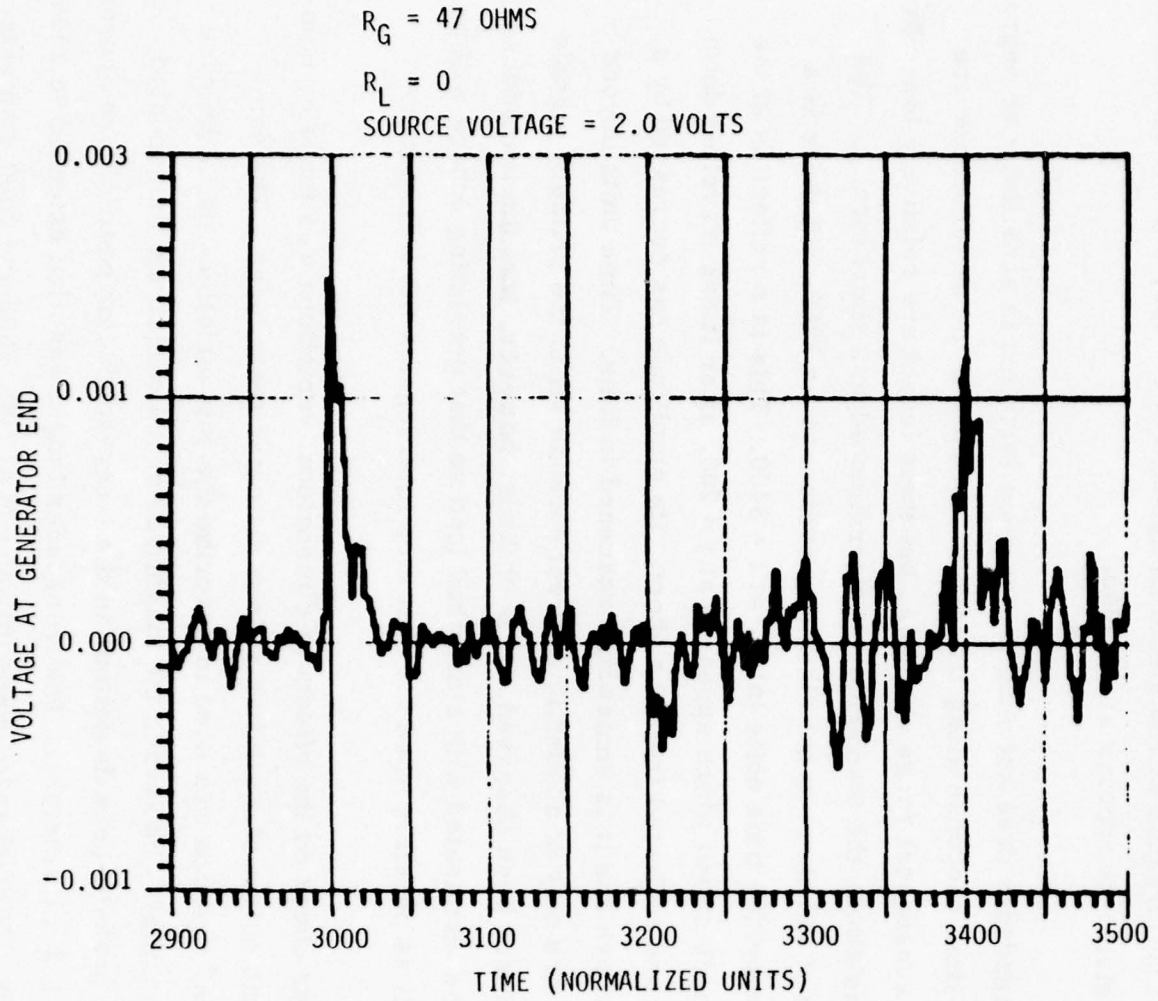

Figure 21. Partial Time-Amplitude History for 1600-Element Transducer (concluded)

to one-half the length of a transducer element. We will discuss the physical significance of these arbitrary time-unit scales later. The response from the disturbance at 100 elements appears at t = 200, and the disturbance at 1500 elements appears at t = 3000.

This transducer does not exhibit a serious variation in sensitivity or degradation in time response along its length. Echoes of the disturbances are seen in subsequent range channels, but their levels are relatively low. In this simulation, the transducer was terminated in a short circuit. The position of the short is not distinctly evident at t = 3200, but there is a strong echo 200 time units later, at t = 3400. This is a reflection of the disturbance signal which appeared at t = 200, after it has travelled down the line and reflected from the short. Its amplitude has decreased by a factor of two and it is somewhat broadened in time. Time units beyond t = 3200 are only of academic interest because all of the primary signals have already been observed. It is obvious, however, that the transducer should be terminated with a matched load so that persisting echoes will be as small as possible when the next step interrogates the transducer.

A further check on the effects of dimensional variations was made by computing the output of a similar $\frac{1}{2}$-inch diameter transducer. The same "random" function was used to describe the gap variations as in the case just described. However, the magnitude of the variations was doubled, so that the peak-to-peak deviations in the inner-conductor position are approximately 1.5 millimeters. The transducer length was also extended to 3200 elements. Disturbances were introduced at 100, 1500 and 3000 elements. Using the same computations as before, Figure 22 (three parts) shows three time-amplitude plots in the region of interest.

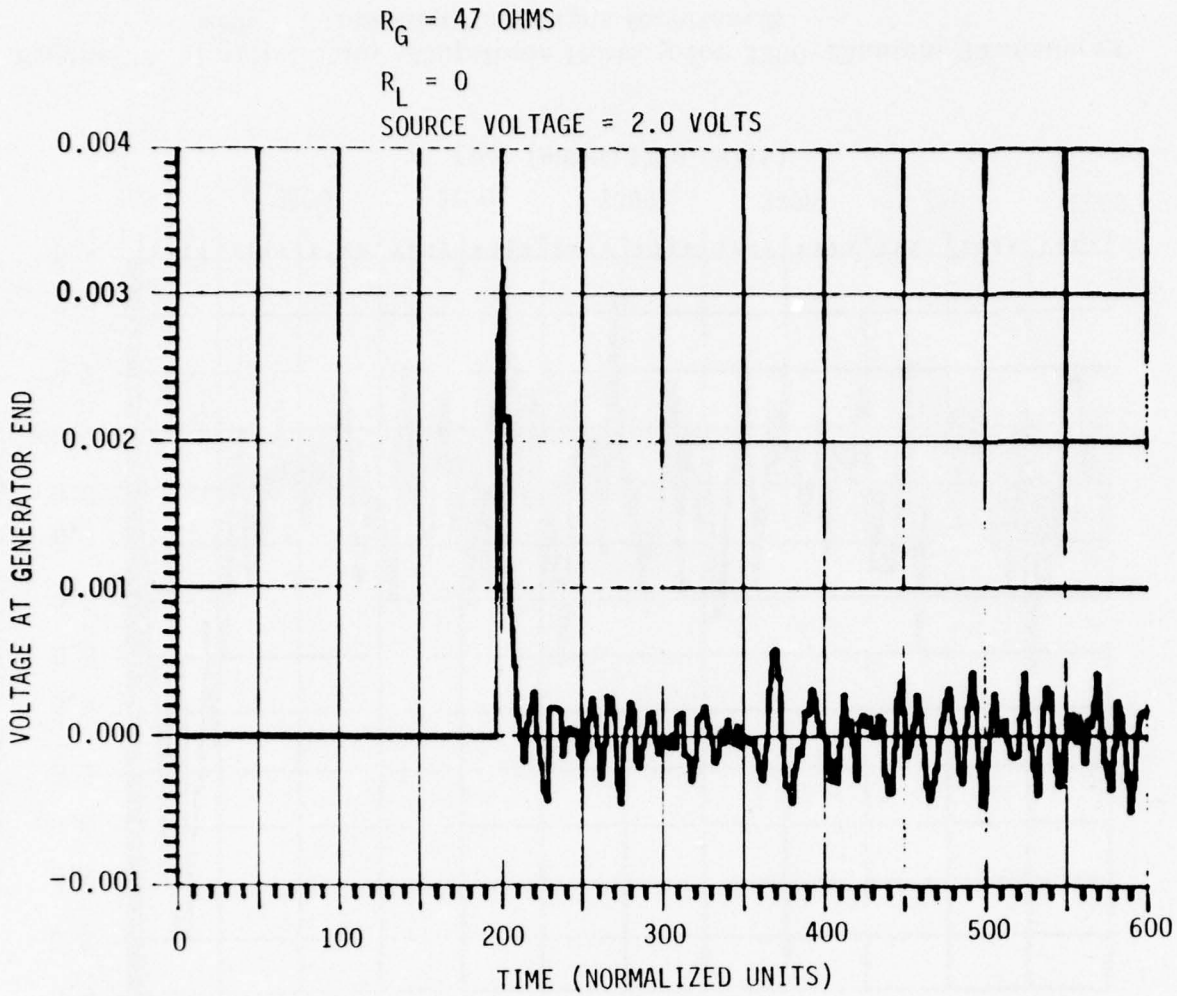

Figure 22. Partial Time-Amplitude History for 3200-Element Transducer with 1.5 mm Gap Variations

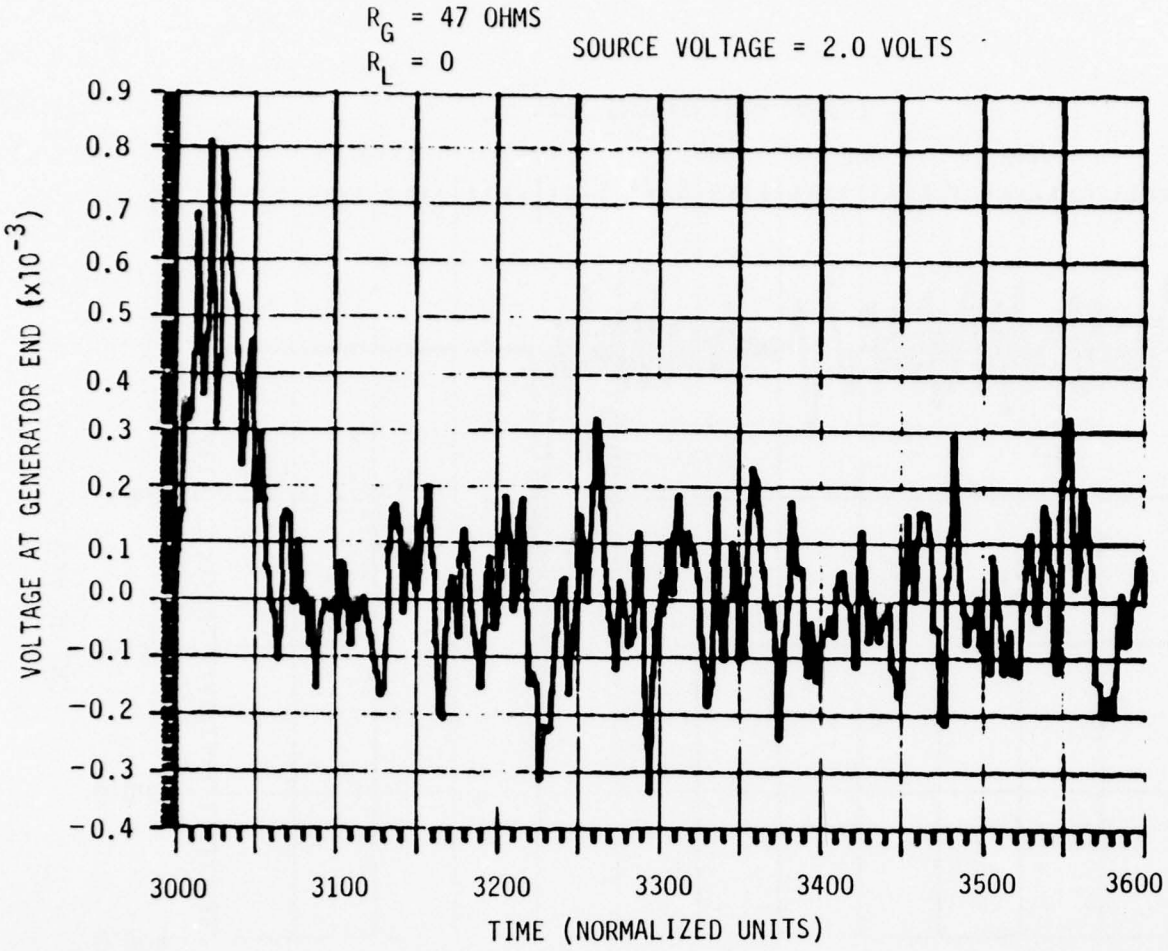

Figure 22. Partial Time-Amplitude History for 3200-Element Transducer with 1.5 mm Gap Variations (continued)

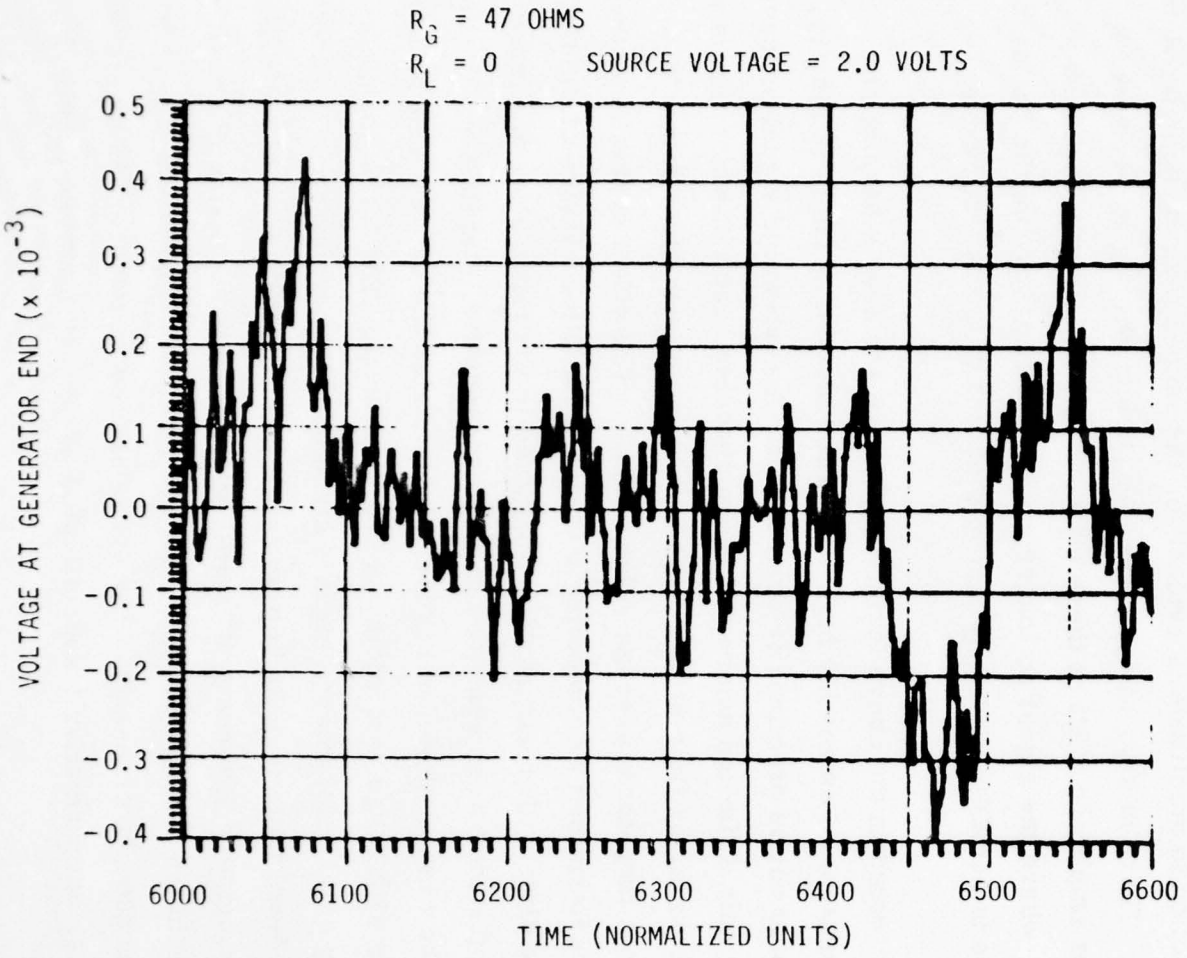

Figure 22. Partial Time-Amplitude History for 3200-Element Transducer with 1.5 mm Gap Variations (concluded)

The first disturbance signal, at t = 200, is very similar to the previous case. However, the echoes following the disturbance are larger in amplitude by approximately a factor of four. A substantial broadening in time and reduction in amplitude is evident for the second disturbance signal at t = 3000. There is also an apparent delay before the signal reaches its maximum amplitude. All of these effects are even more pronounced at t = 6000, where the signal no longer stands out clearly from the "noise". The noise is actually caused by multiple echoes of the other signals.

When presented in the above form, the results are overly pessimistic. They represent an extremely high-resolution picture of the time history, which would not be practical or even useful. A real-world signal processor will have only a limited number of range channels, each of which forms an average over many time units. This will substantially smooth the "noise," which has a long-term average value of zero. The effect of this smoothing has been determined by computing a coarse-resolution version of the time amplitude history that was partially depicted in the three plots of Figure 22. Signal amplitudes were averaged over 25 consecutive intervals of 250 time units. The result, shown in Figure 23, simulates the outputs of a 25-channel processor with range gate widths of 250 time units. The three channels containing actual disturbance signals stand out clearly above the worst-case crosstalk level (note that the bottom level of the histogram is actually a negative voltage). However, it is still apparent that excessive dimensional variations in the transducer will limit the dynamic range of the sensor because of echoes or crosstalk. The crosstalk can be suppressed by signal processing, but a relatively sophisticated processor might be required.

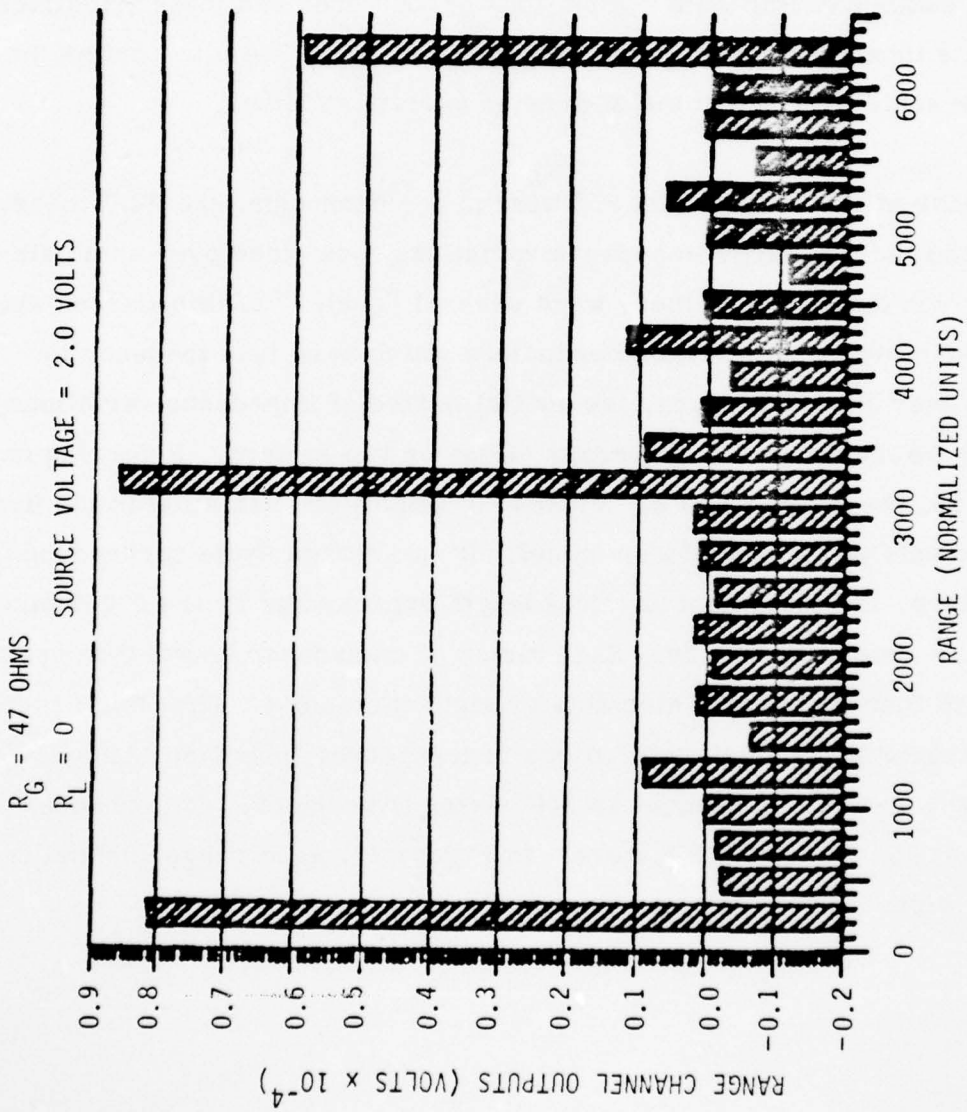

Figure 23. Simulated Processor Outputs for 3200-Element Transducer

All of the multiple-reflection computations for the 0.5-inch transducer have been presented on an arbitrary scale of time units. This is because, for a lossless transducer, the actual physical length (and therefore the time delay) has no influence on the waveform. The only parameters of importance are the number of impedance variations encountered and their magnitudes. To relate these results to actual transducer lengths, we must define the distance scale over which the dimension variations occur.

In the case of the loosely-laid #26 wire in a $\frac{1}{4}$-inch tube, the TDR measurements showed that large impedance variations took place over short distances. On the average, there were several "cycles" of impedance variation per meter. With larger conductors which have less tendency to deform over short distances, the spatial period of impedance variations can possibly be increased to an average of one or two meters. Referring to Figure 20, there are about 65 "cycles" of impedance variation in the first 400 elements of the transducer model. If an average cycle corresponds to 1.5 meters, the equivalent physical length represented by the 400-element picture is about 100 meters. Each meter of transducer length then corresponds to four transducer elements or eight time units. With this assumption concerning the spatial variations in transducer impedance, the 3200-element case would represent an 800-meter transducer. Disturbances are located at 25, 375 and 775 meters. In Figure 23, each range channel is 31 meters wide.

SIGNAL-TO-NOISE ESTIMATES

We have made preliminary estimates of the signal-to-noise ratios attainable with the pulsed-mode, enclosed-wire transducer. These estimates are based upon the simulation results for a uniform transducer, and show the factors limiting the signal-to-noise ratio. The calculations show that even a simple processor can give an acceptable ratio of signal to the theoretical noise floor of the electronics.

For the signal-to-noise calculations, we assumed a single-channel processor of the form shown in Figure 24. It consists simply of a pulse generator which periodically applies a step-function drive signal to the transducer. The generator impedance Z_g is matched to the transducer impedance Z_o to minimize reflections. A video preamplifier is incorporated to overcome the noise contributions of subsequent switching and amplifier circuits. To simplify the noise calculations, we will assume that the preamplifier has unity gain, and that the dominant noise sources are the thermal noise in the transducer and the equivalent input noise of the preamplifier. Following the video preamplifier is a range-gate switch and an integrating capacitor. The range-gate switch closes for a time interval Δt after a delay time t_o following the drive pulse. If the velocity of propagation in the transducer is V, the range gate selects the reflected signals from the range interval $\Delta R = V\Delta t/2$ located at a distance $X = Vt_o/2$.

The integrating capacitor takes the average value of signal plus noise voltage during the time the range-gate switch is closed, and holds this value while the switch is open. A bandpass amplifier following the range-

gate circuit limits the processor bandwidth to the desired signal bandwidth B. We will assume that the range gate interval is centered on the signal pulse.

If the drive voltage is E and the effective reflection coefficient of the disturbed transducer section is ρ_{EFF}, the signal voltage has a peak value equal to $E\rho_{EFF}$. The exact value of signal voltages can be obtained by integrating the signal pulse over the time interval Δt. When the range-gate interval is centered on the signal pulse, we can use simplified expressions which give fairly accurate approximations for the average signal voltage. If the half-voltage width τ of the signal pulse is greater than Δt, the average value of signal voltage is close to the peak value

$$e_s \simeq E\rho_{EFF} \qquad (\tau > \Delta t)$$

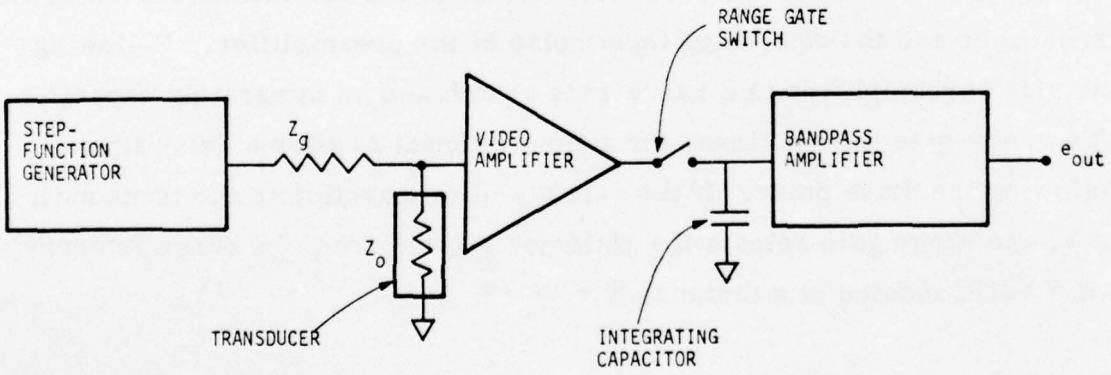

Figure 24. Processor Assumed in Signal-to-Noise Calculations

When the range-gate interval is longer than the pulse width, the average signal voltage is reduced by the factor $K\frac{\tau}{\Delta t}$. The value of K is approximately unity, and e_s can be approximated by

$$e_s \simeq E\rho_{EFF}\frac{\tau}{\Delta t} \qquad (\tau < \Delta t)$$

The rms noise voltage e_{no} from a source at temperature T_o and resistance Z_o in a bandwidth Δf is

$$e_{no} = (4\ k\ T_o\ Z_o\ \Delta f)^{\frac{1}{2}} \text{ volts rms}$$

where $k\ T_0 = 4.14 \times 10^{-21}$ joules at $T_o = 300°K$. A low-noise video preamplifier will add less than three dB to the thermal noise limit. The effective noise bandwidth is approximately $1/\Delta t$. Assuming a 3-dB noise figure for the video preamplifier, we have

$$e_n = \left(\frac{8\ k\ T_o\ Z_o}{\Delta t}\right)^{\frac{1}{2}} \text{ volts rms}$$

Using radar terminology, the "single-pulse" signal-to-noise voltage ratio is approximately

$$\frac{S}{N} \text{ single pulse} = \frac{E\rho_{EFF}(\Delta t)^{\frac{1}{2}}}{(8k\ T_o Z_o)^{\frac{1}{2}}} \qquad (\tau > \Delta t)$$

$$\frac{S}{N} \text{ single pulse} = \frac{E\rho_{EFF}\tau}{(8k\ T_o Z_o \Delta t)^{\frac{1}{2}}} \qquad (\tau < \Delta t)$$

These expressions give the ratio of peak signal to rms noise voltage at the low-frequency amplifier input. The best signal-to-noise ratio is obtained when Δt is "matched" to the pulse width τ.

An improvement in output signal-to-noise ratio is gained if the bandpass amplifier has a bandwidth less than the maximum bandwidth allowed by the Nyquist sampling criterion

$$B_{max} = \frac{PRF}{2}$$

where PRF is the pulse repetition frequency. The signal voltage is proportional to B_{max}/B, and the noise voltage is proportional to $(B_{max})^{\frac{1}{2}}/B$. Thus there is an "integration gain" in the signal-to-noise ratio equal to $(PRF/2B)^{\frac{1}{2}}$.

The maximum pulse repetition frequency is determined by the total transducer length L and the velocity of propagation V.

$$PRF_{max} = \frac{V}{2L}$$

We can also express the optimum gate interval $\Delta t = \tau$ in terms of the transducer range resolution ΔR

$$\tau = \frac{2\Delta R}{V}$$

Combining these factors, the output signal-to-noise voltage ratio when the processor gate time is optimized is approximately

$$\frac{S}{N_{opt}} = \frac{E\rho_{EFF}(\Delta R)^{\frac{1}{2}}}{4(kT_oZ_oBL)^{\frac{1}{2}}}$$

Expressed in dB, the optimum signal-to-noise ratio is

$$\frac{S}{N_{opt}} = 10 \log_{10} \frac{(E\rho_{EFF})^2 \Delta R}{16kT_oZ_oBL}$$

A numerical example of the realizable signal-to-noise ratio with an optimized transducer and processor is given here for the case of a 2 km, $\frac{1}{2}$-inch transducer with a uniform 1-millimeter gap. Assume a drive signal E = 1 volt and the signal bandwidth B = 1 kHz. The transducer impedance Z_o is approximately 50 ohms. From the transducer performance curves, we find that at 2 km, ΔR = 30 meters and $\rho_{EFF} = 3 \times 10^{-5}$. Under these conditions, the output signal-to-noise ratio is approximately 36 dB.

The above signal-to-noise ratio expressions relate the peak signal level to the rms noise voltage. In an intrusion sensor with a threshold-detector alarm circuit, we are concerned with the peak values of both the noise and signal voltage. For Gaussian noise, the peak value will very rarely exceed three times the rms value. The signal-to-noise voltage ratios given above can be divided by three to give a more conservative estimate for false-alarm rate predictions. This reduces the signal-to-noise ratio in the above example to 26 dB, which is still adequate to provide a very low false-alarm rate.

In the calculations presented above, we have not taken into account the cumulative effects of background noise, fluctuations in the drive signal level, or the "clutter" effects caused by multiple reflections. The equations indicate that the signal-to-noise ratio can be improved indefinitely, simply by increasing the drive signal level. However, the background noise due to actual seismic/acoustic disturbances increases in direct proportion to the drive level. Fluctuations in the drive signal level can easily exceed a few parts in 10^6, which sets a lower limit of about 10^{-5} on the minimum effective reflection coefficient for reliable detection.

In the simple processor circuit assumed for the signal-to-noise calculations, the dynamic range of the video preamplifier and range-gating circuits sets a limit on the allowable drive level. This difficulty can be avoided with a slight increase in circuit complexity, as discussed later.

Clutter due to multiple reflections in a non-uniform transducer is a stationary effect, and is not inherently a source of noise. However, crosstalk from multiple reflections can cause background noise along the entire transducer length to contribute to the noise level in each range channel. We expect the cumulative background noise voltage from incoherent sources to be proportional to the square root of the number of range channels, multiplied by the average interchannel crosstalk level. As long as the crosstalk level is low, the cumulative noise contribution will not be severe. With a 3-km transducer and 100 30-meter range channels, the cumulative background noise due to crosstalk from all other channels will not exceed the background noise in a given channel if the crosstalk level is below 20 dB.

Unless the transducer is extremely uniform, the signal-to-clutter ratios will be low. For example, if the displacement caused by an intruder is 0.01 millimeter, and there is a 0.3 millimeter variation in the nominal gap, the signal-to-clutter ratio will be on the order of -30 dB.

Excitation Waveforms

Our sensor analysis was based upon the assumption of a fast-rise step-function drive signal. This is the basic excitation signal used in time-domain reflectometry, and it is convenient for time-domain as well as frequency-domain analysis. However, it is not necessarily the optimum excitation for the pulsed-mode transducer. We did not perform an analysis of more complex excitation signals, but we identified variations of the step function which offer performance advantages.

In the simple case of a step-function drive signal, we must bring the drive voltage back to zero before another step can be applied. Reflections from the transducer will also occur from this "retrace" signal. Rather than accepting the additional 50 percent dead time required for these reflections to damp out, we can just as well use a dual-slope, step-function excitation--in other words, a square wave. All that is necessary is to reverse the polarity of the return signals during alternate half-cycles of the excitation square wave so that the return signals will be combined constructively. When square-wave excitation is used, the actual frequency of the drive signal is one-half the effective PRF.

This square-wave form of excitation has another benefit in addition to reduction of dead time. The drive signal can be made bipolar, with an average value of zero. This removes any unintentional d-c bias from the transducer. Since the polarity of the detection electronics is alternated at a high rate, extraneous d-c or low-frequency signals are cancelled. These features make the pulsed-mode transducer insensitive to the basic low-frequency signals generated by the wire-in-tube transducer when it is biased, either externally or by electret effects in the insulation.

A simple implementation of the square-wave drive technique is shown functionally in Figure 25. The only additions to the basic circuit are a differential video preamplifier, a reference load resistance, and four switching diodes.

Synchronous polarity switching in the detection electronics is automatically provided by a diode ring in combination with the bipolar excitation signal. When the drive signal polarity is positive, the transducer is connected to the non-inverting input of the differential video amplifier and the reference load is connected to the inverting input. A negative drive signal reverses these connections.

As shown in the diagram, the generator and reference load impedances are equal to the nominal transducer impedance. It is necessary to match the generator impedance to the transducer to suppress multiple reflections. A reference load with the same impedance as the transducer provides suppression of noise which may be present in the drive signal itself. It also reduces the dynamic-range requirement of the video preamplifier and subsequent range-gating electronics, which would otherwise have to accommodate the full drive-signal amplitude multiplied by the preamplifier gain.

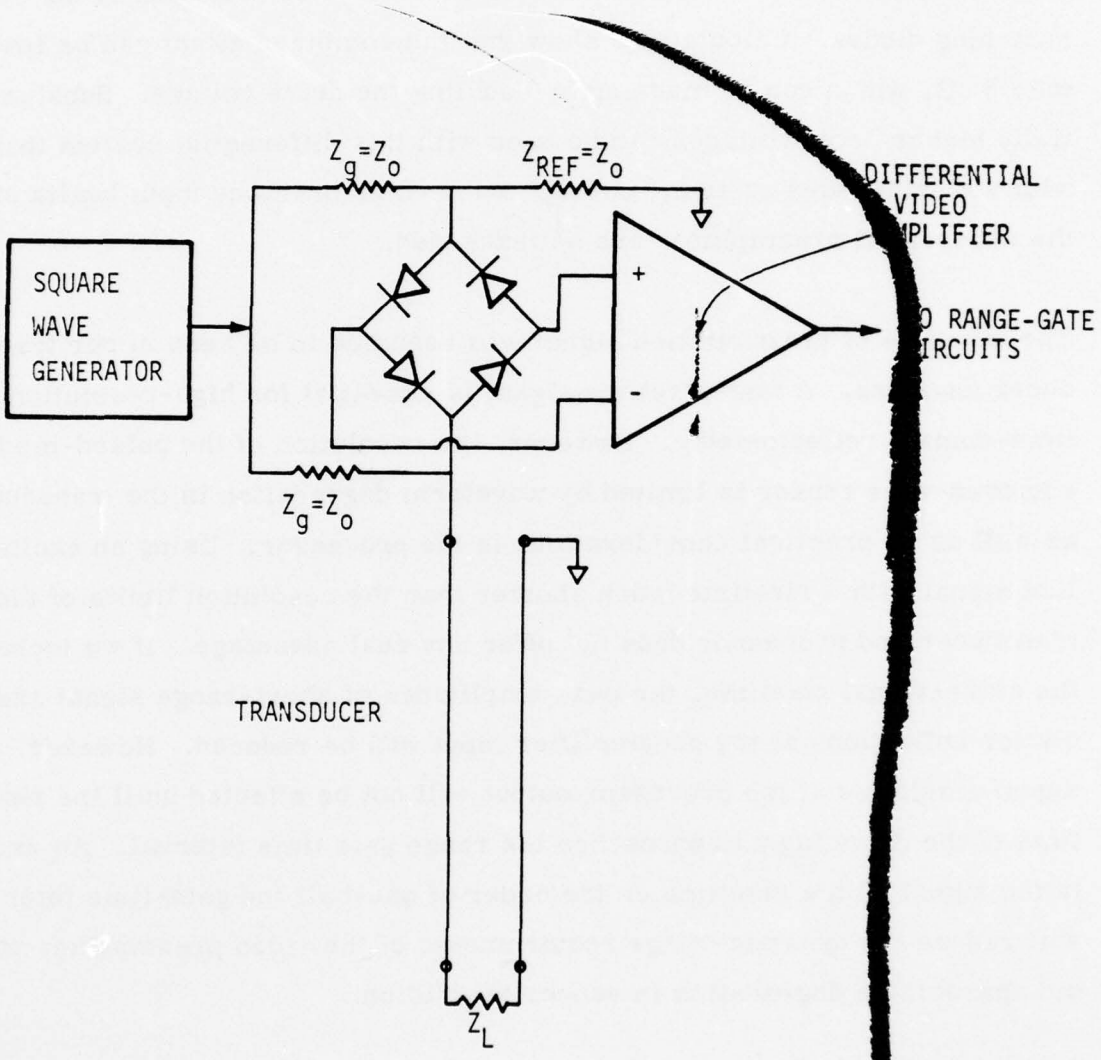

Figure 25. Square-Wave Drive Technique

There is a slight penalty in signal-to-noise ratio with this circuit because of the additional amplifier input and the shot-noise contribution of the switching diodes. Calculations show that the combined effect can be less than 6 dB, which can be made up by doubling the drive voltage. Substantially higher drive voltages can be used with this differential system than with a single-ended system, as long as the common-mode input limits of the differential preamplifier are not exceeded.

The risetime of the excitation signal was assumed to be zero in our transducer analyses. A fast-risetime signal is essential for high-resolution time-domain reflectometry. However, the resolution of the pulsed-mode enclosed-wire sensor is limited by waveform degradation in the transducer, as well as by practical considerations in the processor. Using an excitation signal with a risetime much shorter than the resolution limits of the transducer and processor does not offer any real advantage. If we increase the drive-signal risetime, the peak amplitudes of short-range signal and clutter reflections at the preamplifier input will be reduced. However, the signal amplitude at the processor output will not be affected until the risetime of the drive signal approaches the range gate time interval. An excitation signal with a risetime on the order of one-half the gate-time interval will reduce the dynamic-range requirements of the video preamplifier without appreciable degradation in sensor resolution.

Alternate Signal-Processor Designs

Many of the waveforms and processing techniques used in modern radar and sonar systems may be applicable to the pulsed-mode enclosed-wire sensor. The signal-to-noise estimates show that a simple processor can be used

AD-A040 105 HONEYWELL INC MINNEAPOLIS MINN SYSTEMS AND RESEARCH --ETC F/G 15/3
PULSED-MODE ENCLOSED-WIRE TRANSDUCER ANALYSIS.(U)
APR 77 L E KOEHLER, T RAHMAN, C TETTEMER F30602-76-C-0378
UNCLASSIFIED RADC-TR-77-129 NL

2 OF 2
ADA040105

END

DATE
FILMED
6-77

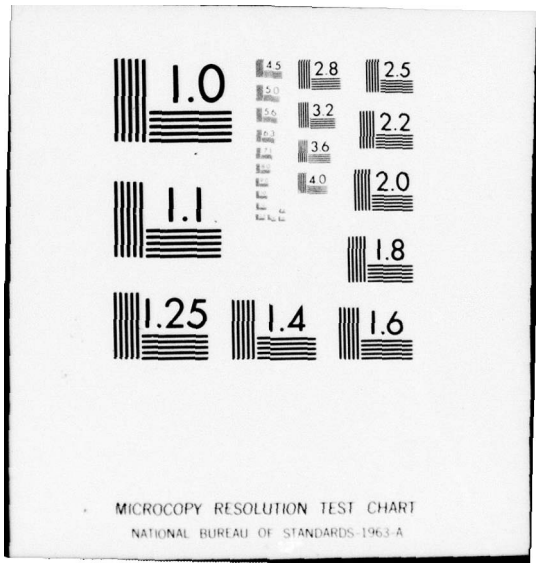
1.0
1.1
1.25
1.4
1.6
1.8
2.0
2.2
2.5
2.8
3.2
3.6
4.0
4.5
5.0
5.6
6.3
MICROCOPY RESOLUTION TEST CHART
NATIONAL BUREAU OF STANDARDS-1963-A

with transducer lengths of two km or more. Because of the presence of clutter, crosstalk and background noise, it is difficult to say how much improvement could be gained with a more complex driving waveform and a sophisticated signal processor. Existing analyses of the pulsed-mode transducer need to be supplemented with experimental data and proof of feasibility before the detailed analysis and design of a complex processor is justified.

One type of processor which could offer a significant cost advantage for a multichannel sensor is based upon charge-coupled devices (CCDs). The functions of a k-channel processor can be implemented with time-shared recursive filters using k-bit CCD analog delay lines. Outputs from all channels can be time-multiplexed to appear on a single line. This would eliminate the need for separate range switches and analog filters in each channel.

SUGGESTED TRANSDUCER CONFIGURATIONS

Our analysis shows that the loosely-laid wire-in-tube configuration is not well suited for pulsed-mode operation. Since the inner conductor can assume any position within the outer tube, the transducer impedance variations are very large. Resulting multiple reflections cause severe attenuation, clutter and crosstalk. An alternate transducer design must be used unless the maximum length is less than a few hundred meters. It is difficult to satisfy all of the conflicting design requirements. The inner conductor must be spaced fairly uniformly within the outer tube. Peak-to-peak variations in the gap should not exceed approximately 1 millimeter. But in order to preserve the sensitivity of the wire-in-tube transducer, the inner conductor must be able to move freely. It is desirable to preserve the

mechanical resonances which are responsible for high sensitivity in the "strumming" mode. The pulsed-mode transducer should also be cheap, rugged and easily deployed. Transducer configurations which show promise of meeting these requirements are identified in this section.

A good compromise between cost and performance can be achieved with a ½-inch diameter aluminum outer conductor. The analysis shows that a signal-to-noise ratio of 25 dB and a range resolution of 30 meters is theoretically possible with a 2-km long, ½-inch diameter transducer. One inch tubing provides comparable performance at 50 percent greater distances, but costs and weighs about three times as much as ½-inch tubing. Aluminum has a slightly higher resistivity than copper, but for high-conductivity alloys the difference is only about 30 percent. High-frequency resistance is proportional to the square root of resistivity and inversely proportional to conductor diameter. Resistive losses in the transducer will be dominated by the inner conductor, and the choice of copper or aluminum for the outer conductor will affect the total resistance by only about 4 percent.

Aluminum tubing also costs much less than copper. Half-inch copper refrigeration tubing costs about 50 cents per foot; aluminum tubing is less than 15 cents per foot. Another advantage of aluminum is its weight. Five hundred meters of ½-inch aluminum tubing weighs less than 100 pounds; copper tubing would weigh nearly 300 pounds. Fabrication may be somewhat more difficult with aluminum than copper, although weather-proof joints and connectors are commonly used in aluminum-jacketed coaxial lines for cable TV systems.

It is also possible to use a braided copper outer conductor with a supporting dielectric. This may offer advantages in fabrication and handling.

The most critical consideration in the transducer design is the inner conductor and the way in which it is supported. For a $\frac{1}{2}$-inch outer conductor the optimum inner conductor diameter is 0.14 inches (equivalent to #7 wire). The inner conductor diameter can be reduced to 0.075 inches before the attenuation becomes excessive. This is approximately the diameter of a #12 wire. We list below a few of the options which can be considered for the inner conductor and its support structure.

Stranded Wires--Solid #12 or larger wire is too rigid to lie in the outer tube without extreme variations in gap. However, multiple-strand wire may be sufficiently flexible to conform to the contour of a deployed $\frac{1}{2}$-inch tube.

Braided Conductors--A hollow braided conductor of the type used for shielded cable has essentially the same high frequency resistance as a solid conductor, but with considerably greater flexibility.

Ribbon Conductors--A very flexible conductor can be made by laminating a copper ribbon between thin sheets of plastic. The desired electrical and mechanical properties might be obtained with a 1/8 inch wide, 0.001 inch thick copper ribbon sandwiched between 1/4 inch wide polyethylene strips. This type of conductor would tend to lie nearly uniformly near the bottom of a $\frac{1}{2}$ inch tube. The edges of the polyethylene strip can be deformed

periodically during manufacture to provide support at discrete points. Another technique for providing periodic support points is to put an intentional twist in the ribbon conductor as the transducer is fabricated.

Formed Conductors--A helical inner conductor configuration can be fabricated by winding a relatively springy conductor such as solid copper or copperweld wire around a mandrel and then stretching it. If the diameter of the resulting helix is slightly smaller than the tubing, it will allow relative motion of the conductors, but will limit the variations in gap to the difference in diameters.

Insulating Supports--Various forms of insulating support structures, such as beads on the inner conductor or deformations in the insulation, should also be considered.

Eccentric Hollow Dielectric--The nominal inner-conductor spacing can be maintained by a dieletric with an eccentric hole, as shown in Figure 26. If the hole is made slightly larger than the inner conductor, the conductor is free to move but its maximum deviation is restricted to an acceptable value. An inexpensive, low-loss dielectric material such as solid or cellular polyethylene will not significantly increase the attenuation as compared to an air-insulated transducer. Any of the conductor configurations described above can be used. This geometry is attractive because it closely resembles the basic wire-in-tube configuration and should be capable of low-cost fabrication.

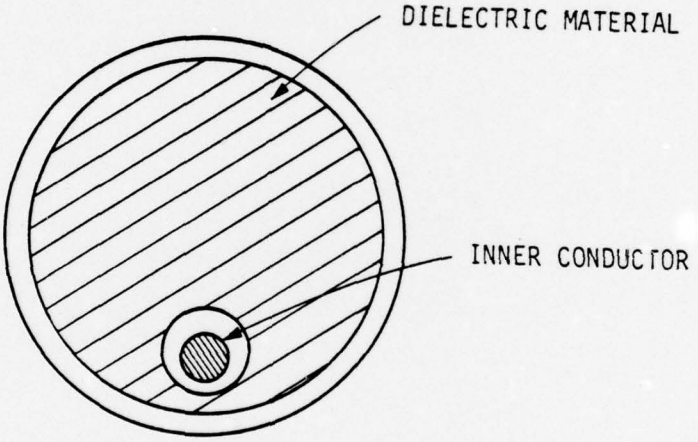

Figure 26. Eccentric Hollow Dielectric Transducer

It is difficult to predict analytically how these conductor configurations will respond to a mechanical disturbance. We recommend that short segments (10 meters or less) of several transducer designs be fabricated for experimental determination of their mechanical and electrical characteristics. A larger-scale feasibility demonstration should then be conducted with a selected transducer design.

REFERENCES

1. Geil, F. G. and H. Gilcher, "Wire-In-Tube Sensor," Proceedings of the 1974 Carnahan Crime Conference, University of Kentucky, Lexington.

2. Wigington, R. L. and N. S. Nahman, "Transient Analysis of Coaxial Cable Considering Skin Effect," Proceedings of the IRE, Vol. 45, No. 2, 1957, pp. 166-174.

3. Bewley, L. V., Traveling Waves on Transmission Systems, 2nd Edition, Wiley, N. Y., 1951.

APPENDIX A
SOIL DISPLACEMENT COMPUTATION

In estimating the soil deformations caused by an intruder, we made use of a computer model which had been developed at Honeywell prior to this study. The approach taken in computing soil displacements is to assume a quasi-static model. This model assumes, in effect, that input load frequencies are relatively small so that soil displacements are proportional to and in phase with the applied loads. This assumption is valid where the wavelength for displacement propagation is much larger than that of the ranges for detection under consideration. Most soils exhibit wave velocities well in excess of 100 feet per second. Therefore, the one-hertz input frequency results in a 100-foot wavelength. Since ranges for detection are for human intruders, well under 10 feet, the quasi-static assumption is valid for that type of traffic. As consideration is given to higher frequencies and larger ranges for detection, i.e., as with vehicular traffic, the quasi-static assumption becomes invalid. One must then resort to analysis of wave propagation within the soil.

ANALYTICAL SOLUTION FOR STRAIN

The solution will be worked out for the case of cylindrical coordinates assuming axisymmetry. The problem is thus cast in two dimensions, r and z, as labeled in Figure A-1. The load produced by the intruder must be assumed to act vertically at $r = 0$.

For the case of uniform elastic soil properties and a concentrated vertical load P at $r = 0$, a closed-form solution may be found in several texts. The solutions for radial and vertical displacements are:

PRECEDING PAGE BLANK-NOT FILMED

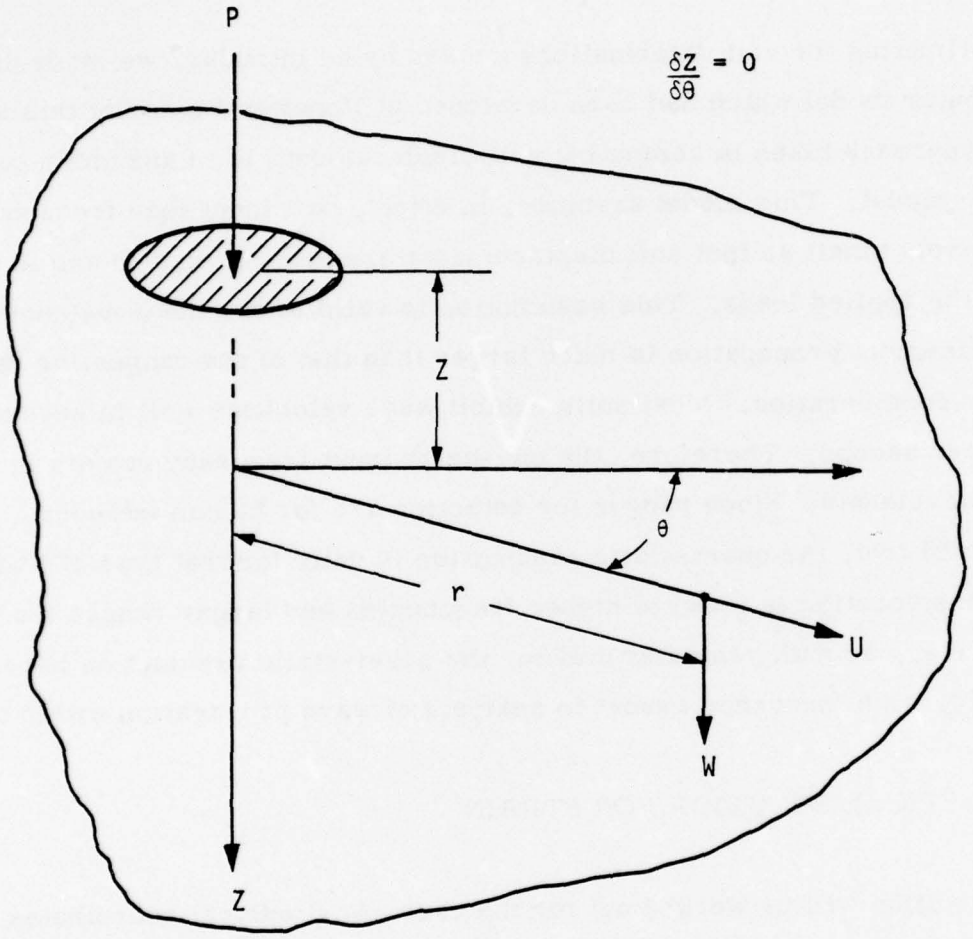

Figure A-1. Coordinates for Soil Displacement Model

$$u = \frac{(1-2\nu)(1+\nu)P}{2\pi E r}\left[\frac{z}{\sqrt{r^2+z^2}} - 1 + \frac{r^2 z}{(1-2\nu)\sqrt{(r^2+z^2)^3}}\right] \qquad \text{(A-1)}$$

$$w = \frac{P}{2\pi E}\left[\frac{(1+\nu)z^2}{\sqrt{(r^2+z^2)^3}} + \frac{2(1-\nu^2)}{\sqrt{r^2+z^2}}\right] \qquad \text{(A-2)}$$

where

E = Young's modulus; ν = Poisson's ratio.

The assumptions of uniform soil properties and a point load limit the applicability of the above equations. The point-load assumption is, according to Saint-Venants' principle, valid for distributed loads at distances from the load large as compared with the dimensions of area of application. Thus, for soil displacements in the immediate vicinity of a footprint, Equations (A-1) and (A-2) would give imprecise results. The assumption of uniform soil properties does not conform to usual conditions of terrains. Soil properties vary considerably with depth either because of harder strata existing at lower depth or because of compaction caused by overpressure.

NUMERICAL SOLUTION FOR DISPLACEMENT

For the case of variable soil properties, and for displacements in the vicinity of a distributed load, one must resort to a numerical solution. Such a solution has been derived and programmed in Fortran IV on the Honeywell 6080 computer.

The basic methodology is to write numerical approximations for the equations of elasticity. We are, of course, assuming the soil behaves according to Hook's law (i.e., stress is proportional to strain). For certain soils,

sufficient water content may produce a more plastic-type behavior which cannot be well represented by this analysis.

For cylindrical coordinates and axisymmetry as illustrated in Figure A-1, the equations of elasticity with variable soil properties are:

$$(\lambda + 2G)\left[\frac{1}{2}\left(\frac{\partial u}{\partial r} - \frac{u}{r}\right) + \frac{\partial^2 u}{\partial r^2}\right] + (\lambda + G)\frac{\partial^2 w}{\partial r\,\partial z} + G\frac{\partial^2 u}{\partial z^2} + \left[\frac{\partial G}{\partial z}\left(\frac{\partial u}{\partial z} + \frac{\partial w}{\partial r}\right)\right] = 0 \tag{A-3}$$

$$(\lambda + G)\left[\frac{\partial^2 u}{\partial r\,\partial z} + \frac{1}{r}\frac{\partial u}{\partial z}\right] + G\left[\frac{1}{r}\frac{\partial u}{\partial r} + \frac{\partial^2 w}{\partial r^2}\right] + (\lambda + 2G)\frac{\partial^2 w}{\partial z^2} + \left[\left(\frac{\partial \lambda}{\partial z}\right)\left(\frac{\partial u}{\partial r} + \frac{u}{r}\right) + \left(\frac{\partial \lambda}{\partial z} + 2\frac{\partial G}{\partial z}\right)\frac{\partial w}{\partial z}\right] = 0 \tag{A-4}$$

where:

$$\lambda = \frac{2E}{(1 + 2)(1 - 2\nu)}$$

$$G = \frac{E}{2(1 + \nu)}$$

The terms highlighted by dashed lines account for property variations in the vertical direction.

The above equations have been expressed in finite difference form and programmed for solution using a relaxation technique.

The program is set up with a graded grid system; that is, as the distance from the point of application increases, the size of the grid also increases as shown in Figure A-2. The basic program is set up for five gradations

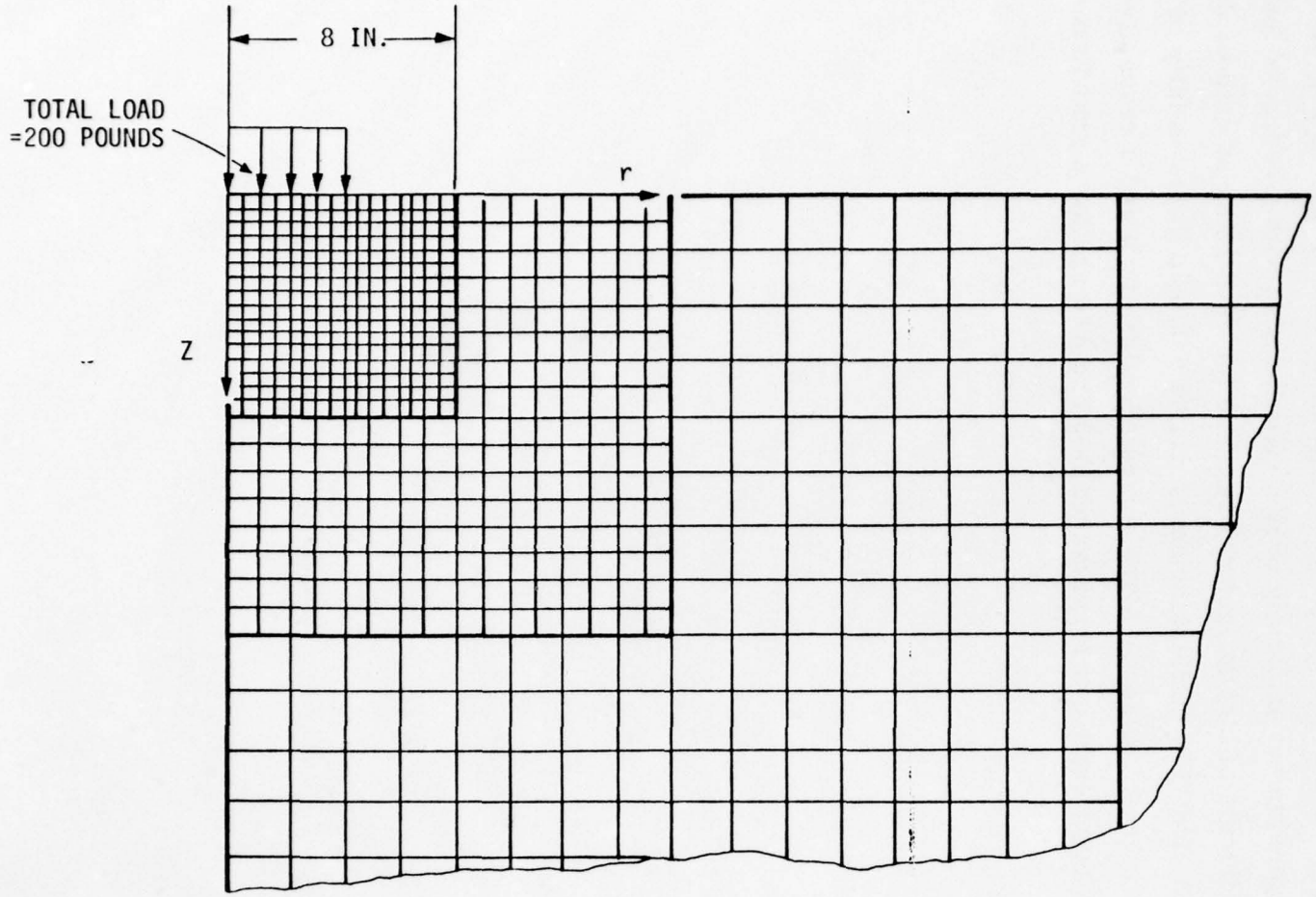

Figure A-2. Graduated Grid System

so that displacements are computed to a range of 128 inches. A 200-pound load is assumed to act uniformly over a circular disk with a radius of four inches. Printouts of displacements are made for each 16 by 16 grid so that a high-resolution view of displacements can be obtained in the vicinity of the load. Figures A-3 and A-4 are computed values of w and u respectively out to a radius of eight inches; Figures A-5 and A-6 are for a grid 16 times larger.

Vertical Distance z, inches \ Radius r, inches	0	0.5	1.0	1.5	2.0	2.5	3.0	3.5	4.0	4.5	5.0	5.5	6.0	6.5	7.0	7.5
0	1737.3	1649.4	1664.0	1620.2	1576.1	1509.3	1426.7	1312.2	1185.5	946.3	834.4	732.5	662.6	604.6	559.2	520.7
0.5	1656.9	1638.2	1622.3	1584.8	1534.7	1468.6	1385.2	1278.5	1143.7	946.4	823.2	730.2	660.2	604.1	558.9	521.4
1.0	1595.6	1599.0	1573.7	1532.8	1479.8	1412.4	1328.7	1224.5	1097.0	940.3	823.0	732.5	662.5	606.4	560.8	523.0
1.5	1532.9	1541.1	1512.2	1469.6	1415.5	1348.4	1266.8	1168.6	1054.3	926.9	820.8	734.7	665.7	609.7	563.8	525.4
2.0	1464.1	1470.6	1441.6	1399.8	1347.0	1282.4	1205.4	1115.6	1015.1	908.7	814.4	734.2	667.7	612.6	566.6	527.9
2.5	1390.6	1393.6	1366.7	1327.6	1277.9	1217.6	1146.8	1066.3	978.3	887.6	804.2	730.6	667.6	614.1	568.7	530.1
3.0	1315.4	1315.2	1291.3	1256.0	1210.6	1155.7	1091.8	1020.2	943.4	865.0	791.0	724.0	665.0	613.8	569.6	531.5
3.5	1241.3	1238.7	1218.3	1187.1	1146.5	1097.3	1040.4	977.2	909.9	841.4	775.7	714.9	660.2	611.7	569.2	531.9
4.0	1170.3	1166.3	1149.1	1122.1	1086.3	1042.7	992.4	936.8	877.7	817.5	759.0	704.0	653.5	608.0	567.4	531.4
4.5	1103.7	1098.9	1084.6	1061.4	1030.2	991.9	947.7	898.7	846.8	793.7	741.5	691.6	645.2	602.7	564.2	529.6
5.0	1041.9	1037.0	1025.1	1005.3	978.3	944.8	905.9	862.9	817.1	770.1	723.4	678.3	635.7	596.2	559.9	527.0
5.5	985.2	980.3	970.6	953.7	930.3	901.0	867.0	829.1	788.7	746.9	705.1	664.3	625.3	588.6	554.6	523.3
6.0	933.4	928.8	920.7	906.2	886.0	860.5	830.7	797.3	761.5	724.4	686.9	649.9	614.2	580.3	548.4	518.9
6.5	886.3	881.8	875.3	862.7	845.2	822.9	796.8	767.3	735.7	702.5	668.8	635.3	602.6	571.3	541.6	513.7
7.0	843.6	839.1	833.9	822.7	807.7	788.0	765.2	739.1	711.0	681.3	651.1	620.6	590.8	561.9	534.1	508.0
7.5	805.2	800.4	796.3	785.8	773.1	755.5	735.8	712.4	687.7	660.9	633.7	606.1	578.7	552.1	526.3	501.9

Figure A-3. Vertical Soil Displacement, w (μin.), 0.5 Inch Resolution, G = 5000 psi, ν = 0.35

Vertical Distance z, inches \ Radius r, inches	0	0.5	1.0	1.5	2.0	2.5	3.0	3.5	4.0	4.5	5.0	5.5	6.0	6.5	7.0	7.5
0	0.	-83.7	-89.7	-137.1	-166.3	-199.3	-235.2	-267.0	-333.9	-329.2	-259.4	-234.8	-207.6	-190.5	-175.7	-163.9
0.5	0.	-47.1	-73.8	-93.2	-109.9	-124.3	-136.3	-145.9	-150.9	-153.2	-152.5	-148.5	-143.7	-138.5	-133.6	-129.1
1.0	0.	-25.4	-39.0	-47.3	-52.7	-55.5	-56.7	-55.6	-54.0	-60.6	-73.7	-83.5	-90.0	-93.6	-95.4	-95.7
1.5	0.	-5.5	-7.5	-7.6	-6.3	-3.7	-0.4	2.6	2.4	-6.1	-21.3	-35.9	-47.8	-56.8	-63.2	-67.7
2.0	0.	10.2	16.4	21.8	27.0	32.1	36.4	38.6	36.6	27.6	13.2	-2.0	-15.7	-27.0	-35.9	-42.5
2.5	0.	21.1	32.5	41.3	48.7	54.8	59.0	60.3	57.4	48.9	36.1	21.9	8.2	-4.0	-14.2	-22.6
3.0	0.	27.9	42.2	53.1	61.6	68.0	72.0	72.8	69.7	62.2	51.2	38.5	25.8	14.0	3.6	-5.1
3.5	0.	31.4	47.2	59.1	68.2	74.8	78.6	79.4	76.6	70.2	60.9	49.9	38.5	27.4	17.2	8.1
4.0	0.	32.8	49.1	61.4	70.7	77.3	81.2	82.1	79.9	74.7	67.0	57.6	47.6	37.6	28.1	19.5
4.5	0.	32.8	48.9	61.2	70.5	77.1	81.1	82.4	80.9	76.7	70.4	62.6	53.9	45.0	36.2	27.9
5.0	0.	31.9	47.5	59.5	68.7	75.3	79.4	81.1	80.3	77.2	72.1	65.6	58.2	50.4	42.6	35.1
5.5	0.	30.5	45.5	57.1	66.0	72.6	76.9	78.9	78.7	76.5	72.5	67.2	60.9	54.1	47.1	40.1
6.0	0.	28.9	43.1	54.2	62.9	69.4	73.8	76.1	76.5	75.1	72.0	67.7	62.5	56.7	50.5	44.4
6.5	0.	27.3	40.7	51.2	59.6	66.0	70.5	73.1	73.9	73.2	70.9	67.5	63.2	58.2	52.8	47.2
7.0	0.	25.5	38.2	48.2	56.3	62.6	67.1	69.9	71.2	71.0	69.4	66.8	63.3	59.1	54.4	49.6
7.5	0.	23.4	35.7	45.4	53.2	59.2	63.8	66.8	68.4	68.6	67.7	65.7	62.9	59.3	55.4	51.0

Figure A-4. Horizontal Soil Displacement, u (μin.), 0.5 Inch Resolution, G = 5000 psi, ν = 0.35

Vertical Distance z, inches \ Radius r, inches	0	8	16	24	32	40	48	56	64	72	80	88	96	104	112	120
0	1737.3	490.0	256.0	176.9	135.7	110.0	92.1	79.1	69.3	61.6	55.2	49.9	45.4	41.7	38.2	35.4
8	771.5	473.1	261.7	179.4	136.6	110.1	92.1	79.0	69.1	61.2	54.8	49.6	45.7	41.4	38.0	35.1
16	450.9	370.8	252.4	179.9	137.5	110.8	92.5	79.2	69.0	61.1	54.7	49.4	45.0	41.2	37.9	35.0
24	318.5	288.7	227.2	173.7	136.1	110.5	92.6	79.3	69.1	61.1	54.6	49.4	44.9	41.2	37.9	35.0
32	247.7	232.5	198.9	162.1	131.7	108.8	91.9	78.9	68.9	61.0	54.6	49.3	44.9	41.1	37.9	35.1
40	201.8	193.0	173.4	148.5	125.0	105.8	90.7	78.1	68.4	60.7	54.4	49.7	44.8	41.1	37.9	35.2
48	169.2	164.0	151.8	134.8	117.1	101.2	87.7	76.6	67.5	60.1	54.0	49.0	44.7	41.1	37.9	35.2
56	145.2	141.9	133.9	122.0	118.8	95.5	84.5	74.6	66.3	59.3	53.5	48.6	44.5	41.0	37.9	35.3
64	127.6	124.4	119.0	110.5	100.5	90.3	80.7	72.1	64.0	58.2	52.8	48.1	44.2	40.8	37.8	35.3
72	112.8	110.1	106.4	100.3	92.7	84.6	76.7	69.3	62.7	56.9	51.9	47.5	43.8	40.5	37.7	35.2
80	100.3	98.2	95.6	91.2	85.4	79.0	72.5	66.3	60.5	55.4	50.8	46.8	43.2	40.1	37.4	35.1
88	89.8	88.1	86.4	83.1	78.8	73.7	68.4	63.2	58.2	53.7	49.6	45.9	42.6	39.7	37.2	34.9
96	80.9	79.5	78.3	76.0	72.7	68.7	64.4	60.1	55.9	51.9	48.3	44.9	41.9	39.2	36.8	34.6
104	73.2	72.0	71.3	69.6	67.1	64.0	60.6	57.0	53.5	50.1	46.8	43.9	41.1	38.6	36.4	34.3
112	66.7	65.6	65.2	64.0	62.1	59.7	57.0	54.0	51.1	48.2	45.4	42.7	40.3	38.0	35.9	33.9
120	61.2	60.3	60.1	59.1	57.6	55.7	53.5	51.2	48.7	46.3	43.8	41.5	39.3	37.2	35.3	33.5

Figure A-5. Vertical Soil Displacement, w (μ in.), 8-Inch Resolution, G = 5000 psi, ν = 0.35

Vertical Distance z, inches \ Radius r, inches	0	8	16	24	32	40	48	56	64	72	80	88	96	104	112	120
0	0.	-156.0	-84.5	-58.6	-48.6	-36.4	-30.1	-25.4	-22.1	-19.0	-16.5	-14.5	-12.7	-11.3	-10.0	-9.2
8	0.	48.3	0.4	-13.7	-16.9	-16.8	-15.8	-14.6	-13.3	-11.9	-10.7	-9.6	-8.6	-7.7	-6.9	-6.1
16	0.	40.9	25.9	9.7	1.1	-3.1	-5.1	-6.1	-6.2	-6.1	-5.8	-5.4	-5.0	-4.6	-4.2	-3.8
24	0.	28.4	28.0	19.1	11.3	6.0	2.6	0.5	-0.7	-1.4	-1.7	-1.9	-2.0	-1.9	-1.8	-1.7
32	0.	20.6	24.5	21.4	16.2	11.5	7.9	5.4	3.6	2.4	1.6	1.0	0.7	0.4	0.3	0.1
40	0.	15.9	20.8	20.6	17.8	14.4	11.3	8.7	6.8	5.4	4.3	3.5	2.8	2.4	2.0	1.8
48	0.	12.7	17.5	18.8	17.7	15.5	13.1	10.9	9.1	7.6	6.4	5.4	4.6	4.0	3.5	3.1
56	0.	10.4	14.9	16.8	16.8	15.7	14.0	12.2	10.6	9.2	7.9	6.9	6.0	5.3	4.8	4.3
64	0.	8.9	12.9	15.0	15.6	15.2	14.2	12.9	11.5	10.2	9.0	8.0	7.1	6.4	5.7	5.2
72	0.	7.8	11.3	13.4	14.4	14.4	13.9	13.0	11.9	10.8	9.7	8.8	7.9	7.1	6.5	5.9
80	0.	6.8	10.0	12.0	13.1	13.5	13.3	12.7	11.9	11.0	10.1	9.2	8.4	7.7	7.0	6.4
88	0.	6.0	8.8	10.8	11.9	12.5	12.5	12.2	11.7	10.9	10.2	9.4	8.7	8.0	7.3	6.8
96	0.	5.3	7.8	9.6	10.8	11.4	11.7	11.5	11.2	10.7	10.0	9.4	8.7	8.1	7.5	7.0
104	0.	4.6	6.8	8.4	9.6	10.3	10.7	10.7	10.5	10.2	9.7	9.2	8.7	8.1	7.6	7.1
112	0.	3.8	5.7	7.1	8.2	9.0	9.5	9.7	9.7	9.5	9.2	8.8	8.4	8.0	7.5	7.1
120	0.	2.9	4.4	5.6	6.7	7.5	8.1	8.5	8.6	8.6	8.5	8.3	8.0	7.7	7.3	7.0

Figure A-6. Horizontal Soil Displacement, u (μ in.), 8-Inch Resolution, G = 5000 psi, ν = 0.35

APPENDIX B

CHARACTERISTIC IMPEDANCE OF AN ECCENTRIC COAXIAL CABLE WITH A NONHOMOGENEOUS DIELECTRIC

THE INVERSION TRANSFORMATION OF A CIRCLE

Consider the properties of a regular function of the type

$$Z = f(t) = x(\mu, \nu) + jy(\mu, \nu) \tag{B-1}$$

which defines a complex variable $Z = x + jy$ as some function of another complex variable $t = \mu + j\nu$. A particular value, t', can be represented by a point in the Argand diagram of t. Through equation (B-1) some particular value Z' corresponds to t' and it may be represented by a point in the Argand diagram of Z. Further, there is a similar correspondence for a succession of pairs of points in the t and Z planes so that to some curve t't'' there corresponds a curve Z'Z'' which is said to have been transformed from t't'' by equation (B-1).

Consider the inversion transformation

$$Z = 1/t \tag{B-2}$$

The equation of a circle, center (a, o), and radius r in the t plane,

$$r = |t-a| \tag{B-3}$$

Substituting (B-2) into (B-3),

$$r = \left|\frac{1}{(x+jy)} - a\right|$$

$$= \left|\frac{(1-ax) - jay}{x+jy}\right| \qquad \text{(B-4)}$$

Therefore,

$$r^2 = \frac{(1-ax)^2 + a^2y^2}{x^2 + y^2} \qquad \text{(B-5)}$$

which may be rearranged as

$$\left(x - \frac{a}{a^2 - r^2}\right)^2 + y^2 = \left(\frac{r}{a^2 - r^2}\right)^2 \qquad \text{(B-6)}$$

Equation (B-6) represents a circle, radius $r/(a^2-r^2)$, center $((a/(a^2-r^2)), 0)$, in the Z plane, mapped by equation (B-2) from the circle, radius r, center (a, o), in the t plane.

THE IMPEDANCE OF AN ECCENTRIC COAXIAL CABLE WITH A NONHOMOGENEOUS DIELECTRIC FILLING

Consider the eccentric coaxial cable shown in Figure B-1. From equation (B-6), it is seen that the smallest circle, center (d, 0), and radius R_3 in the t plane transforms into a circle in the Z plane with center coordinates $((d/(d^2-R_3^2)), 0)$ and radius

$$r_3 = \frac{R_3}{d^2 - R_3^2} \qquad \text{(B-7)}$$

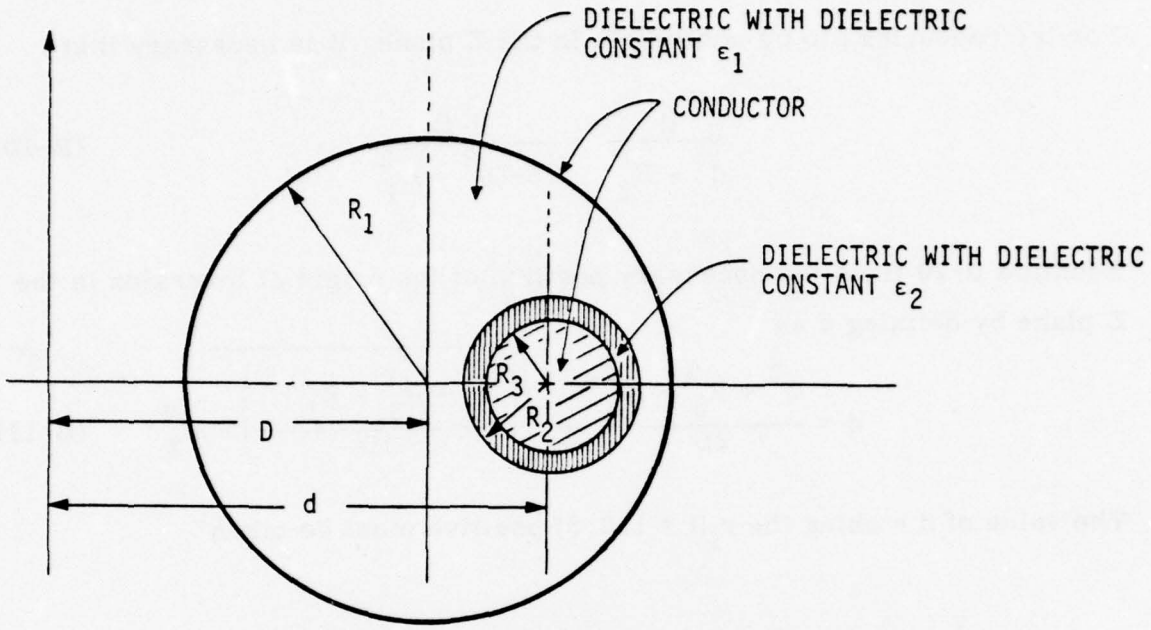

Figure B-1. Eccentric Coaxial Cable with Nonhomogeneous Dielectric

Similarly, the circle with center (d, 0) and radius R_2 in the t plane transform into a circle in the Z plane with center coordinates $((d/(d^2-R_2^2)), 0)$

$$r_2 = \frac{R_2}{d^2 - R_2^2} \tag{B-8}$$

Also, the circle with center ((d-D), 0) and radius R, in the t plane transforms into a circle in the Z plane with center coordinates $((d-D)/(d-D)^2 - R_1^2, 0)$ and radius

$$r_1 = \frac{R_1}{(d-D)^2 - R_1^2} \tag{B-9}$$

For the conductors to be concentric in the Z plane, it is necessary that

$$\frac{d}{d^2 - R_3^2} = \frac{d-D}{(d-D)^2 - R_1^2} \qquad \text{(B-10)}$$

Equation B-10 fixes the necessary position of the origin of inversion in the Z plane by defining d as

$$d = \frac{D^2 + R_3^2 - R_1^2}{2D} \pm \sqrt{\left(\frac{D^2 + R_3^2 - R_1^{2\,2}}{2D}\right) - R_3^2} \qquad \text{(B-11)}$$

The value of d making the $r_i (i = 1, 2, 3)$ positive must be taken

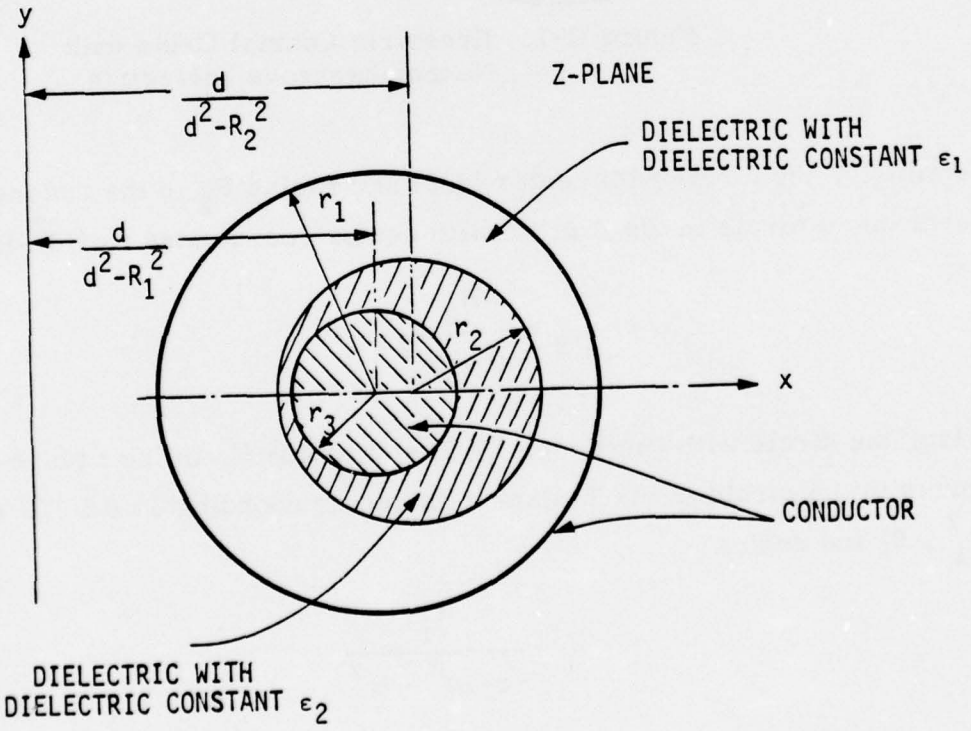

Figure B-2. Transformed Cable

The configuration of Figure B-2 can be broken up into infinitesimal wedges as shown in Figure B-3.

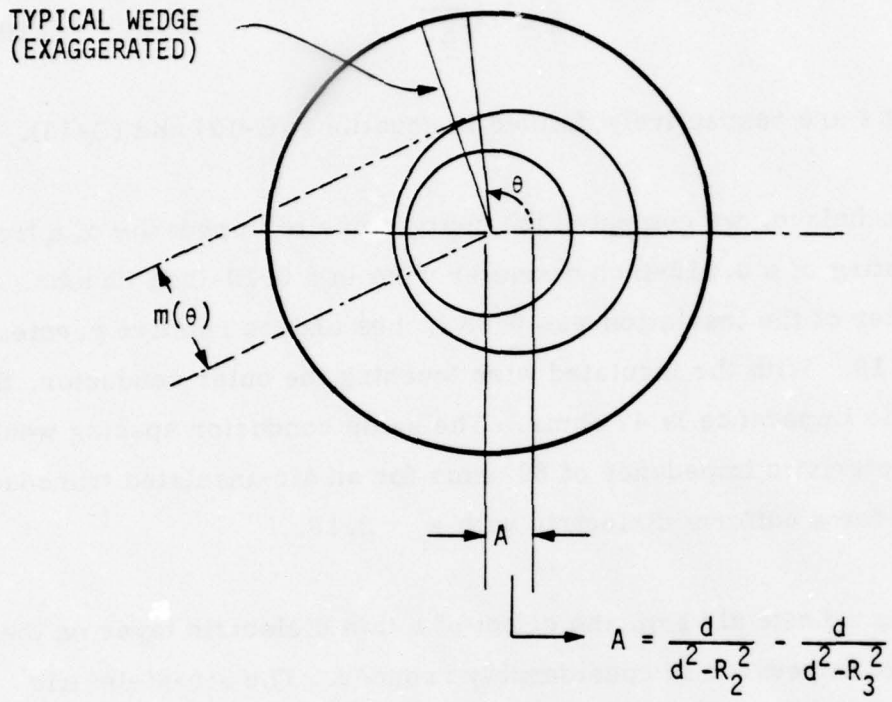

Figure B-3. Wedge Configuration

The approximate capacitance per unit length of the cable is

$$C = 2\varepsilon_o \int_o^{\pi} \left(\frac{d\Theta}{1/\varepsilon_1 \ln \frac{r_1}{m(\theta)} + 1/\varepsilon_2 \ln \left(\frac{m(\theta)}{r_3} \right)} \right) \qquad \text{(B-12)}$$

The inductance per unit length of the cable is

$$\ell = \frac{\mu_0}{2\pi} \ln \left(\frac{r_i}{r_3} \right) \qquad \text{(B-13)}$$

The characteristic impedance of the cable is

$$Z = \sqrt{\frac{\ell}{C}} \qquad \text{(B-14)}$$

where C and ℓ are respectively defined in equations (B-12) and (B-13).

Using this technique, we computed the characteristic impedance of a transducer consisting of a 0.018-inch diameter wire in a 0.19-inch ID tube. The outer diameter of the insulation was 0.03 inches and its relative permeability was 2.18. With the insulated wire touching the outer conductor, the characteristic impedance is 47 ohms. The same conductor spacing would give a characteristic impedance of 62 ohms for an air-insulated transducer, and 42 ohms for a uniform dielectric with $\varepsilon_r = 2.18$.

When there is a finite air gap, the effect of a thin dielectric layer on the characteristic impedance is considerably reduced. The air-dielectric approximation for the transducer impedance then becomes reasonably accurate.

APPENDIX C

REFLECTIONS FROM ABRUPT AND GRADUAL DISTURBANCES IN A LONG TRANSMISSION LINE

This appendix describes the equations used in predicting reflected signal waveshapes for a uniform, lossy transducer. Our computations were simplified by using a double-step approximation for the line displacement. We include in this appendix an independent computation of the signal waveshape for a case in which the impedance variation is described as an exponential function. Results of the two computation methods are nearly identical for long transducers, where frequency-dependent losses dictate the signal waveforms.

STEP-FUNCTION RESPONSE OF A TRANSMISSION LINE

According to the theory developed by Wigington and Nahman (Reference 1), the response of a lossy transmission line to a step-function input is

$$v(t) = \text{CERF} \quad \frac{T}{t} \tag{C-1}$$

where t is the time after arrival of the step and T is defined by

$$T = \frac{\alpha^2 L^2}{4 Z_o^2} \tag{C-2}$$

L is the length of the transmission line and Z_o is its characteristic impedance. The attenuation per unit length α is

$$\alpha = \frac{1}{2\pi}\left(\frac{\mu}{\sigma}\right)^{\frac{1}{2}}\left(\frac{1}{a_1} + \frac{1}{a_2}\right) \qquad \text{(C-3)}$$

a_1 and a_2 are the conductor radii, and for copper conductors

$$\mu = \mu_o = 4\pi \times 10^{-7} \text{ Henries/meter}$$

$$\sigma = 5.8 \times 10^{7} \text{ mhos/meter}$$

CERF(x), the complementary error function of x, can be computed very accurately from

$$\text{CERF}(x) = \frac{1}{\left(1 + a_1 x + a_2 x^2 + a_3 x^3 + a_4 x^4\right)^4} \qquad \text{(C-4)}$$

$a_1 = 0.278393$

$a_2 = 0.230389$

$a_3 = 0.000972$

$a_4 = 0.078108$

REFLECTIONS FROM A DOUBLE-STEP DISTURBANCE IN LINE IMPEDANCE (METHOD 1)

When an intruder crosses the transducer, the impedance of a short section is affected. In our analysis, we assumed that the disturbance can be approximated by step-function changes in the line impedance (Figure C-1). Let us denote the line impedance of the disturbed section as Z_o', and the length Δx. We now want to calculate the reflected wave. This is, in fact, a

multiple reflection problem. However, we can make a "one pass" approximation by realizing the fact that Z_o and Z_o' are almost equal; therefore, the transmission is nearly complete. Let us assume that an incident wave $v(t)$ arrives at junction 1. The reflection coefficient is:

$$\rho_1 = \frac{Z_o' + Z_o}{Z_o + Z_o'} \tag{C-5}$$

The transmission coefficient is:

$$\tau_1 = \frac{2Z_o'}{Z_o + Z_o'} \tag{C-6}$$

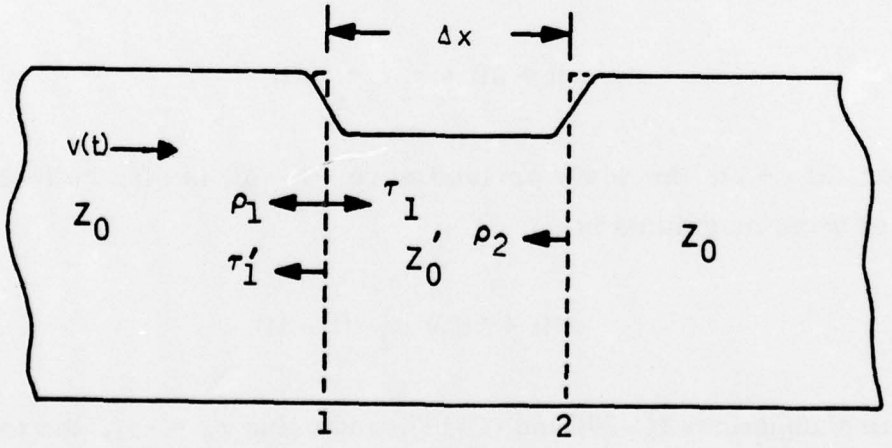

Figure C-1. A Disturbed Section of Transmission Line

This transmitted wave propagates forward and is reflected at junction 2. The reflection coefficient is:

$$\rho_2 = \frac{Z_o' - Z_o}{Z_o + Z_o'} \tag{C-7}$$

This reflected wave propagates backward and is transmitted at junction 1, where the transmission coefficient is:

$$\tau_1' = \frac{2Z_o}{Z_o + Z_o'} \tag{C-8}$$

Now this wave has travelled a distance of $2\Delta x$, and the time spent is

$$\Delta t = \frac{2\Delta x}{c_o} \tag{C-9}$$

Combining Equations (C-6), (C-7) and (C-8), the reflected wave has a magnitude

$$v(t + \Delta t) = \tau_1 \tau_2 \tau_2' v(t) \tag{C-10}$$

However, at $t + \Delta t$, the newly arrived wave $v(t + \Delta t)$ is also reflected, the reflected wave magnitude is:

$$v''(t + \Delta t) = \rho_1 v(t + \Delta t) \tag{C-11}$$

Combining Equations (C-10) and (C-11), and using $\rho_2 = -\rho_1$, the total reflected wave magnitude is

$$v_r(t + \Delta t) = \rho_1 [v(t + \Delta t) - \tau_1 \tau_2' v(t)] \tag{C-12}$$

Since $Z_o' \approx Z_o$, we get:

$$\tau_1 \approx 1 \tag{C-13}$$

$$\tau_2' \approx 1 \tag{C-14}$$

Equation (C-12) becomes

$$v_r(t + \Delta t) \approx \rho_1[v(t + \Delta t) - v(t)] \tag{C-15}$$

This is equivalent to

$$v_r(t) \approx \rho_1[v(t) - v(t - \Delta t)] \tag{C-16}$$

We can consider this as a superposition of two separate reflected signals displaced in time. Each signal is a linearly-scaled version of the incident wave $v(t)$. As these signals propagate back toward the generator, they continue to undergo the same degradation in risetime as the forward-going incident wave. We can compute the actual waveshape of the superposed reflected signals by using the expression previously developed for $v(t)$ evaluated at a distance L equal to twice the distance from the generator to the disturbance.

REFLECTIONS FROM AN EXPONENTIAL VARIATION IN LINE IMPEDANCE (METHOD 2)

As a check on the validity of the double-step approximation for the transducer impedance variation, we computed the signal waveshape from an exponential disturbance. The expression for the variation in impedance

was taken from a cable sensor analysis performed by Frazier and Shiau (Reference 2). They expressed the impedance of the disturbed section as

$$Z_o(x) = Z_o \exp\left[-k(x - L)/\Delta x\right], \quad L < x < L + \frac{\Delta x}{2} \tag{C-17}$$

$$Z_o(x) = Z_o \exp\left\{-k\left[1 - (x - L)/\Delta x\right]\right\}, \quad L + \frac{\Delta x}{2} < x < L + \Delta x \tag{C-18}$$

The parameter k is determined from the impedance at the center of the disturbed section Z_o' by

$$k = 2\ell n \frac{Z_o}{Z_o'} \tag{C-19}$$

Note: For small variations in impedance, the expression for $Z_o(x)$ is nearly a triangular function.

For time domain reflectometry purposes, the reflected waveform, $v_r(t)$, in a uniform transducer with an exponential disturbance when interrogated by a unit step voltage is given by the expression

$$v_r(t) = -\frac{1}{2\Delta x} \ell n \frac{Z_o}{Z_o'} \left[u(t) * F^{-1}\left\{\left[\exp(4\gamma L - \gamma \Delta x) - \exp(4\gamma L)\right]^2 / \gamma\right\}\right] \tag{C-20}$$

where L = the distance between the reflectometer and the disturbance

Δx = the length of the disturbance

Z_o = the characteristic impedance of the transducer

Z_o' = minimum impedance along the exponential disturbance

γ = propagation coefficient of the transducer

$u(t)$ denotes a unit step function

F^{-1} is the inverse Fourier transform

The propagation coefficient, γ, of the transducer is given by the expression

$$\gamma(jw) = \sqrt{(R + jw\ell)/jwc} \qquad \text{(C-21)}$$

where ℓ = inductance per unit length of the transducer

c = capacitance per unit length of the transducer

$R = k(jw)^{\frac{1}{2}}$

$$k = \frac{1}{2\pi}\left(\frac{\mu_o}{\sigma}\right)^{1/2}\left(\frac{1}{r_1} + \frac{1}{r_2}\right)$$

r_1 = inner conductor radius

r_2 = outer conductor radius

σ = conductivity of the inner conductor

μ_o = permeability of free space

COMPARISON OF RESULTS

Figure C-2 shows a reflected signal waveform computed by the first method, assuming a step discontinuity in the line impedance. The disturbance is located at one km from the generator end of a transducer with a_1 = 4.2 mm and a_2 = 15 mm. The gap between conductors is 0.06 mm, except for the 1-meter-long disturbed section where the gap is 0.05 mm. A 1-volt step is used as the excitation signal. For this case, the peak amplitude of the reflected pulse is -4.1×10^{-4} volts, and the half-amplitude width is about 3×10^{-7} seconds.

For comparison, we used the second method to compute the reflected signal from an exponential impedance variation on an identical transducer. The total disturbance length was again chosen to be one meter. We set the

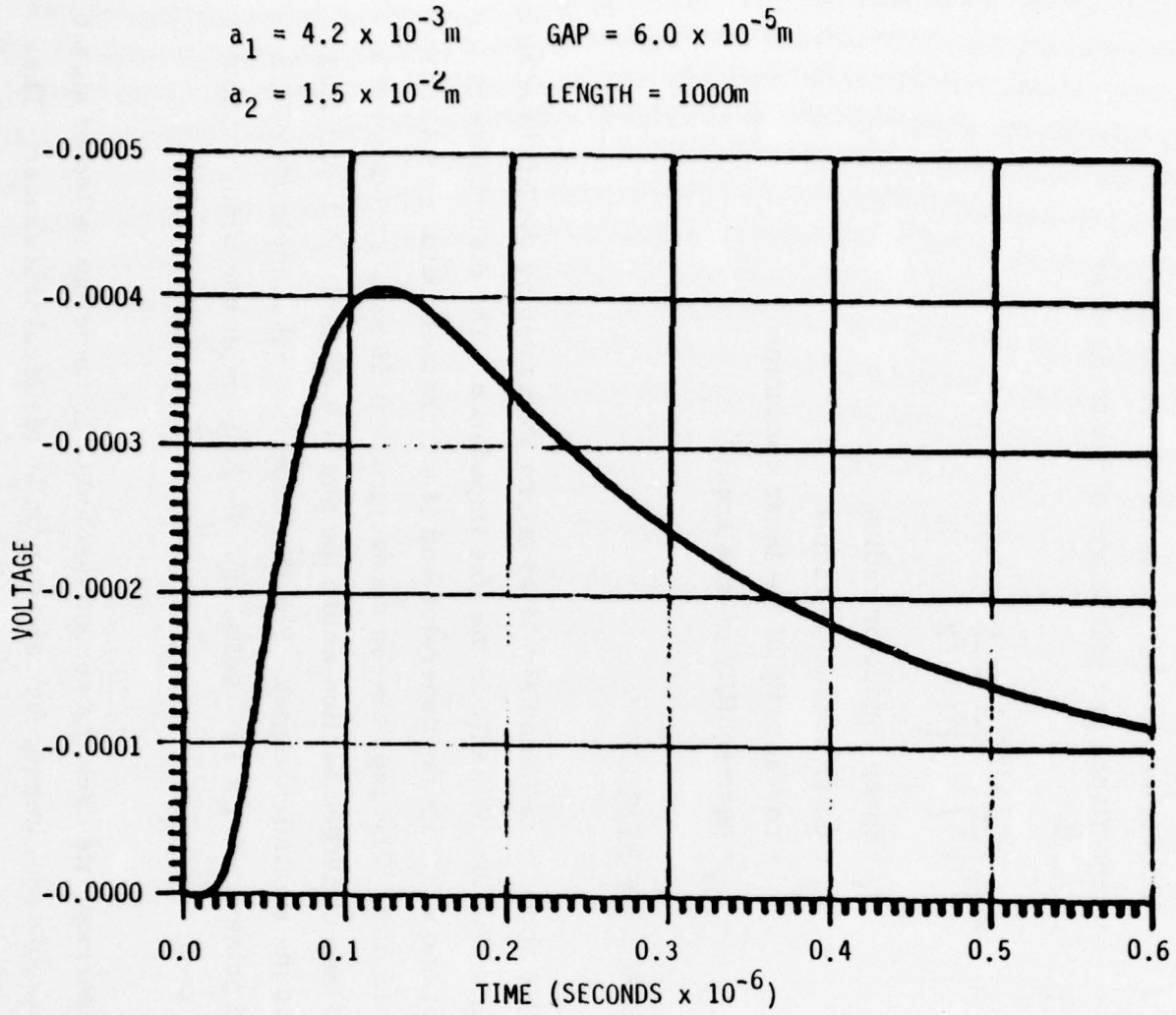

Figure C-2. Signal Waveform Computed by Method 1

impedance Z_o' in the center of the disturbed section to be equal to Z_o' for the previous case.

A 512-point Fast Fourier transform and discrete convolution with the unit step input were performed on a SDS 9300 computer. Results of the computation over the time interval of interest are shown in Figure C-3. The peak amplitude of -2.2×10^{-4} volts is about half the amplitude for the double-step case, but the pulse width is essentially unchanged.

We would obtain almost identical results with Method 1 if we replaced the impedance Z_o' of the one-meter disturbed section by $(Z_o' + Z_o)/2$. Integrating the exponential expression for the variation in transducer impedance over the disturbance length, we find that the average value is in fact very close to $(Z_o' + Z_o)/2$.

This comparison of numerical results does not constitute a proof of the validity of Method 1. However, we feel that the method provides accurate results for long transducers, where the response in the time domain is limited by the frequency response of the transducer. Under these conditions, the amplitude of the received signal from a disturbance will depend upon the integral of the impedance variation over the disturbed length.

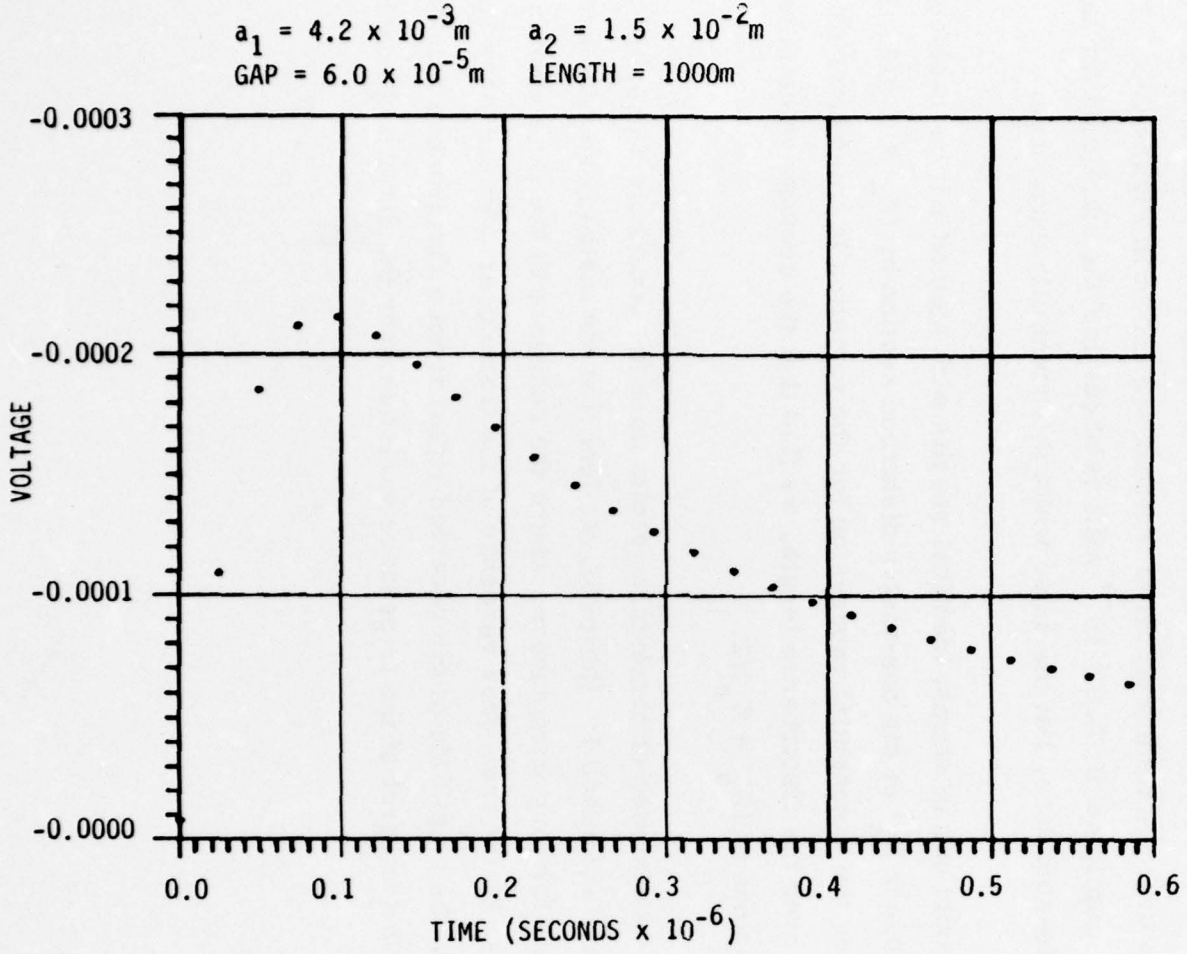

Figure C-3. Signal Waveform Computed by Method 2

REFERENCES FOR APPENDIX C

1. Wigington, R. L. and N. S. Nahman, "Transient Analysis of Coaxial Cable Considering Skin Effect," Proc. IRE, Vol. 45, No. 2, 1957, pp. 166-174.

2. Frazier, M. J. and Y. Shiau, Cable Sensor Analysis, Final Report, NUC Contract N66001-75-C-0176, June 1975.

METRIC SYSTEM

BASE UNITS:

Quantity	Unit	SI Symbol	Formula
length	metre	m	...
mass	kilogram	kg	...
time	second	s	...
electric current	ampere	A	...
thermodynamic temperature	kelvin	K	...
amount of substance	mole	mol	...
luminous intensity	candela	cd	...

SUPPLEMENTARY UNITS:

plane angle	radian	rad	...
solid angle	steradian	sr	...

DERIVED UNITS:

Acceleration	metre per second squared	...	m/s
activity (of a radioactive source)	disintegration per second	...	(disintegration)/s
angular acceleration	radian per second squared	...	rad/s
angular velocity	radian per second	...	rad/s
area	square metre	...	m
density	kilogram per cubic metre	...	kg/m
electric capacitance	farad	F	A·s/V
electrical conductance	siemens	S	A/V
electric field strength	volt per metre	...	V/m
electric inductance	henry	H	V·s/A
electric potential difference	volt	V	W/A
electric resistance	ohm		V/A
electromotive force	volt	V	W/A
energy	joule	J	N·m
entropy	joule per kelvin	...	J/K
force	newton	N	kg·m/s
frequency	hertz	Hz	(cycle)/s
illuminance	lux	lx	lm/m
luminance	candela per square metre	...	cd/m
luminous flux	lumen	lm	cd·sr
magnetic field strength	ampere per metre	...	A/m
magnetic flux	weber	Wb	V·s
magnetic flux density	tesla	T	Wb/m
magnetomotive force	ampere	A	...
power	watt	W	J/s
pressure	pascal	Pa	N/m
quantity of electricity	coulomb	C	A·s
quantity of heat	joule	J	N·m
radiant intensity	watt per steradian	...	W/sr
specific heat	joule per kilogram-kelvin	...	J/kg·K
stress	pascal	Pa	N/m
thermal conductivity	watt per metre-kelvin	...	W/m·K
velocity	metre per second	...	m/s
viscosity, dynamic	pascal-second	...	Pa·s
viscosity, kinematic	square metre per second	...	m/s
voltage	volt	V	W/A
volume	cubic metre	...	m
wavenumber	reciprocal metre	...	(wave)/m
work	joule	J	N·m

SI PREFIXES:

Multiplication Factors	Prefix	SI Symbol
1 000 000 000 000 = 10^{12}	tera	T
1 000 000 000 = 10^{9}	giga	G
1 000 000 = 10^{6}	mega	M
1 000 = 10^{3}	kilo	k
100 = 10^{2}	hecto*	h
10 = 10^{1}	deka*	da
0.1 = 10^{-1}	deci*	d
0.01 = 10^{-2}	centi*	c
0.001 = 10^{-3}	milli	m
0.000 001 = 10^{-6}	micro	μ
0.000 000 001 = 10^{-9}	nano	n
0.000 000 000 001 = 10^{-12}	pico	p
0.000 000 000 000 001 = 10^{-15}	femto	f
0.000 000 000 000 000 001 = 10^{-18}	atto	a

* To be avoided where possible.

*U.S. GOVERNMENT PRINTING OFFICE: 1977-714-025/228

MISSION
of
Rome Air Development Center

RADC plans and conducts research, exploratory and advanced development programs in command, control, and communications (C^3) activities, and in the C^3 areas of information sciences and intelligence. The principal technical mission areas are communications, electromagnetic guidance and control, surveillance of ground and aerospace objects, intelligence data collection and handling, information system technology, ionospheric propagation, solid state sciences, microwave physics and electronic reliability, maintainability and compatibility.